Design of a New Electron Gun for LINAC2 at ELSA

Samuel Kronenberg

Masterarbeit in Physik
angefertigt im Physikalischen Institut

vorgelegt der
Mathematisch-Naturwissenschaftlichen Fakultät
der
Rheinischen Friedrich-Wilhelms-Universität
Bonn

April 2023

I hereby declare that this thesis was formulated by myself and that no sources or tools other than those cited were used.

Bonn, ...

Date Signature

1. Gutachter: Prof. Dr. Klaus Desch
2. Gutachter: Prof. Dr. Hartmut Schmieden

Contents

CHAPTER 1

Introduction

In this thesis the design process of a new electron gun for the accelerator facility ELSA is presented. The new gun is set to be integrated at the 3 GHz linear accelerator (LINAC2) of the facility. The development starts with an investigation of the current electron gun with the goal to determine the beam parameters of the existing setup, which should be matched by the new assembly. Different types of electron guns are presented and evaluated regarding their usability as an injector for the LINAC2. The structure of the new gun layout is presented, its design is simulated and refined in several steps, optimizing the beam parameters while ensuring good usability and easy maintenance. Beside the existing multi-bunch mode (electron pulse duration of 1 µs), a single-bunch mode, where the duration of emitted electron pulse is equivalent to a single RF bucket in the Linac, is to be realized. Furthermore, an outlook to the future work and research regarding the new electron gun is presented.

1.1 Electron Accelerator Facility ELSA

At the Physics Institute of the University of Bonn, the 3.2 GeV electron stretcher accelerator (ELSA) is operated since 1987. An overview of the facility is given in Figure 1.1. The facility utilizes three accelerator stages to provide the experimental sites with spin-polarized or unpolarized electrons. The first stage consist of a travelling wave linear accelerator (LINAC2). LINAC2 is equipped with two electron guns: One thermionic gun for the production of unpolarized electrons, and a second one for the production of polarized electrons, which is based on a photo-cathode. Both guns emit electron beams with an energy of 50 keV which are accelerated up to 26 MeV using the 3 GHz Linac. The second accelerator stage of the facility is the combined function booster synchrotron, which is in operation since 1967. It was constructed as an 2.5 GeV synchrotron and was formerly used for hadron physics experiments. After the construction of the third stage, the ELSA stretcher ring, it was utilized as an pre-accelerator for ELSA. The stretcher ring, capable of accelerating a beam current of 30 mA at the maximal energy of 3.2 GeV. The external electron beam is provided via slow resonance extraction from the storage ring. Thus, a maximal external quasi-continuos current of 100 nA can be extracted towards the two experimental sites of CBELSA/TAPS [1] and BGOOD [2]. Furthermore an external beamline for detector tests is available, which is also used for medical experiments recently.

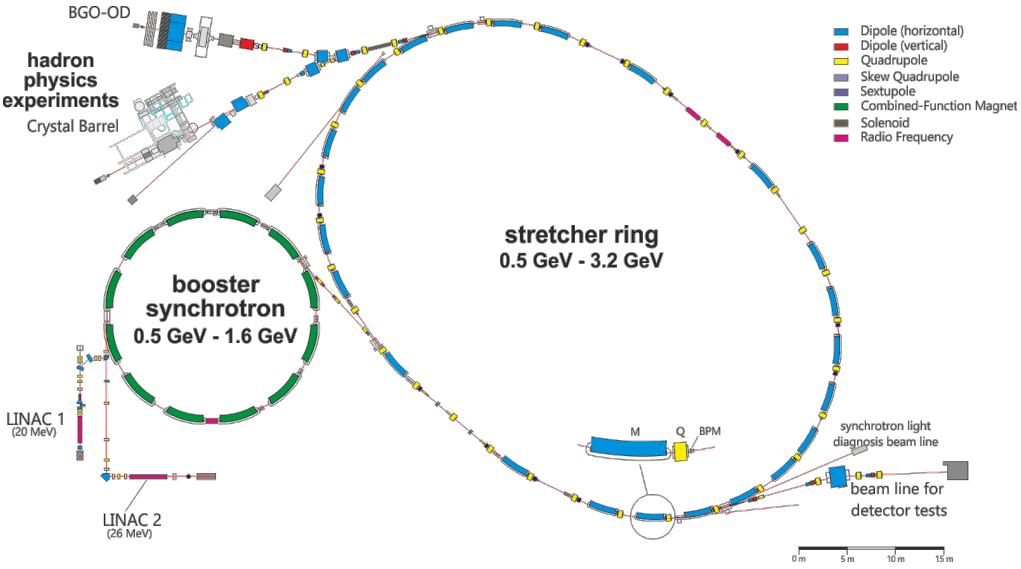

Figure 1.1: The plan of the ELSA facility

1.2 Current Layout of the Injector Infrastructure

The linear accelerator (LINAC2) was formerly used as part of the 300 MeV linear electron accelerator at the University of Mainz. The thermionic electron gun, used as a source for unpolarized electrons, was constructed around 1975 also at the University of Mainz. In the 1990s the Linac as well as the thermionic gun were given to the University of Bonn. First operation of the new setup was in 2000.
The layout of the transfer beamline is shown in Figure 1.2. The gun is positioned below the transfer beamline. The α-Magnet is used to switch between operation with the thermionic gun or the source of spin-polarised electrons. The position of the gun causes it to be difficult to reach, which makes it difficult to work on. This is particularly inconvenient for recurring tasks, which are therefore more time-consuming. Due to the limited space at LINAC2, no other positioning is possible.

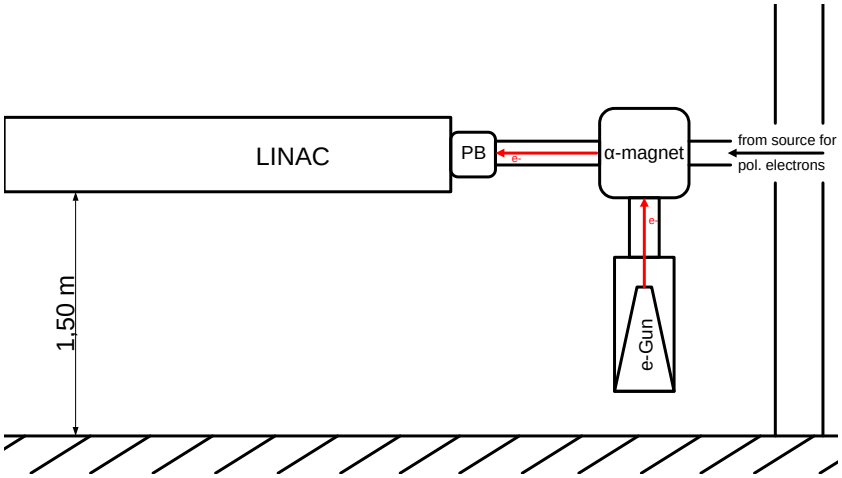

Figure 1.2: Schematic drawing of the position of the thermionic gun at LINAC2 and the transfer beamline.

1.3 Requirements for an Injector Upgrade

Since the start of operation in 2000 the electron gun was in operation without severe technical problems. However, due to ageing effects, especially on vacuum seals at the prebuncher and the gun, it became increasingly difficult to maintain a vacuum pressure in the needed range of 10^{-8} mbar inside the transfer beamline. Furthermore damages at the structure of the electron gun were observed, mainly at the cathode mount. Due to this a remaining lifetime in the order of a few years was estimated. Thus the development of a new electron gun has to be considered.
In addition to solving the vacuum problems, the new electron gun should provide a new mode of operation: The so-called single bunch mode. This new mode allows the filling of a single RF bucket in the linear accelerator and the following accelerator stages. This would allow arbitrary filling patterns in the stretcher ring, which would also be available for external experiments if desired. It is also needed for additional accelerator research, such as advanced beam stability measurements. The use of a single high intensity bunch would enable the wake impedance in the stretcher ring and its influence on the beam to be measured. This is of great interest for the desired intensity upgrade of ELSA [3]. The single-bunch filling pattern allows the influence of multi-bunch instabilities to be neglected for these measurements. This feature was already introduced at the former LINAC1 [4] but was later lost as part of the decommissioning of this injector.

CHAPTER 2

Background Information

To understand the design choice made in the planning process of the new electron gun, it is necessary to introduce some basic knowledge regarding the beam dynamics in a particle accelerator and the occurring effects which are of special interest in electron guns. This chapter will mainly be based on [5] and [6].

2.1 Transverse Beam Dynamics

The motion and behaviour of electrons inside particle accelerators resides from their transport through an ion optical system with drifts as well as dipole and quadrupole magnets. To describe their trajectory – position and angular displacement as well as momentum deviation of single particles - one can use a matrix formalism similar to regular optics. This formalism is described for example in [5] or other accelerator physics textbooks. The beam inside a particle accelerator is made up of a many different particles. Combining all these single particle trajectories enables the beam the description of the beam as an ensemble with statistical quantities. An introduction to this formalism is given below.

2.1.1 Coordinate System

In accelerators - this can be circular or linear accelerators as well as beam lines of any shape for beam transport. A co-moving curvilinear coordinate system is used, as shown in Figure 2.1 . This coordinate system is based on the design orbit. The origin of the system moves along this orbit with the design velocity. The s axis always points in the direction of motion. The x axis is oriented parallel to the $\mathbf{R}$ vector of used dipole magnets (the horizontal plane for ELSA) and perpendicular to s. The z axis is orientated perpendicular to the s- as well as the x-axis. Additionally, the derivatives of the transversal coordinates along the longitudinal direction

$$x' = \frac{\mathrm{d}x}{\mathrm{d}s} \quad \text{and} \quad z' = \frac{\mathrm{d}z}{\mathrm{d}s} \tag{2.1}$$

are used to describe the particles trajectory and position. Assuming that the deviations from the reference orbit are small, the beam dynamics can be described in a linear approximation. To describe a particle in longitudinal direction the position deviation l and the relative momentum deviation δ are used:

$$l = -v_0(t - t_0)\ , \quad \delta = \frac{p - p_0}{p_0}. \tag{2.2}$$

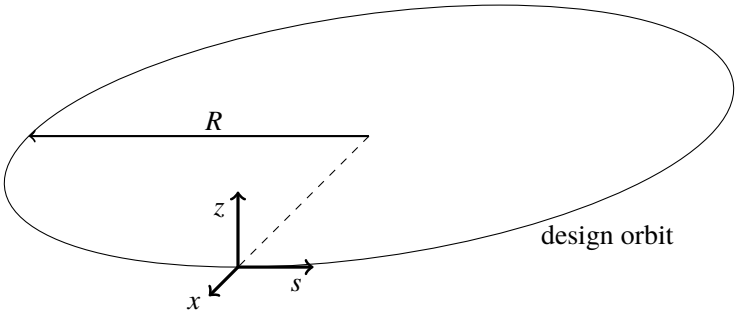

Figure 2.1: In accelerators a co-moving coordinate system is used - here depicted exemplary in a circular accelerator. The axis s always points in the direction of the design orbit. The axis x is oriented in the horizontal plane and the axis z in the vertical plane.

The longitudinal position deviation is given by the difference between the time t, where the described particle passes the position s and the time t_0, where the central particle passes the same location. The projection of this time difference onto the longitudinal displacement is done using the velocity v_0 of the central particle. One could describe a particle using a six-dimensional vector $\mathbf{x}(s)$:

$$\mathbf{x}(s) = \begin{pmatrix} x \\ x' \\ y \\ y' \\ l \\ \delta \end{pmatrix} = \begin{pmatrix} \text{radial position displacement} \\ \text{radial angular displacement} \\ \text{axial position displacement} \\ \text{axial angular displacement} \\ \text{longitudinal position displacement} \\ \text{relative momentum deviation} \end{pmatrix} \tag{2.3}$$

Instead of using the six-dimensional phase space, typically three two-dimensional phase spaces are used. These are two transversal phase spaces (x, x'), (z, z') and the longitudinal phase space (l, δ).

2.1.2 Transverse Phase Space

In order to describe a particle beam in an accelerator, it is not sufficient to describe a single particle and its trajectory, but the entire beam must be described as an ensemble of many individual particle trajectories. The particle beam is completely described if the density distribution $\rho(\mathbf{x}) = \rho(x, x', z, z', l, \delta)$ is known. As introduced in the previous section we will describe the particle in the transversal phase space. We consider the phase space (x,x') as an example, but the statements can also be transferred to the axial phase space (z,z').

Distribution in Phase Space

The vector $\mathbf{x}(s)$ is a two-dimensional vector in this phase space, consisting out of the radial position displacement and the angular displacement. The assumed density distribution in this phase space is a two-dimensional Gaussian function. The normalized two-dimensional Gaussian function is given by:

$$\rho(\mathbf{x}) = \frac{1}{2\pi\epsilon_x} \exp\left(-\frac{1}{2}\mathbf{x}^T \sigma_x^{-1} \mathbf{x}\right). \tag{2.4}$$

The entity ϵ_x is the radial emittance of the beam, both its mathematical as well as its physical meaning is explained later on. The vector $\mathbf{x}(s)$ is a column vector and the vector $\mathbf{x}(s)^T$ the corresponding row vector. The contour lines of the distribution are ellipses. Those ellipses can be described by the beam matrix σ_x, which can be expressed as:

$$\sigma_x = \begin{pmatrix} \sigma_{11} & \sigma_{12} \\ \sigma_{21} & \sigma_{22} \end{pmatrix} = \begin{pmatrix} \sigma_{11} & \sigma_{12} \\ \sigma_{12} & \sigma_{22} \end{pmatrix} . \tag{2.5}$$

The matrix has a positive determinant and is symmetric (the off-diagonal elements are equal). The diagonal elements of the matrix are the variances in x and x' and the off-diagonal elements are the covariances.
If one consider the contour line, where the density is decreased by the factor $\exp(-1/2)$, 39.3 % of all beam particles are inside this contour line. To simplify the description of the beam in the phase space this ellipse is used and the underlying distribution is omitted. Analogous to the 1σ interval of a Gaussian function, this ellipse is the 1σ ellipse of the density distribution and is commonly referred to as the phase space ellipse.

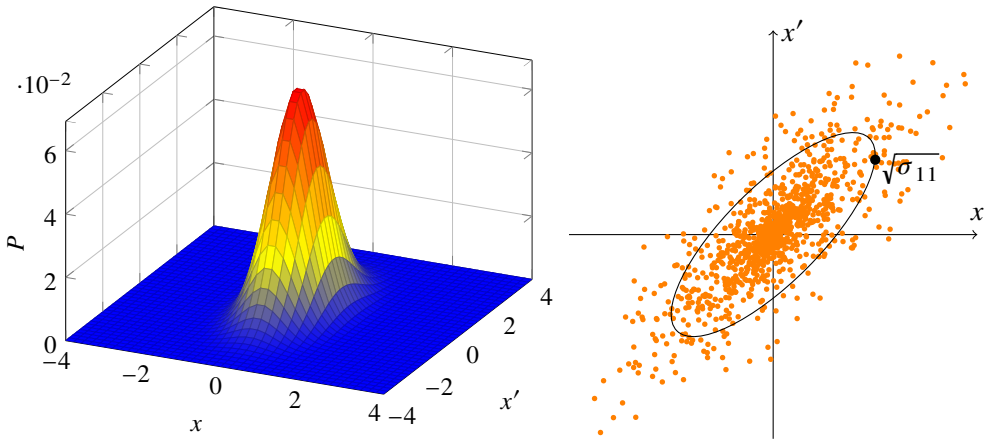

Figure 2.2: On the left a bivariate normal-distribution is shown, which is the underlying distribution for all the particles in the transverse phase space. The right shows individual particles in the phase space as a scatter plot. The distribution of the particles is described by the phase space ellipse. This ellipse is the 1σ-contour line of the underlying normal distribution.

The area of the 1σ ellipse is given by ϵ_x the radial emittance of the beam. To clarify which contour line is used to define the emittance, it is also called 1σ-emittance and it is given by

$$\epsilon_x = \epsilon_x^{1\sigma} = \sqrt{\det(\sigma_x)} . \tag{2.6}$$

The shape and orientation of the phase space ellipse represents the characteristics of the particle beam. The tilt of the ellipse represents the correlation between position displacement and angular deviation. The correlation is negative or positive for a convergent or divergent beam. The emittance is a measure for the beam quality, more precisely for the expansion of the beam around the central particle.

2.1.3 Emittance and Emittance Measurement

As already described above, in the spacial regime the transverse emittance is a measure of the spacial expansion of the particles in the transverse plane.
In simple terms, a low-emittance beam is tightly focused and confined to a small spot, while a high-emittance beam is more spread out and covers a larger area. A low-emittance beam can be tightly focused and precisely guided through accelerator components, while a high-emittance beam is more challenging to focus and steer with precision. There is also a risk of cut-off at the aperture for high emittance beams.
There is one important distinction to make if one speaks about emittance: As introduced in the previous section the emittance is defined at a position s along the accelerator using the distribution of all particles in the transverse phase-space. We introduced therefore also the concept of the phase-space ellipse. If one speaks about circular accelerators, one often comes across another ellipse which is defined in the transverse phase-space, called the machine ellipse. This is not defined by any distribution but rather by an idealized particle, which is in a state of equilibrium - which will be true in circular accelerators after a sufficient number of turns. If this requirement is fulfilled, this particle will move along this ellipse as it passes the accelerator multiple times. Therefore it is describing the particles at a position s over several turns. The machine ellipse describes the acceptance of the accelerator in the transverse phase space.
The area of the machine ellipse is defined by the Courant-Snyder-Invariant. In general, this quantity is not equal to the emittance. In circular accelerators, when all particles are in a corresponding state of equilibrium and have adjusted to the machine ellipse, the exceptional case is valid that emittance and Courant-Snyder-Invariant are equal. In this case the beam matrix introduced in formula 2.5 can be described in the form:

$$\sigma_x = \begin{pmatrix} \sigma_{11} & \sigma_{12} \\ \sigma_{12} & \sigma_{22} \end{pmatrix} = \begin{pmatrix} \epsilon\beta & -\epsilon\alpha \\ -\epsilon\alpha & \epsilon\gamma \end{pmatrix} \tag{2.7}$$

Where ϵ is the Courant-Snyder-Invariant and α, β and γ are optical functions, which are machine properties. A more in-depth treatment of these quantities can be found in every accelerator physics textbook. With regard to the emittance in accelerators, Liouville's theorem is often quoted. It shows that the emittance is a conserved quantity as long as the beam is only subjected to conservative forces. There are methods to reduce the emittance in an accelerator (so-called cooling methods), both based on naturally occurring effects and on special techniques. The fact that emittance is otherwise conserved motivates the importance of minimising it from the beginning.
At an accelerator facility the emittance is not only from great interest for the accelerator itself, but also for the experiments located at the facility. This is due to the fact that the emittance correlates to the angular divergence of the beam, meaning that a low-emittance beam is much more collimated than a high-emittance beam. One can see that the emittance is both a critical entity as well as an suitable performance metric to characterize the accelerator and beam characteristics. Therefore it is important to be able to measure and observe this quantity.
To measure the emittance of a beam the two-dimensional density distribution (in (x,x') phase space) is measured and the ellipse parameters are evaluated based on a two-dimensional Gaussian fit to the measured distribution. Using the ellipse parameters one can obtain the emittance of the beam.
A different approach is to measure the beam-profile at three location across the accelerator. Using the propagation of beam characteristics across an accelerator (i.e. the matrix formalism) the emittance can be calculated.
An additional method, which is often used, is the so-called quadrupole scan. Here one measures the beam-profile behind a quadrupole depending on the quadrupole strength k. One can then again use the propagation of beam parameters to calculate the emittance. A more in depth description of these methods is given in [5].

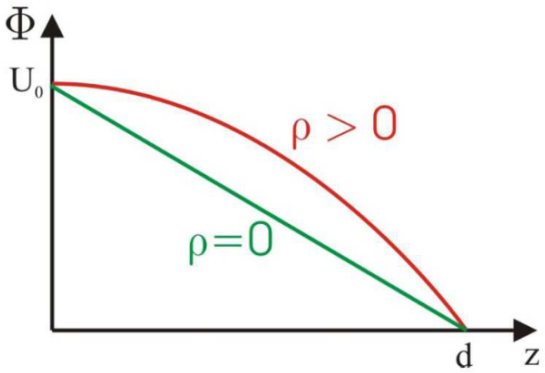

Figure 2.3: Electric potential inside an electron gun as a function of the distance z from the cathode. Compared is the potential in the absence of any charge $\rho = 0$ and if there is charge in the field $\rho > 0$. One can see that the existing space charge shields some of the potential. Especially near the cathode ($z = 0$), where the charge density is high, the potential difference is almost zero. [4].

2.2 Space Charge in Electron Guns

In an electron gun a non-divergent electron beam is desired. With increasing current density this becomes an severe problem. Every electron beam is subject to space charge effects, which is due to the fact that particles with same signed charge repel each other. In a dense electron beam this leads to significant repelling forces which subsequently leads to a broadening of the beam and therefore increased divergence. Furthermore, the charge of the beam also reduces the effective accelerating electric field inside an electron gun, which limits the maximal current, which can be accelerated inside the gun.
To describe effects in electron guns or RF cavities, typically a coordinate system is utilized, which differs from the previous described one. Here the longitudinal axis is represented by the z-axis, and the second transverse axis is designated as y. However, the definition of the x-axis remains unchanged. This coordinate system will be employed in the subsequent sections.

2.2.1 Space Charge Limited Current

In an electron gun, a voltage is applied between two electrodes, the cathode and the anode. Electrons are emitted from the cathode and then accelerated towards the anode, typically leaving the gun through a hole in the anode.
Without the presence of an electron beam ($\rho = 0$) one expects a constant progression of the potential between cathode and anode. With the presence of an electron beam ($\rho > 0$) this progression is no longer linear (see Fig. 2.3). Electrons travelling towards the anode are shielding the electric field due to their collective space charge. As a consequence following electrons will experience less accelerating voltage. This effects increases with a higher number of electrons since the space charge of these electrons again compensates a portion of the electric field, until emitted electrons are shielded completely from the field and therefore experience no acceleration. This leads to a limitation on the number of electrons, which can be accelerated in a field. The maximal current, which can be accelerated is called space charge limited current.
This effect was described first by C. Child (1911) and I. Langmuir (1913). The space charge limited current density J - which is the maximal current I_{max} through an area S - is therefore mainly influenced by the

acceleration voltage U and the geometry of the gun, described by d, the distance between cathode and anode. It is given by

$$J = \frac{I_{\max}}{S} = K \cdot U^{\frac{3}{2}} \cdot d^{-2} \,. \tag{2.8}$$

Where K is a factor depending on the particle type. For electrons it is given by

$$K = \frac{4}{9}\epsilon_0 \sqrt{\frac{2e}{m_e}} \,. \tag{2.9}$$

Therefore the space charge limited current can be altered by the accelerating voltage and by the distance between anode and cathode. Typically the former is fixed by the following accelerator but the latter can be changed.
If the possible emission current I of the cathode is higher than the space charge limited current $I_{\max}$, this is called the space charge limited operation mode. If this operation mode is desirable or not is not an easy question to answer and surely depends on the use case. The inverse squared dependency of the current on the distance of the electrodes implies that one is sensible on manufacturing tolerances as they influences this distance. These geometry imperfections therefore significantly influences the actual achievable currents. The dependency on the accelerating voltage also implies that jitter on the accelerating voltage would be transferred onto the particle current in the space charge limited operation.

2.2.2 Compensating Space Charge Effects

Besides the limitation of the maximum achievable particle current, the space charge has further effects on the particle beam. The high density of particles of the same electric charge leads to a broadening of the beam. To decrease this effect, a special geometry of the electrodes in the gun is used, which introduces transverse focussing electric field components. This geometry is called Pierce-geometry, since it was first described by J. R. Pierce in [7]. A sketch of such a setup is shown in Figure 2.4. However, it is important to keep in mind that this geometry was optimized for the space charge limited operation mode. Assuming an uniform rectilinear flow of electrons, he used the Laplace's equation at the interface between the electron beam and the surrounding charge-free region to find a potential that produces a parallel beam of electrons. At the position of the cathode, the equipotential lines of this potential intersect with the beam direction at an angle of 67.5°. To form such an electric potential the cathode needs to be shaped conforming to these equipotential lines. In a typical rotationally symmetrical gun assembly this means, that the cathode has the form of a cone with a half opening angle of $\Theta_{\text{Pierce}} = 67.5°$. Sometimes this angle is alternatively defined as the slope angle of the cathode with a value of 22.5°, which is equivalent. The anode in this setup also needs to be parallel to the equipotential lines. This needs to be evaluated for the individual setup.

2.3 Acceleration of Electrons in RF Fields

Besides static electric fields also radiofrequency (RF) fields are used - characterized by their frequency ν_{RF} - for the acceleration of charged particles. The motivation for this is the achievable electric field strength, which is typically higher in RF structures than in static electric fields. This is due to the fact that the breakdown voltage is dependent on the frequency of the applied voltage and increases for higher frequencies. This enables the use of field-gradients in RF cavities, which are excluded in a DC structure due to the breakdown

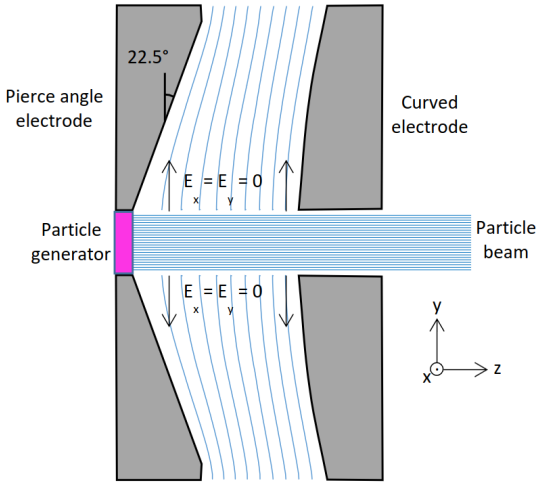

Figure 2.4: A simplified sketch of a pierce-type electron gun is shown. The pierce angle is here given in relation to a perpendicular axis to the particle beam and therefore given as 22.5°. One can see that the anode is parallel to the equipotential lines at this position. This setup compensates the space charge effects and produces a parallel beam. Taken from: [8].

limit. Higher field strengths are desirable in accelerator physics, since amongst other effects they reduce the space required for a given energy increase of the particles and because they have a positive impact on beam properties. Exemplarily, the larger effect of adiabatic damping reduces the emittance stronger for larger field gradients.

Inside a typical cylindrical cavity, the TM_{01} mode is used for acceleration. This mode has a longitudinal electric component, necessary for particle acceleration. The time evolution of the z-component (longitudinal component) of the electric field is shown in Figure 2.5.

Charged particles can only be accelerated in such a structure, when they experience an attractive field gradient ($E_z > 0$). In an alternating field this gradient is only present in a certain phase-range of the RF wave. The sections of the wave, where a stable acceleration is possible are called RF buckets. Therefore a continuous beam cannot be accelerated in a RF accelerator, but the beam needs to have a microstructure, consisting of so-called bunches. The separation of two bunches needs to be an integer multiple of the RF cycle $T_{\mathrm{acc}} = \frac{1}{\nu_{\mathrm{RF}}}$ and the length of the bunch must not exceed the phase acceptance of the accelerator.

The phase acceptance of an RF-accelerator is visualized in Figure 2.5. In this depiction of the E_z component the injection time range T_{inj} is marked. A bunch of charged particles of length t_{bunch} inserted at this time will span from $T_{\mathrm{inj}} - \frac{t_{\mathrm{bunch}}}{2}$ to $T_{\mathrm{ins}} + \frac{t_{\mathrm{bunch}}}{2}$. Therefore different particles in different positions inside the bunch will experience different accelerating field gradients. If the length of the bunch is greater than half a period of the accelerating wave, the particles at the end of a bunch will experience a decelerating field gradient. Dependent on the difference of T_{acc} and t_{bunch} and the electric field strength, these particles are slowed down, stopped or even accelerated back towards their source. The phase acceptance is therefore the area around the nominal phase, where an charged particle will be accelerated through the section without being lost. The velocity modulation of the particle beam in dependency of the phase difference to the nominal phase can be advantageous in a small region around T_{inj}, this effect is called phase-focussing and decreases the length (in time) of a bunch. An explanation of this effect can be found in [5] or other text books.

For typical linear RF accelerators the phase acceptance is rather small, in the order of some degrees. This

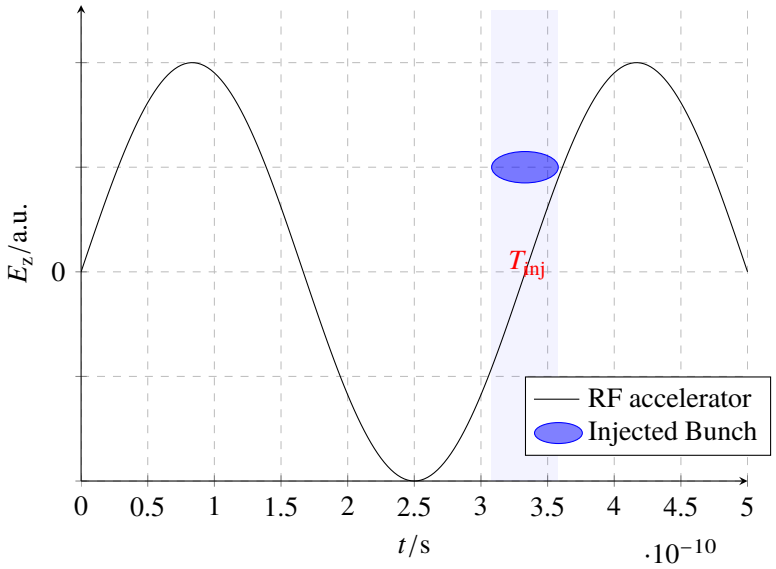

Figure 2.5: Time evolution of the E_z-component inside a RF accelerator. This component of the RF mode is used for acceleration of the particles. There is also shown the ideal injection time T_{inj} to accelerate a charged particle. Furthermore one can see an bunch which spreads around T_{inj}, the electrons inside the bunch will experience different accelerating gradient depending on their position in time.

leads to the loss of many particles in such a accelerator section if the incoming beam is not correctly prepared. The preparation of a particle beam before a RF Cavity is called *bunching*.

2.3.1 Bunching of Electron Beams

The bunching can be done upstream of the accelerating structure - separated from or inside the first section of the RF accelerator. At linear accelerators with injection velocities $v_{inj} \ll c$, typically a mixture of both is used to achieve the highest possible transfer efficiency. The first section in such an accelerator is used to match the phase velocity v_{ph} of the RF wave to the increasing particle velocity v_{part}. Additionally, this section is also used as an buncher. To increase the phase-acceptance and the transfer-efficiency of such an accelerator, an additional buncher is used before the accelerating structure.
There are different methods available to achieve the bunching, which can mainly be categorized into buncher and chopper.

(Pre-)buncher

As already mentioned a buncher can be also the first part of the accelerator structure. Often one uses a cavity which is placed at a distance L before the accelerating structure, therefore bunchers are often also referred to as prebunchers. The setup of such a buncher is shown in Figure 2.6(a). A buncher is an RF cavity to which a voltage is applied to generate a longitudinal electric field. Ideally a sawtooth-voltage would be used, but in practice this kind of voltages are not available in typical frequency ranges. Therefore a sinusoidal voltage, with the same frequency ν_{RF} as the RF accelerator is used, which is often separated from the power input of the main accelerator. In bunchers significantly smaller amplitudes are used than in a Linac. The time evolution of these modes in a prebuncher are shown and compared to the accelerating mode inside the main accelerator in Figure 2.7.

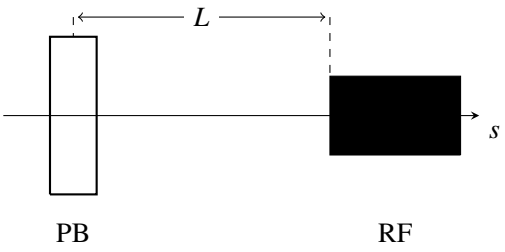

(a) Setup of the prebuncher (PB) and the accelerating RF structure

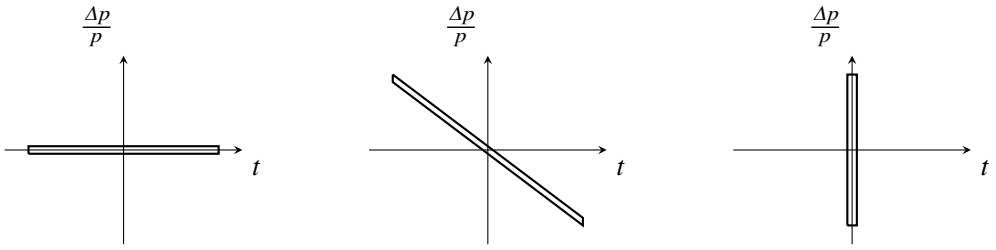

(b) $s = 0$ (c) $s = \frac{L}{2}$ (d) $s = L$

Figure 2.6: The working principle of a prebuncher is depicted. A prebuncher is placed at distance L to an accelerating RF structure. In a prebuncher a the time spread (see (b)) is transferred into a momentum deviation and therefore a velocity modulation (comp. (c)). After a suitable drift length L this momentum deviation will result in a sharp particle bunch in time domain. The bunch at position $s = L$ is depicted in (d). Inspired by: [5].

The energy modulation of the RF wave leads to an energy and velocity modulation of the particles. This principle is depicted in Figure 2.6. A bunch with small momentum deviation is injected into the prebuncher. The energy modulation shown in Figure 2.7 leads to a velocity modulation in the bunch. Particles towards the end of the bunch are accelerated stronger and particle towards the front are decelerated. Therefore the momentum deviation of the particles inside the bunch is dependent on their longitudinal position (comp. Fig. 2.6(c)). After a drift of length L, this modulation results in a sharp pulsed particle bunch in time domain. At the same time the momentum deviation of the beam is increased compared to the injected beam.
For the bunching, the linear part of the buncher mode is critical. This is why the sawtooth wave would be ideal. With a sawtooth prebuncher, one could achieve a phase acceptance of 2π. The phase acceptance of a sinusoidal prebuncher is smaller since the range, where the field strength rises linear with time, is smaller. Especially around the discontinuity of the sawtooth function particles cannot be bunched by a real prebuncher. A prebuncher can be used to divide a very long pulse, with a phase-spread way higher than the phase acceptance of the RF cavity - $\Delta\Phi_{\text{bunch}} \gg \Delta\Phi_{\text{acc}}$ - into multiple smaller bunches or to compress a bunch with $\Delta\Phi_{\text{bunch}} > \Delta\Phi_{\text{acc}}$ to a smaller phase phase-spread. The suitable distance between prebuncher and accelerator is dependent on the velocity and momentum of the central particle and the RF properties (voltage and frequency) of the prebuncher. A formal derivation can be found in [5]. A more detailed introduction into bunchers and prebunchers is available in [9].

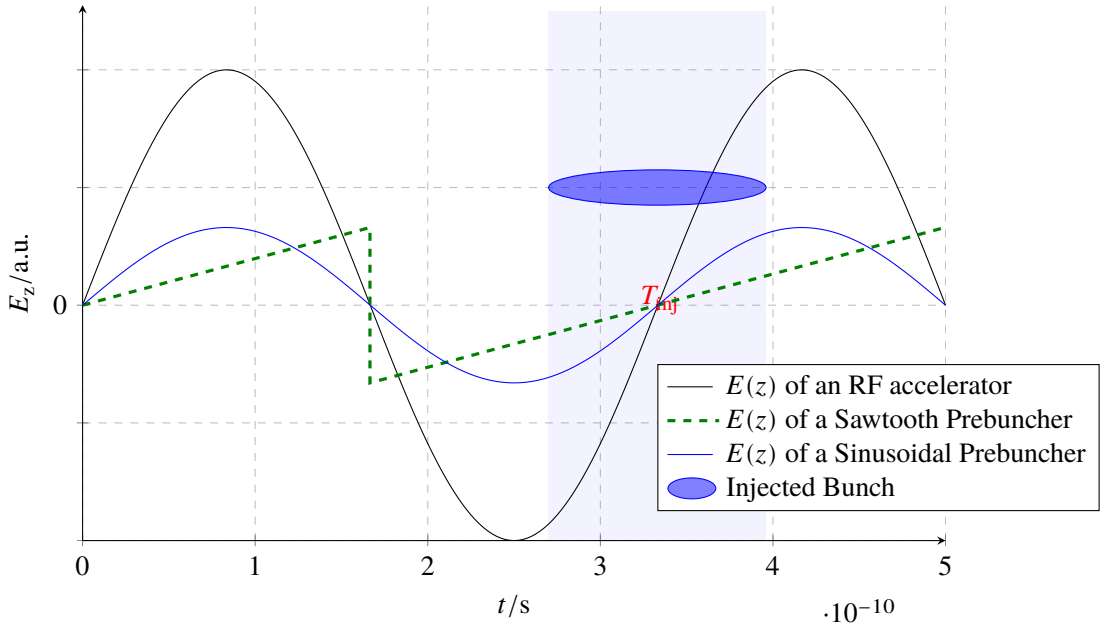

Figure 2.7: The evolution of E_z over time for an RF accelerator is compared to the one of a prebuncher. Prebunchers are used to give incoming pulses the required microstructure. Ideally E_z of the prebuncher cavity would be describable by an sawtooth function. This idealized case is shown as a dashed line. Practically only sinusoidal energy modulations are available.

Chopper

A buncher compresses the particle density into the phase acceptance of an RF accelerator. Another way to achieve bunching is to discard all particles which are outside of the phase acceptance of the accelerator. This process is called chopping, the principle is depicted in Figure 2.8. Inside a cavity, a continuous beam is deflected periodically in the transversal plane. Only particles with no transverse deflection can pass the aperture. Therefore, the beam is chopped into several short bunches. The length of this bunches depend on the width of the aperture as well as the amplitude and frequency of the transverse deflection. The major disadvantage of this method - and the reason it is not used in ELSA - is the poor transfer efficiency, as all particles outside the phase acceptance of the Linac are discarded.

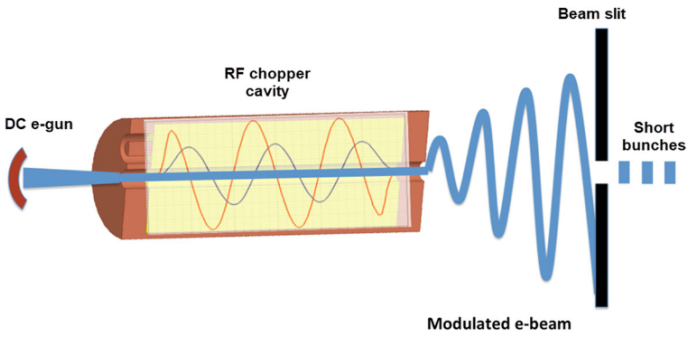

Figure 2.8: The principle of a chopper is depicted [9].

CHAPTER 3

Current Status of the Electron Gun at LINAC2

After the theoretical introduction to the topic, it is now possible to take a look at the current gun assembly and its performance.
LINAC2 was previously built and operated at the University of Mainz and later transferred to ELSA, where it became operational in 2000. It was originally intended to be used only in combination with the 50 keV source for polarised electrons, which was completed around the same time.
However, reliability problems with LINAC1 led to these plans being abandoned and LINAC2 being prepared for operation with non-polarised electrons. For this reason, LINAC2 was also equipped with a thermal source. The original electron gun built in 1975 for the Mainz accelerator was used for this purpose.
To allow operation with two sources, an alpha magnet is used as a beam switch. The pre-buncher cavity - originally located at the gun output - is therefore not used for the LINAC2 operation, instead a cavity was installed in vicinity of the Linac input.

3.1 Operational Status

As mentioned the Linac and the current gun were constructed at the University of Mainz and later installed at the ELSA facility. Nevertheless they are already more than twenty years in operation at the facility. In the last years a worsening vacuum performance was observed. Especially the vacuum quality in the beam pipe connecting the two electron sources to the Linac decreased drastically. The vacuum quality inside the gun is still acceptable at the moment, but a negative influence of the beam pipes vacuum can be observed. Therefore a complete replacement of this beam line section is necessary. The gun assembly itself also shows increasing signs of ageing, especially the holder of the cathode exhibits damages, which leads to the assumption, that after the next cathode replacement the lifetime of the gun will end with the lifetime of the cathode. Therefore the remaining lifetime of the current gun is estimated to be two and a half to three years.
A negative consequence of the deteriorated vacuum quality in the beam pipe is that the analysis structures installed there had to be replaced by additional vacuum pumps. This results in a loss of critical diagnostics between the current electron source and the Linac, preventing experimental determination of the current gun's properties. Therefore this investigations have to be based on simulations. The gun model underlying these simulations is developed based on original technical drawings available.

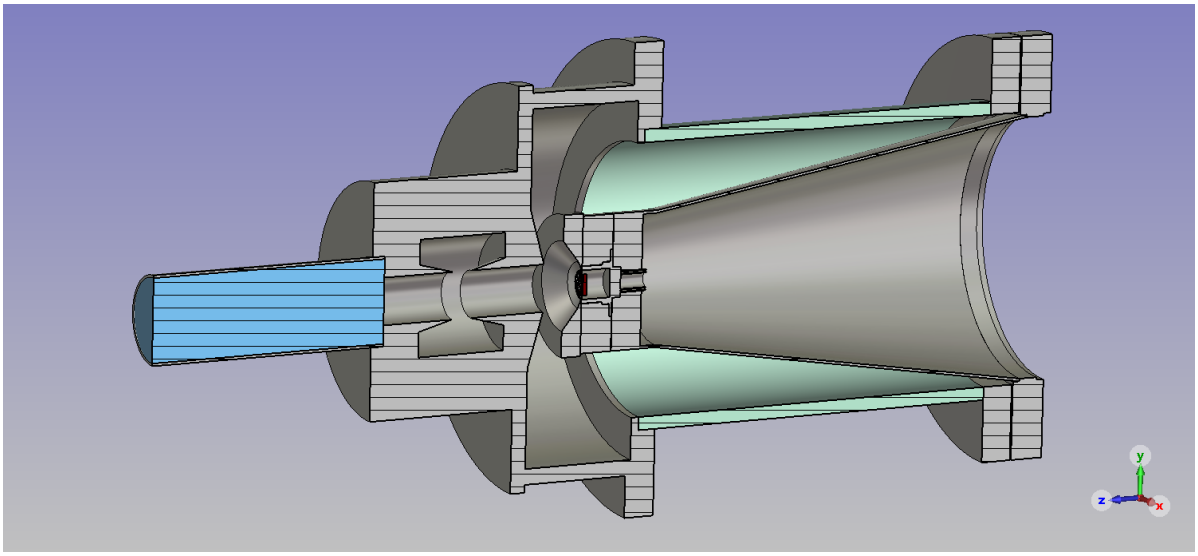

Figure 3.1: Three dimensional model of the current electron gun in CST [11]. Used for simulating the beam behaviour in the gun to determine the beam characteristics.

3.2 Structure of the Current Electron Gun

Currently in use is a thermionic triode electron gun using a static electric field for acceleration. The gun is designed with a pierce geometry. The cathode used is a dispenser cathode, made out of tungsten and impregnated with caesium. The cathode is of the type Y646-B made by Varian Eimac[10]. The specifications of the gun are given in table 3.1.

Cathode Area	Flange Size	Grid			Emission Current	Filament	
		D_{GC}	$\varnothing_{wire}$	d_{wire}		Current	Voltage
0.5 cm^2	2 3/4″	150 µm	25.4 µm	150 µm	0.75 A	1.4 A	6 V

Table 3.1: The specifications of the Varian Eimac thermionic dispenser cathode used in the current electron gun [10]. Where D_{GC} is the distance between the surface of the cathode material and the grid, $\varnothing_{wire}$ is the diameter of a single grid wire and d_{wire} is the distance between two adjacent grid wires.

The only source regarding the actual design of the gun is a technical drawing dated from 1975. With regard to the beam properties, there are different statements, some of which are contradictory. In addition to the properties of the cathode already mentioned, the beam energy of approx. 48.7 keV and the pulse length of 1 µs are certain. Therefore, before starting to plan the new gun, the characteristics of the current setup should be determined. This is done by performing simulations with the program CST [11]. These simulations are described in more detail in the following section.
Based on the available technical drawing a three dimensional model was set up. This model features the basic geometry of the gun including the cathode assembly and the grid. The model is depicted in Figure 3.1.
On the right one can see the high-voltage cone which is connected to the insulator (depicted in green) via a vacuum flange. At the end of the high-voltage cone the cathode is mounted, surrounded by a component that introduces the pierce angle into the geometry of the gun. The insulator is necessary to separate the potential

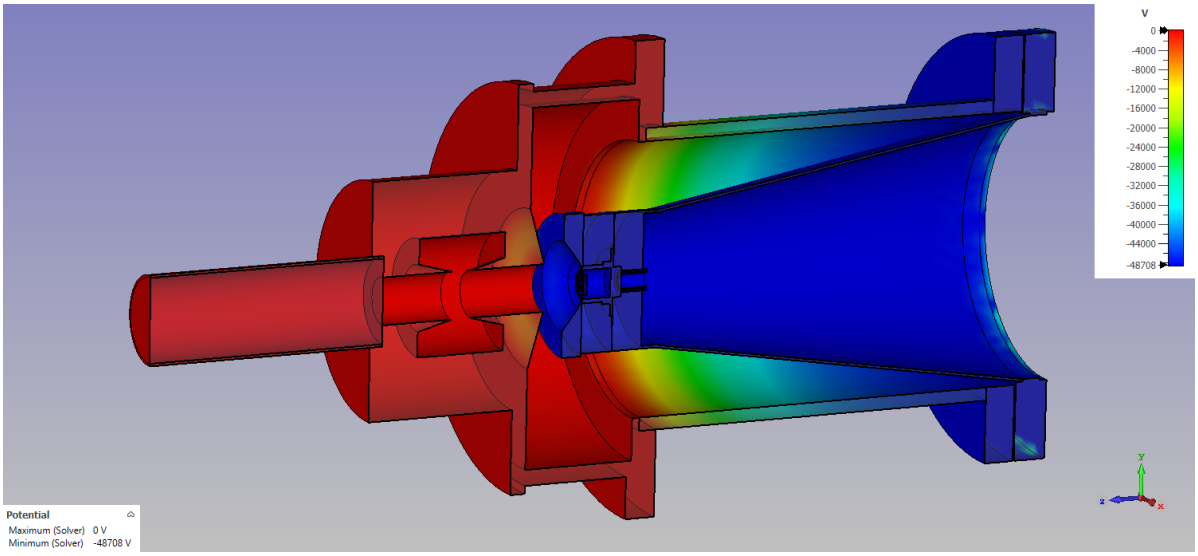

Figure 3.2: The electric potentials inside the current electron gun are depicted. The simulation was performed using CST [11].

of the high voltage cone from the potential of the anode. The high-voltage cone and the cathode housing as well as the component responsible for the pierce geometry are on a potential of approx. −50 kV, where as the anode is on ground potential. The potential of the grid is influenced by a special pulser electronic, which is typically inserted right into the high-voltage cone.
On the left of the model one can see the anode, which is connected to the other end of the insulator. Important for the pierce geometry is also the conical design of the centre of the anode. The electrons leave the assembly through the hole in the anode.
In this model one can see the pre-bunching cavity right behind the anode exit, which is not used at ELSA. Connected to the cavity is a beam pipe, to extend the scope of the simulation behind the gun exit.

3.3 Simulation of Beam Parameters

For the simulation of an electron gun CST offers several possible solvers dependent on which problem one try to examine. In the following the electrostatic and the particle-tracking solver are used.
The electrostatic solver allows to simulate the electric potentials inside the gun. The particle-tracking solver takes electric and magnetic fields into account and tracks the movement of particles through this fields. This solver offers a special algorithm for the simulation of particle guns. The algorithm tracks the particles iteratively several times, taking into account the influence of the space charge on electric fields as well as the electrodynamic effects of the electron current.
Using the electromagnetic solver one can simulate the electric potentials and fields in the gun, the output of the solver is shown in Figure 3.2. One can see, that the whole high-voltage is on the grid potential of −48 650 kV, the cathode is on a even lower potential of −48 708 kV. The potential decreases over the insulator towards the anode, which is on ground potential.
This simulation was performed to verify that the model and the definition of the potentials are correct. After this simulation provided the desired confirmation, simulation of the beam in the gun began. The already

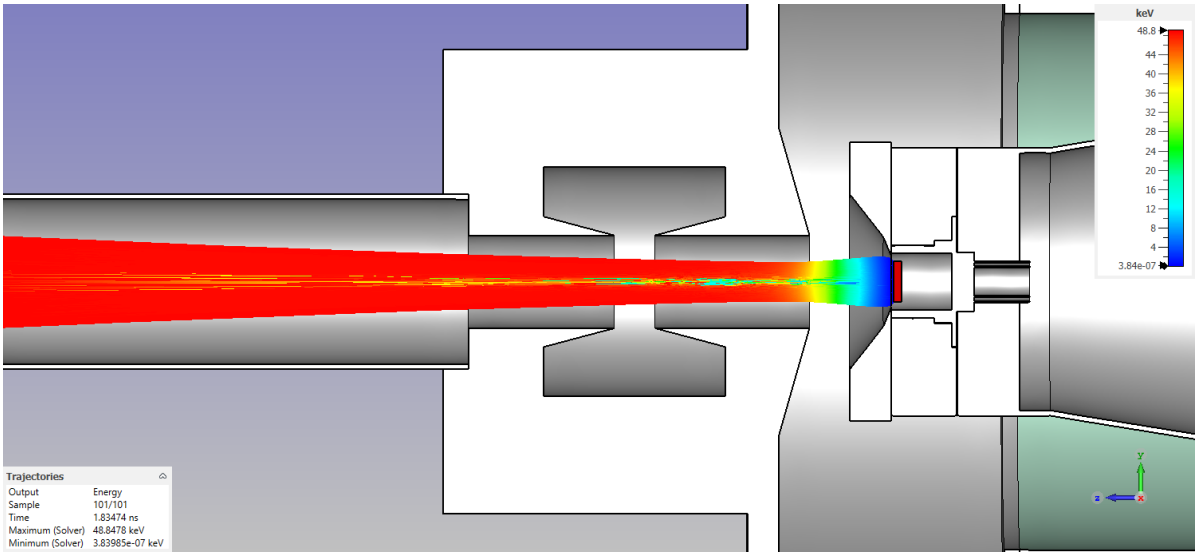

Figure 3.3: Depicted is a cut along the zy-plane. The trajectories of electrons leaving the cathode is shown. The acceleration takes place inside the cathode-anode gap.

mentioned particle-tracking solver was used for this. Once the individual particle paths are simulated, it is possible to calculate the width of the beam in $x-$ and $z-$axis and the transverse emittances ϵ_x and ϵ_z, also the energy dispersion can be analysed.

In Figure 3.3 one can see the individual particles paths, the colour of the paths denotes the energy of the particles at this point. One can observe the acceleration and focussing of the electron beam inside the cathode-anode gap. The focussing is due to the pierce-geometry of the gun.

A simulation artefact can be seen in these trajectories. Some of the electrons in the centre of the beam are tagged with a lower energy, which could be observed in any CST simulation. There is no physical explanation for this effect. It is unclear where this artefact originates from. However, it has been verified that the lower energy is only assigned to a very small fraction of the electrons.

In CST so-called particle monitors are defined, which tracks all particles at a specific position along the s-axis. If multiple of those monitors are defined along the particle paths it is possible to analyse beam properties, such as the emittance, the emission current or the beam envelope.

In Figure 3.4 one can see the clear decrease of the emittance in the acceleration gap, which is an indicator of the focussing. The increase of the emittance in the drift section of the gun is due to space charge, which have a broadening effect on the beam. The transversal emittances at the gun exit are determined to be:

$$\epsilon_x = 8.4\,\text{mm mrad} \quad \epsilon_z = 8.3\,\text{mm mrad}$$

The difference between the analysed emittances is a consequence of the grid in front of the cathode. All other parts of the gun are rotationally symmetric. This symmetry is broken by the grid. An axial symmetry is not valid either, because the grid itself is not necessarily symmetrical. The meshing of the simulated volume, which must not perfectly match the structure of the grid, is another reason why the axial symmetry can be broken.

The analysis of the beam divergence allows further understanding of the focussing happening inside the acceleration gap. In Figure 3.5 it is visible that the beam is initially divergent until it has passed the grid.

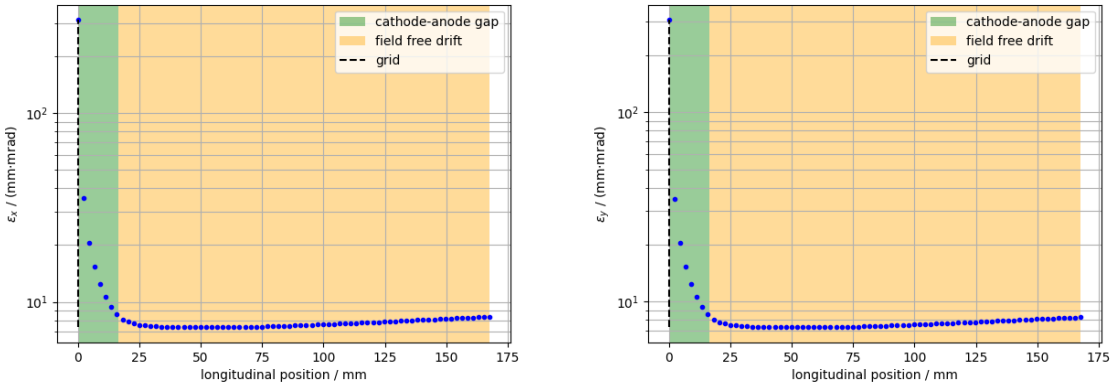

Figure 3.4: Horizontal and vertical emittance in the current electron gun, based on the simulation utilizing CST. One can see a strong decrease in the acceleration gap between anode and cathode and a slow rise in the following drift section - due to space charge and the absence of focussing magnetic fields.

Inside the acceleration gap, the focussing leads to a strongly convergent beam. Towards the end of the acceleration gap as the focussing (transversal) component of the electric field decreases, the convergence decreases as well. Behind the anode the beam starts to diverge again, which is also due to space charge effects and the absence of focussing fields. This could be compensated for by a solenoid magnet, which is typically mounted right behind the gun exit in most electron gun assemblies. In the current assembly there is also a solenoid in the vicinity of the gun exit. Those effects onto the focussing of the electron beam can also directly be seen, if one analyse the beam envelope - this can be seen in Figure 3.6. The beam envelope at the gun exit is roughly 9 mm wide. The radius of the anode aperture and the aperture inside the pre-bunching cavity is also 9 mm. The aperture of the beamline is slightly wider in the assembly. As the aperture is almost equal to the envelope, the risk of particle loss at the aperture is obvious, making the envelope a critical parameter.
The electron current inside the gun can also be analysed and the transfer efficiency η_I, defined as:

$$\eta_\mathrm{I} = \frac{I(z)}{I_\mathrm{emitt}}, \tag{3.1}$$

where I_emitt is the total emitted current by the cathode, can be estimated. From this it can be deduced where electrons are lost within the gun and thus concluded how well the gun is adjusted.
In Figure 3.7 the transfer efficiency for the current gun design is depicted. One can see that approximately 15 % of the emitted electrons are lost at the grid, which is characteristic for a triode electron gun. After the grid no further loss of electrons is identifiable. As mentioned earlier, the installation of an solenoid magnet at the gun exit can compensate for further beam loss due to aperture limitations.

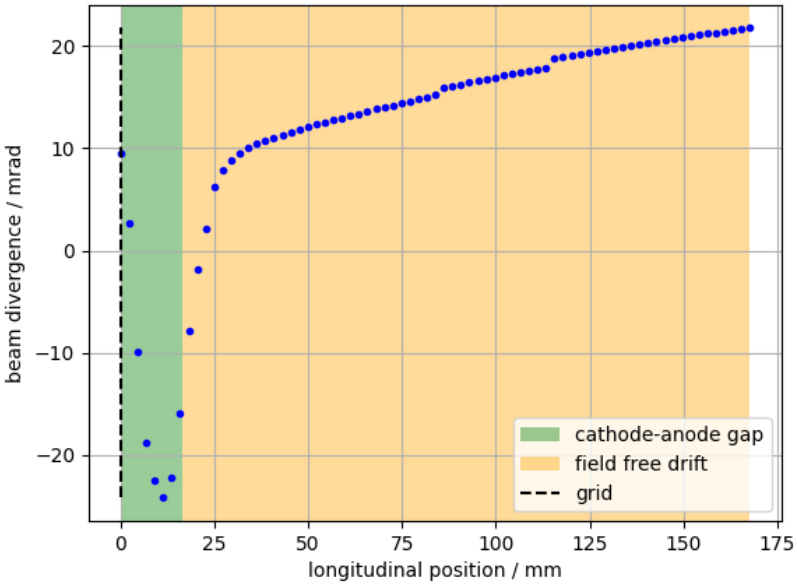

Figure 3.5: Beam divergence angle in the current electron gun as a function of the distance travelled from the cathode, based on the simulation utilizing CST. One can see that the initially divergent beam becomes convergent in the acceleration gap. Towards the end of the gap the convergence starts to decrease and behind the anode the beam diverges again.

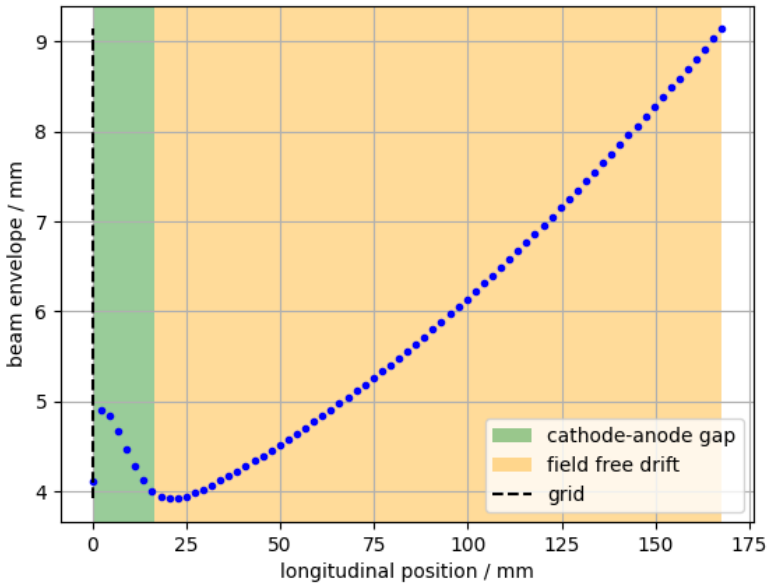

Figure 3.6: Beam envelope in the current electron gun, based on the simulation utilizing CST. The beam waist is actually located behind the anode. At gun exit the beam envelope is roughly 9 mm.

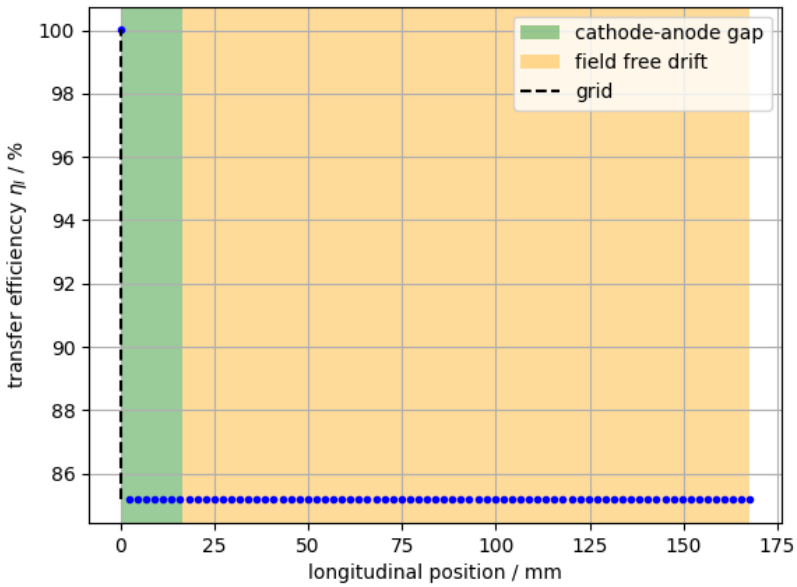

Figure 3.7: The simulated transfer efficiency along the *s*-axis (direction of motion) in the current gun.

CHAPTER 4

Suitable Electron Gun Types for LINAC2

Based on the analysis of the current gun (see Chapter 3) it is possible to define design goals, which the new gun assembly should fulfil. The justification and derivation of these goals will take place in this chapter. Furthermore these goals will be used to filter the large number of possible types of electron guns and to identify and select a suitable type for LINAC2.

4.1 Design Goals

The simulations presented in the previous chapter enable us, to quantify the behaviour of the current electron gun. Since the behaviour was not investigated experimentally before and cannot be investigated in the current assembly, this was the only possibility to achieve this knowledge. The beam properties found via the simulations should act as a guide for the new gun assembly.

4.1.1 Basic Properties

Some properties have dedicated goals that are fixed and cannot or should not be changed. For example the maximum extracted current is set to 2 A, this was also the goal in the redesign of LINAC1 [4, 12]. Looking into Table 3.1 one can also see, that this means, that a new dispenser cathode must be found, which can be used in the new gun, to fulfil this requirement. The electron energy and therefore the potential difference in the gun is also fixed to match the expected input energy of the travelling wave Linac, which is equipped with a so-called $\beta < 1$ section, which is used to match the phase velocity v_{ph} of the travelling wave to the velocity of the particle v_{particle}. Since for electrons in the energy range of 50 keV v_{particle} still varies significantly with the kinetic energy of the particles, the acceptance of the Linac depends strongly on the input energy. Besides the design energy of the electron gun to be fixed to the corresponding value of the Linac of 48.5 keV, the ability to vary the accelerating voltage by a small amount is a way to optimize the transfer efficiency through the Linac.
As described in the introduction, two operation modes are to be implemented that differ in the length of the electron pulses; these modes and their requirements are briefly described below.

Property	Value
acceleration voltage	48.5 kV
extraction current	2 A
pulse length (multi bunch mode)	1 µs
pulse length (single bunch mode)	≈ 70 ps
transverse emittance	≤ 8.3 mm mrad
divergence	≤ 22 mrad
beam envelope	≤ 8 mm

Table 4.1: The required parameters for the new electron gun. Those design goals are chosen to match or improve the beam quality of the old gun and to be suitable for single and multi-bunch operation mode.

Multi-Bunch Mode

The multi-bunch mode or long-pulse mode is characterised by electron pulses with a length of 1 µs. These pulses are transformed into a bunch train conforming to the 3 GHz structure of LINAC2 by a prebuncher. As described in Section 2.3.1, the bunching results in a significant loss of particles. To achieve a current of 2 A at the gun exit (within a bunch), bunch charges of 2 µC are needed. This mode represents the standard operating mode on the injector, as already described in the introduction.

Single-Bunch Mode

The aim of the single-bunch mode is to fill individual buckets in the 3 GHz structure of the linear accelerator. Since the phase acceptance of linear accelerators is very small, bunch lengths of 1 to 2 ps would be required for this. However, as described in Section 2.3.1, the prebuncher can also be used to compress a bunch. The exact phase acceptance of the prebuncher can be calculated – such a calculation can be found for LINAC1 in [4] - in this work the length of the still compressible bunch was estimated at 70 ps [13]. With this bunch length an almost loss-free insertion in the Linac in ensured, which improves the overall transfer efficiency significantly.

4.1.2 Technical Specifications and Performance Metrics

In Section 3.3 the beam emittance in both transverse directions, the beam divergence and the transfer efficiency were presented. The emittance of the electron beam after the linear accelerator is not dependent on the emittance before the linear accelerator, therefore an improvement of the emittance is not required. The beam divergence at gun exit was found to be around 22 mrad, this amount of collimation should be also achieved with the new assembly to ease the handling of the beam in the subsequent beamline. For the new gun the design goal should be to achieve a beam envelope which is smaller than 8 mm to ensure some safety margin to the aperture - which has a radius of 9 mm - to prevent particle loss.
Based on the desired operating modes and on the analysis of the current electron gun, various requirements for the new design were identified in the previous sections. In order to later simplify the comparison with these design goals, these requirements are summarized below in Table 4.1. For the divergence, the beam envelope and the transverse emittance only upper limits are defined. This is due to the fact that smaller values of those properties correspond to a better focussing of the electron beam. Nevertheless those three properties should act as performance metrics, if it is possible to optimize them without too much complications in

other areas it should be strived for. One property which was analysed for the existing electron gun, which is not shown in Table 4.1, is the transfer efficiency. In the existing setup one could see that this is mostly dependent on the characteristics of the grid - as long as the focussing inside the gun is sufficient. Since the characteristics of the grid are specific on the cathode model it was decided to not include this property to the design goals and rather add the *effective* extraction current - not the current extracted from the cathode, but the current leaving the gun. Nevertheless as described in Section 3.3 the transfer efficiency is an important performance metric and therefore it should maximized at the gun exit.

4.2 Overview of Electron Gun Types

A multitude of different types of electron guns is known and available. It is therefore crucial to carry out an evaluation of the individual methods with regard to their usability at LINAC2. In the following the different types of electron guns are shown, explained and rated.

4.2.1 Method of Acceleration

A possibility to categorize all this different methods is to differentiate based on the method of accelerating the electron beam. This can be achieved by a static electric field or using a normal- or superconducting RF-Cavity.

Static Electric Field

The acceleration inside a static electric field is the easiest technical achievable sort method of acceleration, since no timing is required for the high-voltage generating the field. The maximal achievable energy inside the static field is limited to a acceleration gradient of several keV cm^{-1} due to the risk of a vacuum breakdown. A higher acceleration gradient has a positive influence on the emittance of the electron beam. In the energy regime of 50 keV, which is used at LINAC2, this method could be used.

Alternating Electric Field (RF)

Acceleration inside an alternating electric field yields the opportunity, that higher acceleration gradient can be achieved, which has a positive influence on the emittance as mentioned in Section 4.2.1. According to [14] field gradients of roughly 20 $\mathrm{MV\,m}^{-1}$ and acceleration voltages of $\approx$ 500 kV are necessary for this effect to be influential - the latter is already well above the required energy at LINAC2. Another advantage of this method is that no pre-bunching in front of the Linac is needed, which simplifies the injector setup. However, the complexity of the system is increased since the phases of the field in the electron gun and in the Linac have to be synchronized.

Normal Conducting Normal conducting cavities are operated at room temperature and thus do not need a complex cooling system. The supply of the cavity with sufficient RF-power on the other hand requires additional infrastructure compared to the method using a static electric field. Typical beam energies of normal conducting RF guns are in the magnitude of several MeV (comp. [15, 16]), there are also electron guns with lower energy of a couple of hundred keV [17], which is still an order of magnitude greater than the required beam energy at LINAC2.

Super Conducting Super conducting RF-cavities offer the benefit of even higher achievable field gradients and beam energies. The typical energy range for this kind of electron guns is in the order of several MeV and above. In terms of the infrastructure in place at ELSA, this would be rather a replacement of LINAC2 than the gun. However, this is not feasible as LINAC2 is still required for operation in combination with the polarised electron source. Furthermore, it would likely not be possible to set up and operate the required cooling infrastructure at LINAC2.

4.2.2 Type of Cathode

Another way to categorise the variety of electron guns is by the type of cathode used in the assembly.

Thermionic Cathodes

For thermionic cathodes a material with a low work function is used. The material is heated by a heating filament, such that the electrons leave the surface of the cathode due to the thermionic excitation. Typical materials used for this kind of cathode are tungsten compounds. In modern thermionic cathodes so-called dispenser cathodes are used [18–20]. This cathodes consist out of a "metal sponge" (e.g. tungsten), which is doped with an active material, which provides additional electrons. Through the heating of the cathode the active material is repeatedly spread over the cathode surface, which extends its lifetime. Additionally, it is also possible to heat the surface by a laser [21, 22] or by electron bombardment [12].
Achievable beam currents are dependent on the area of the cathode and the desired lifetime and can be in the order of several ampere. The use of cathodes with a greater surface area leads on the other hand to a larger emittance of the electron beam [12]. Possible beam energies are dependent on the method of acceleration which is combined with this cathode. The beam emittance is furthermore influenced by the design (diode, triode), method of acceleration and the cathode used [23].

Photo-cathodes

Photo-cathodes are based on the photoelectric effect. By the radiation with a laser electrons are excited and leave the cathode surface. Wavelength and power of the laser are dependent on the used photo-cathode. The cathodes are typically divided into metal cathodes and semiconductor cathodes. Former exhibit a longer lifetime and lower demands on the quality of the vacuum. The latter achieve significantly higher quantum efficiency (number of emitted electrons per laser photon), but they also have a significantly shorter lifetime and high demands on the quality of the vacuum [24]. The lifetime of some photo-cathodes is measured in hours of beam time, strongly dependent on the emission current, which is achieved during operation. While the number of low energetic photo-cathode based electron guns is rather small, the 50 keV source for polarized electrons already at LINAC2 [25–29] is exactly such a gun. The reason for the small number of low energetic photoemitter electron guns, is that the advantage in terms of emittance of the photo-cathode is (partially) compensated by the low field gradients and beam energies of low energetic electron guns.

Plasma Cathodes

For this type of cathodes hydrogen gas is injected and split into protons and electrons by a high electric field. The electrons are then accelerated by a static electric field towards the following accelerator structure, the protons are dumped on the opposite site. Depending on the required electron current, the beam dump must be additionally cooled. Because of the non negligible initial momentum of the electrons inside the gas,

the expected emittance and energy dispersion are larger than for other types of cathodes. Such a cathode deteriorates the vacuum significantly and therefore introduce higher demands on the surrounding vacuum pumps. The achievable emittances and also the degradation of the vacuum argue against the use of such a cathode at LINAC2.

Field-emission Cathodes

This kind of cathode is mainly used for electron microscopy, but is being researched as an alternative to photo-injectors at FELs. On sharp edges and points electrons are emitted by applying a very strong electric field. The emission current of a single tip is in the magnitude of µA, for the use with higher emission currents there are arrays with multiple tips available [30]. Publications regarding cathodes with a total emission current of roughly 1 A are not to be found. The needed field gradients of $10^7 - 10^{10}\,\mathrm{V\,m^{-1}}$ are also very challenging to obtain.

Secondary Emission

There are materials, which emit electrons when bombarded with electrons initially and thereby amplify the electron current. An electron gun utilizing this concept consists of two electron sources. The first electron gun can only have a low electron current density, since the material of the second source amplifies the electron current. The achievable emittance of this type of electron guns is worse compared to photo-cathodes or thermionic cathodes, since the initial direction of motion of the secondary electrons can not be restricted and thus the angular dispersion is comparably high. The initial source can also be ion source [31]. The advantage of this method is the moderate vacuum demands even compared to thermionic cathodes [31].

Mixed Forms

Additionally to the already described “classic” methods of electron emission there are mixed forms or special implementations, which try to combine the advantages of different methods of emission or to use a method in a new way.

Photo-emission off Dispenser Cathodes As described in Section 4.2.2 the lifetime of semiconductor photocathodes is often short and the demand on the vacuum quality is relatively high. Hence the search for a more durable and robust alternative is an important field in the development of photoinjectors. Dispenser cathodes are used - as described in Section 4.2.2 - as thermionic electron sources and are known to be durable and robust. Theoretical and experimental investigations regarding the usage of dispenser cathodes as photo-cathodes are available from the universities of Maryland and Paris-Sud and other research groups [32–36]. Most of the approaches are based on the heating of the cathode material to a point were thermionic emission is suppressed. The remaining energy required to release electrons out of the materials is applied by a laser utilizing the photoelectric effect. This method is also called thermally assisted photo-emission (TAPE). A further advantage of this method is that through heating of the cathode the surface properties can be enhanced during operation and by intense heating the original quantum efficiency can be restored to a large extent after a long period of use. Furthermore the wavelength of the laser can be varied by adjusting the operating temperature.
Furthermore this type of cathode usage enables the possibility to operate the electron source in different modes: a pure thermionic mode and a TAPE mode. Hereby longer lifetimes - when used as a thermionic

source in normal operation - and the needed properties for a single-bunch or a multi-pulse mode can be achieved.
Experimental research was carried out at the Stanford Synchrotron Radiation Laboratory (SSRL) [37, 38] and the MAX-lab facility [39, 40], which successfully operated a TAPE-type gun.

Self-bunching/Microbunch Electron Guns Another special type of an electron gun is the so-called micro-bunch electron gun (or self-bunching electron gun) which use the effect of multipacting to emit bunched pulses of electrons. The central component of such an electron gun is a RF-cavity in which a grid is built-in as a anode, the cathode is made out of a material, which emits secondary electrons under electron bombardment. Primary emitted electrons are accelerated toward the anode, some of them leave the cavity through the grid. The remaining electrons are accelerated towards the cathode and release secondary electrons there. The secondary electrons are again accelerated towards the anode. Through this process the so-called micro-bunches are generated, since electrons accumulate in a specific RF bucket. Descriptions of this method can be found in [41–47].

4.3 Selecting an Electron Gun Type for LINAC2

In Section 4.2.1 the different methods of acceleration usable in a electron gun were presented. The acceleration in RF-fields needs infrastructure, which is difficult to install and operate at the current location. Furthermore the typical beam energies for this type of guns is significantly higher than the 50 keV, which are needed at LINAC2. As a result, only the acceleration in a static electric field seems reasonable.
At the moment a thermionic dispenser cathode is used at LINAC2, this emission method can be used for different applications with different demands and is known to be durable and comparably simple. The requirements placed on the electron source at LINAC2 can be met by a triode structure with a grid. The usage of the gun for a single-bunch mode make higher demands on the pulsing electronics as described for LINAC1 in [12]. The source of polarized electrons at LINAC2 is a photo-cathode based source, this method allows a lot of freedom regarding the bunching of the electron beam, since this can be implemented via the laser system. Using a pulsed laser to create a pulsed electron beams leads to the need for an exact timing of the laser system and linear accelerator's RF system.
As described in Section 4.2.2 the lifetime of modern and particularly efficient photocathodes is very low. Because of that the use of dispenser cathodes as photocathodes seems to be satisfying. By using the TAPE-effect significantly higher lifetimes are possible to achieve with acceptable quantum efficiency at the same time. A more in depth examination of this operation mode is performed in the following chapter. Furthermore it would be interesting to use a electron gun with a dispenser cathode both as thermionic as well as photo source. However, the use as a purely thermal cathode would necessitate a triode structure. In the following it would be necessary to examine the influence of the grid on the laser beam or alternatively the usability of a wehnelt cylinder as a control electrode.
An electron gun for LINAC2 based on plasma, field emission or secondary emission cathode fails because of the required emission current or the desired emittance.
Micro-bunch electron guns are described since the beginning of the 1990s. Publications covering the use of such an electron gun as a productive injector for an electron accelerator were not to be found. Furthermore the lifetime of such an gun is not only limited by the lifetime of the cathode but also by the lifetime of the RF cavity, since secondary electrons are also released from the inside of the cavity, which leads to wear of the cavity. This makes this type of gun a costly - when the lifetime of the cavity is reached - and not entirely proven alternative.

As a result of this investigation, the new gun is to be planned based on a thermionic dispenser cathode and using a static electric field. The single-bunch mode is to be implemented by using the cathode as a photocathode (TAPE effect). The aim is to implement this source in a hybrid structure. This approach envisages using the cathode as a thermal source with normal heating power in normal operation, and reducing the heating power for special applications that require the use of the single-bunch mode, operating the cathode using the TAPE operation mode and a suitable laser system. In the following chapter a deeper examination of this operation mode is presented, to show if the hybrid usage is feasible and if a switch of the operation modes is possible without the need of hardware replacements. Should this turn out to be unfeasible in the future, the single-bunch mode can also be implemented in a purely thermionic mode using special pulser electronics, as has already been accomplished with the LINAC1.

CHAPTER 5

Thermionic Dispenser Cathode as Photoemitter

In the previous chapter, different types of electron guns were described as well as the TAPE operation mode. It was also identified as a possible candidate for the implementation of the single-bunch operation mode. In this chapter, the previous experimental work of the groups at SSRL [38] and MAX-lab [39, 40] is analysed in more detail in order to characterise the operation mode more precisely and to find requirements for this mode of operation according to the facility needs. In the further course, it will be clarified what consideration have to be made for such an electron gun and whether the concept of combining them into a hybrid gun is feasible. Afterwards, first considerations will be presented on how this setup can be integrated into the existing infrastructure.

5.1 Analysis of Past Research on Photoemission off Thermionic Dispenser Cathodes

In the previously mentioned papers initial experimental analysis was done to analyse the TAPE operation mode using dispenser cathodes. Both experiments were carried out using a barium oxide impregnated tungsten dispenser cathode embedded in a RF gun structure. The lasers used provide pulses in the picosecond range (SSRL: 2 ps, MAX-lab: 9 ps). This is necessary since they operate there cathode already inside an RF cavity. To match the phase acceptance of the gun cavity such short pulses are used to prevent problems due to back-bombardment. In both experiments lasers with a wavelength of 263 nm were used. However the group at SSRL performed a test to measure the quantum efficiency (QE, emitted power in form of electrons per incident laser power) in dependency of the wavelength. For this they used a Xenon arc lamp and a monochromator. Results of this experiment are shown in Figure 5.1.
They performed this measurement both for a heated as well as an unheated dispenser cathode. For wavelengths shorter than 250 nm the QE are almost similar in both cases, but for longer wavelengths of 350 to 500 nm the quantum efficiency of the heated cathode (using TAPE effect) is significantly higher. This is very promising as it indicates that the use of a dispenser cathode in TAPE mode with a laser with a wavelength in the blue or green spectral range is efficient. This will facilitate the design as these wavelengths have significantly smaller demands on e.g. vacuum windows and such devices also typically have longer lifetimes when using these wavelengths. In this spectral region the QE of a heated dispenser cathode is constant - according to their measurements - and around QE = $2 \cdot 10^{-4}$. The quantum efficiency would be even higher in the ultraviolet range. However, this places additional requirements on the vacuum windows, for example. The

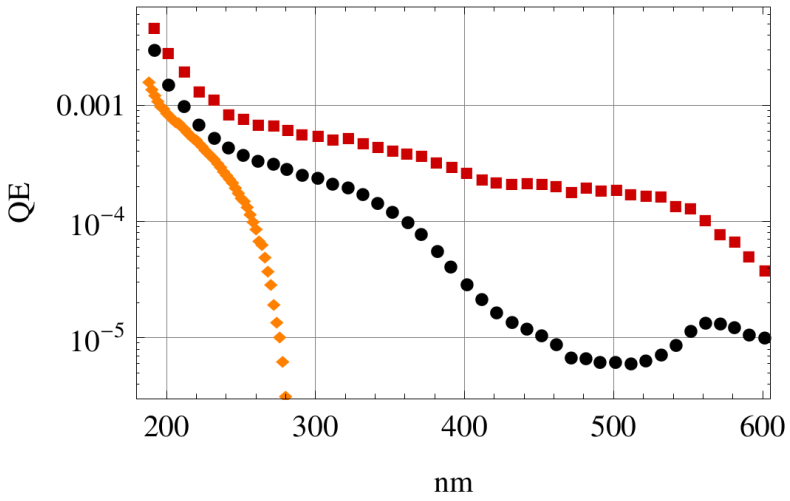

Figure 5.1: Measurement of the quantum efficiency of both an unheated (black circles) and heated (red squares) dispenser cathode in dependency of the incident wavelength. These measurements were taken at the gun test stand at SSRL. For reference the quantum efficiency of a copper cathode is shown. [38]

choice of wavelength is therefore a compromise between the higher extraction charges achievable and the higher demands on the installed components and their shorter lifespan.
Regarding the achievable pulse charges both experiments measured this in dependence of the incident laser peak energy. This can be seen in Figure 5.2. In both experiments a striking space-charge effect could be observed. This is due to initially extracted electrons, which are shielding the accelerating field from the following electrons. Since the charge is measured outside the gun, those later electrons will not be measured, as they are not accelerated through the gun. The position of the effect deviates between both experiments, this is because the space-charge effects are influenced by the geometrics and available field-gradient, rather than the emission process. MAX-lab estimates the quantum efficiency for their setup to be QE = $1.1 \cdot 10^{-4}$ for the energy range without saturation, SSRL has calculated QE = $(7.4 \pm 0.8) \cdot 10^{-4}$ at very low energies (1.8 µJ).
In order to place the conditions of the presented investigations in relation to the intended use, some differences should be highlighted. The gun setup differs from our planned setup in two respects. Both guns use an RF structure for acceleration, which could have an influence on the emittance depending on the field gradients reached, but a different emittance can be assumed due to the different geometry. The investigations at MAX-lab suggest emittances in the order of 5 mm mrad, which is suitable for the requirements of use at LINAC2. The other difference is in the cathode used: whereas we have used cesium-impregnated dispenser cathodes so far, both experiments used barium-impregnated cathodes. In thermal mode, these cathode types behave almost identically. It is not yet known whether there are differences in quantum efficiency, but since the energetic properties of both types of cathode are similar, it is assumed that any differences are not significant. Regarding pulse length, it should be noted that our target pulse length of 70 ps is longer than the pulses used in the experiments. However, this should not affect the behaviour of the cathodes.

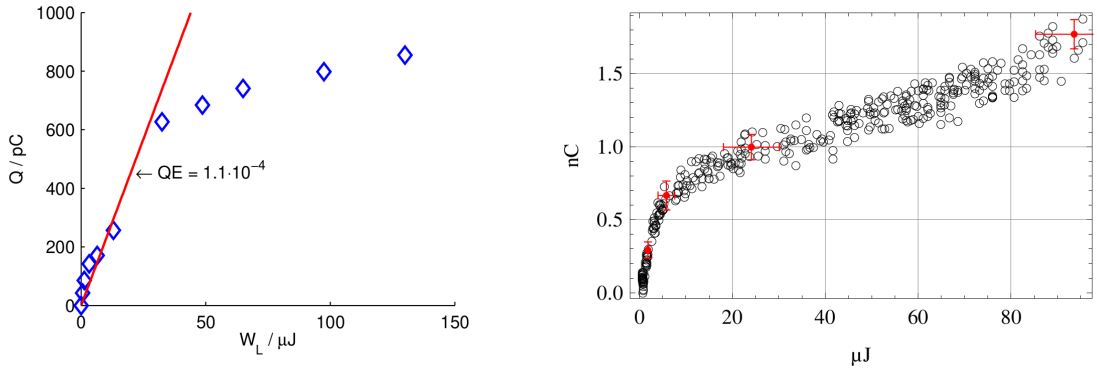

(a) MAX-lab [39]

(b) SSRL [38]

Figure 5.2: Both experiments measured the pulse charge Q in dependency of the pulse-energy of the incident laser beam. Both experiments experienced saturation for higher laser energies, which they explained as space charge effects (shielding of the extracting field by initially extracted electrons). However the laser energy from which the effect can be observed is different for both experiments.

5.2 Preliminary Laser System Properties

From the previous experimental work some preliminary laser design parameters can be concluded. This should act as a guide for the setup of a laser system at ELSA. Since there is at the moment only few experiences with the operation of dispenser cathodes in the TAPE mode of operation, it is likely that minor deviations from the properties described in the previous section will be observed, thus altering the necessary laser requirements. To what extent and how exactly these results will correspond to the behaviour of the cathode used in the setup at LINAC2 is to be tested experimentally, when the gun is operational. However, the presented properties are suitable as an orientation to check how realistic and sensible the implementation of this operation mode is. Using the experimentally found quantum efficiency one can obtain the laser power and pulse energy needed, to match our demands regarding the extraction currents. For this one need to take a look at the formula of the quantum efficiency, which is given, for example, in [48]:

$$QE = \frac{1}{e} \cdot \frac{I \cdot E_{\text{photon}}}{P_{\text{laser}}}$$
$$\Leftrightarrow P_{\text{laser}} = \frac{1}{e} \cdot \frac{I \cdot E_{\text{photon}}}{QE} = \frac{1}{e} \cdot \frac{I \cdot hc}{QE \cdot \lambda} \tag{5.1}$$

We will use 400 nm as a lower wavelength limit. This consideration is based on the additional problems regarding vacuum windows, when operating below $\lambda = 400\,\text{nm}$. The advantage in regard to the higher QE is rather small and does not justify the additional complications. A typical wavelength around 500 nm results from a frequency doubled Nd:YAG laser with a wavelength of $\lambda = 532\,\text{nm}$, which will be our upper limit. With $I = 2\,\text{A}$ and $QE \approx 2 \cdot 10^{-4}$ from the SSL paper, we can calculate the laser power for both wavelengths. With this we can conclude:

$$\lambda = 400\,\text{nm}\text{: } P_{\text{laser}} = 31.00\,\text{kW} \qquad \lambda = 532\,\text{nm}\text{: } P_{\text{laser}} = 23.31\,\text{kW}.$$

For a pulse length of 70 ps we can calculate the pulse energy using:

$$P_{\text{laser}} = \frac{E_{\text{pulse}}}{\Delta t} \Leftrightarrow E_{\text{pulse}} = P_{laser} \cdot \Delta t. \tag{5.2}$$

For the different laser wavelengths this results in:

$$\lambda = 400\,\text{nm}\text{: } E_{\text{pulse}} = 2.17\,\mu\text{J} \qquad \lambda = 532\,\text{nm}\text{: } E_{\text{pulse}} = 1.63\,\mu\text{J}$$

The spot size should be in the order of magnitude of the size of the cathode. In [39] it was analysed that the emittance is dependent on the spot size also one would expect that there is a dependency between illuminated area and achievable extraction current, however it is to be determined if this is dominated by the described space-charge effects.

5.3 Optical Simulations of Grid Influence on Laser Beam in TAPE Mode

Thermionic cathodes typically have a grid installed near the emitting surface. This enables a pulsed mode of the cathode, which is also needed in our operation mode. The grid serves as a control electrode; depending on the potential of the grid, electrons may or may not enter the area between the cathode and the anode. When used as a photocathode, however, this grid is in the laser's beam path and diffraction at the grid could be a challenge for the operation of such an cathode in this mode. In the following, considerations and simulations will be presented that examine and describe the influence of the grid.
To understand which regime of the phenomenon we are in, the Fresnel number was calculated. This is given as[49]:

$$F = \frac{a^2}{\lambda \cdot d}, \tag{5.3}$$

where a is the characteristic dimension of the diffracting object - in our case the distance between neighbouring grid wires - and d is the distance between diffracting object and the observation plane - in our case the distance between cathode and grid. Looking at the specifications of the grid of our current cathode one can see, that $a = d$ in our application. With $a = 150\,\mu\text{m}$ and $400\,\text{nm} \leq \lambda \leq 532\,\text{nm}$ we obtain:

$$\lambda = 400\,\text{nm}\text{: } F = 375 \qquad \lambda = 532\,\text{nm}\text{: } F = 282$$

The different regimes of diffraction are separated according to:

- $F \ll 1$**:** Fresnel diffraction
- $F \approx 1$**:** Fraunhofer diffraction
- $F \gg 1$**:** Geometric optics

The last regime is valid for very high distances between the grid wires and - as in our case - if the plane if observation is very near the diffracting object. Here no diffraction patterns can be observed and the image is dominated by sharp shadows of the object. Since we observe quite high values of the Fresnel number, we expect this to happen. However it is not sure how sharp the shadows really are and how significant the influence of diffraction in this case.
For that matter an optical simulation was carried out. For this the `python3`-library `LightPipes` [50]

was used. With this package the propagation of a laser beam and its influencing via lenses, apertures and other objects can be studied. For our purpose a very simple optics was simulated to achieve a suitable spot size at the grid and the intensity pattern at distance $d = 150\,\mu m$ was observed. This intensity distribution without the presence of a grid as well as with a grid in the beams path is shown in Figure 5.3. As expected we can see distinct shadows of the grid. The shadows can be further inspected by the use of a cross-section. This

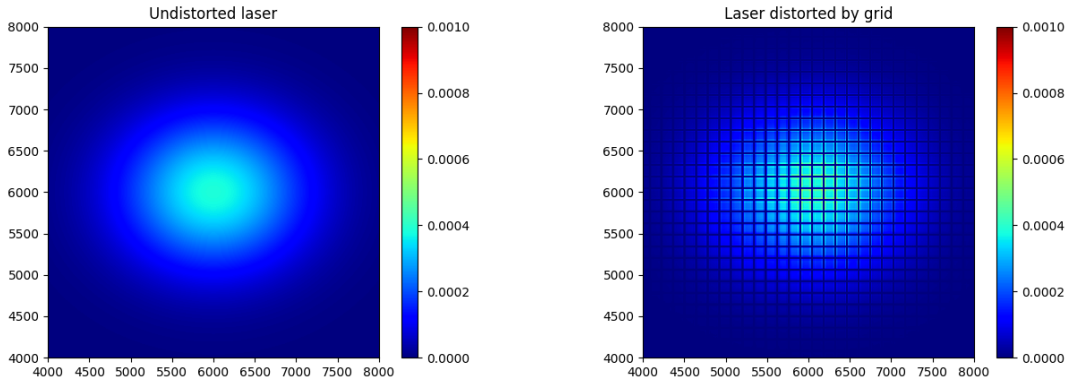

(a) without grid (b) with grid

Figure 5.3: The intensity distribution at the position of the cathode was simulated - using `LightPipes` [50] - with a grid in the path of the laser and without this grid. The dimensions of the grid are according to 3.1. The axis are given in pixel defining the simulation area, here the width of a pixel is equal to 1.25 µm.

can be seen in Figure 5.4. Some smaller diffraction effects are apparent. The intensity inside the shadow is not exactly zero, but there is a small underlying intensity. Also one observes some over-amplification around the edges of the shadows. The latter effect is greatest at the edges of the shadows, where one observes up to 25 % exaggeration. If one integrates over the whole range for both intensity distributions one observes 26.85 % of intensity lost at the grid. This is significant and therefore should be considered in future planning

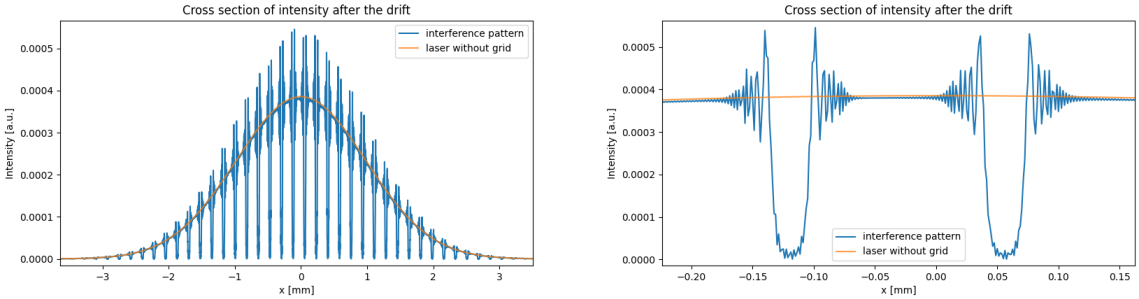

(a) whole spot (b) centre of the spot

Figure 5.4: A slice through the intensity distribution at the cathode position is performed along the middle of the cathode. The distributions with a grid and without the grid are compared. Effects of diffraction at the edges of the shadows can be observed. This leads to an intensity behind the grid also inside the shadows and some over-amplification around the edges.

of the laser system. However the amount of energy that is deposited in the grid as a result, should not be any problem for the grid itself. Based on the observed intensity distributions it is assumed, that the operation of a gridded thermionic gun in a TAPE operation mode is feasible. Since no knowledge could be obtained as to whether the cathodes used in the SSRL and MAX-lab experiments had such a grid, it remains to be seen whether and what influence the grid has on the beam properties. The assumption that an effect is present results from the fact that the initial space charge distribution is very discontinuous. A simulation of this effect could not be carried out due to the limitations of the simulation environment.

5.4 Conceptual Design of Possible Setup

Before further development of the gun is started, it should be considered how the TAPE operation mode can be realised on the current setup. In this respect, attention should also be paid to whether the requirements for the laser system are within reasonable limits. The results of this consideration will be presented in the following:

- **Wavelength:** Below $\lambda = 400\,\mathrm{nm}$ the aging of structures as vacuum windows for the laser beams is speeded up, furthermore very low wavelengths create the need of vacuum windows made from special materials, which are more expensive. A wavelength between $\lambda = 400\,\mathrm{nm}$ and $\lambda = 450\,\mathrm{nm}$ seems to be appropriate since the quantum efficiency is expected to be slightly higher (as can be seen in Figure 5.1), but the laser would be still in the visible range, which simplifies optical monitoring.

- **Positioning of the laser setup:** The positioning of the laser itself is uncritical, since the usage of a glass fibre to transport the laser beam near the beam line is suitable. The easiest approach of placing the optics would be to place it neighbouring to the beam line and use a vacuum window to transport the beam into the vacuum structure. In the current setup this could easily be done above the alpha magnet (compare Figure 1.2).

- **Optics:** An adjustable spot size can be achieved using a single focusing lens, as the targeted spot sizes are very large (a few millimetres). For this, the laser beam would be decoupled from the optical fibre, resulting in a very divergent beam, which would then be focused to the desired size on the cathode. If this lens can be moved, the spot size can be adjusted.

- **Monitoring:** Using a special (semi-transparent) mirror one could reflect the laser beam into the vacuum structure and using a camera setup above the mirror to monitor the laser through it.

- **Feasibility:** The preliminary design parameters outlined in section 5.2 are technically realizable. There are many systems available which fulfil this requirements. For testing low cost laser diodes could be used to measure quantum efficiency - also in different wavelengths. When this tests are finished a better suited system could be acquired, since this diodes are not originally designed for this usage.

A positioning of the laser optics above the existing alpha magnet would allow the TAPE operation mode. A deviation from the design for a purely thermionic electron gun does not seem to be necessary. The grid in the path of the laser beam seems to oppose no problem for this operation mode.

CHAPTER 6

Development of a new gun assembly

In chapter 3 challenges with the existing electron gun were presented and a suitable type of a new electron gun was identified. As described in chapter 4 a thermionic electron gun using an electrostatic field for acceleration is the most appropriate method for the needs of the ELSA facility. To enable the single bunch operation mode the gun will be developed as a hybrid mode gun, using the dispenser cathode both as a thermionic as well as a photo-cathode. The operation mode was analysed in the previous chapter. It was found that the design of a thermionic DC gun is suitable to achieve our planned hybrid gun. The following section describes the design process of this gun.
In the beginning a very basic structure was planned, which shows strong similarities to the existing structure with some optimizations and simplifications being made. After that the influence of some dimensions on the performance metrics was analysed to optimize those dimensions. This was followed by an in-depth simulation and analysis of the whole assembly using different solvers to find also problems, which are not directly obvious from the beam parameters, such as high field gradients somewhere in the assembly for example, which could introduce the risk of vacuum breakdowns. In the scope of the mechanical engineering it was determined which parts we could build by ourselves and for which parts we rely on other producers. After the exact dimensions of the components, which have to be planned and manufactured commercially, will be known, the simplified "physical" model will be transferred into an finished "mechanical" model, including all details. This model will then be imported to CST to validate its performance based on the performance metrics specified in the section above. In the scope of this thesis the development of the "physical" model and all the optimizations and analyses done can be presented. In the end work, which was necessary to develop the constructive requirements of those parts, is presented.

6.1 Conceptualization of the basic Electron Gun Assembly

Before the start of the modelling process it is important to think about which basic methods one wants to use for this assembly. As reasoned in section 4.3 a thermionic cathode and acceleration within a static electric field - as used in the current electron gun - is the most suitable way for this application. To compensate for space charge effect the Pierce geometry (comp. 2.2.2) will be used in the new gun. The single bunch mode will be realized by using the TAPE operation mode. In section 5.4 it was stated, that there will be no modification necessary for this operation mode.
It was decided to use the same dimensions of the existing beam pipe at gun exit, to simplify the installation into the existing infrastructure. In contrast to the current electron gun there is no need for a prebunching

cavity at the end of the gun, so the beam pipe will directly be connected to the anode of the new gun assembly. There were several ideas for optimizations in comparison to the existing structure, which are taken into account for the new electron gun from the beginning:

- **Optimization of the cathode holder:** The cathodes in use at the moment are not mounted on a vacuum flange. To create a vacuum seal the cathode is pressed between two pieces of metal. This connection is sealed by gold rings, which are also squeezed in between to close any gaps. In the past years it was necessary to increase the thickness of this rings, to create a suitable vacuum seal. Nevertheless in recent accelerator operations one could observe continuos worsening of the vacuum inside the gun, which leads to the assumption that the service life of the seal has been reached. Besides the problems due to the ageing this kind of seal has some basic problems. The work needed to create an appropriate seal is time consuming and especially inside the high voltage cone rather difficult. Furthermore the positioning of the cathode cannot be reliably reproduced. This leads to the decision to use a cathode already mounted on a CF type vacuum flange for the new gun assembly. That way a good vacuum seal, reproducible positioning and rather easy switching of the cathode can be ensured. Moreover this means that the interface between the high voltage cone and the cathode is a standardized component, which is a great advantage if the type of cathode has to be changed in the future or if different cathodes will be used.

- **Optimization of insulator and high-voltage cone:**The high-voltage cone in the gun is used to hold the cathode in place and to transfer the high-voltage potential to it. It is also a barrier of the guns vacuum. Therefore it has to fulfil multiple demands. Furthermore the inside of the high-voltage cone is also used to place the pulser electronic as close as possible to the grid. At the moment the high-voltage cone is rather deep and narrow, which complicates tasks as the replacement of the cathode since the corresponding screws are hard to access. For the new assembly it should be aimed for a broader and - if possible - shorter high-voltage cone to simplify these tasks. Since the accessibility of the gun in general is already a problem due to the positioning of the gun in the injector facility the optimization of the accessibility inside the high-voltage cone is an important focus in the redesign of the electron gun. Due to the general layout - the high-voltage cone inside the insulator - the design of those two components is strongly linked together. A broader insulator therefore creates the need for a fitting, wider insulator. Another point which one could optimize with regard to the high-voltage cone is the space which is available for the pulser electronic. An increase of this space would enhance the cooling of the electronics, which could be beneficial, furthermore it could simplify the design of the electronics by lessening the size constraints.

- **Modularity of the assembly:** The old assembly consisted mainly of two parts: The anode part, which is flanged to the beam pipe at one end and permanently connected to the insulator at the other end, which in turn is connected via flanges to the second main component, the high-voltage cone. This should be done differently in the new assembly, which will consists of three main parts: the anode section, the insulator and the high-voltage cone, which will be connected via standard vacuum flanges. The cathode holder will also be achieved by a standard vacuum flange as already described. This setup should simplify later upgrades, reparations or replacements if necessary. This also simplifies the design of some parts as the insulator, since a standard assembly mounted with vacuum flanges on both ends can be used. This modular approach could also make future upgrades of the individual components more viable, because they are not longer linked to a replacement of other components. For example the high-voltage insulator is a quite cost-intensive component, separating this from the

anode section would make any changes to the anode independent of the insulator as long as the vacuum flange is preserved.

- **Vacuum Optimizations:** The optimization of the cathode holder was already mentioned before. One of the motivations for this optimization was to achieve a more reliable vacuum seal. Since the vacuum quality in the injector facility was generally an important reason for this project, the vacuum quality is also an important topic to consider. Besides the already mentioned usage of standard vacuum flanges as component interfaces and the also mentioned rework of the cathode holder, the usage of standardized vacuum parts should be sufficient to achieve the goals regarding the vacuum optimization.

- **Usability with different cathodes:** Another feature which should be considered for the new assembly is the possibility to use different cathodes. This would have multiple advantages: First of all it reduces the dependency on one manufacturer of cathodes and on the availability of the chosen cathode. The latter was experienced with the current cathode, since it was only available at one distributor which made the procurement of a sufficient number of cathodes more difficult, since the reserves of this special cathode were typically low. Furthermore while the performance in a thermionic operation mode are given, the performances (i.e. the quantum efficiency) for the TAPE operation mode are unclear. Having the possibility of using different cathodes grants the chance to analyse and explore the differences in their behaviour for the TAPE operation mode and eventually settle for a different cathode later, which is ideal for both operation modes.

6.2 Screening and Selection of Optimal Cathodes

The cathode used in the current electron gun was already described in section 3.2. As justified beforehand a cathode for the new assembly should be premounted on a vacuum flange. Furthermore the cathode needs to be able to fulfil the requirements regarding the extraction current of 2 A.
However the maximum extraction current, which is given by most manufacturers, is in reference to a continuos extraction. In a pulsed extraction mode the pulse current

$$I_{\text{pulse}} = \frac{Q_{\text{pulse}}}{t_{\text{pulse}}}$$

can be slightly higher as long as the averaged current

$$I_{\text{avg}} = I_{\text{pulse}} \cdot f_{\text{pulse}} \cdot t_{\text{pulse}} \tag{6.1}$$

does not exceed the given current. Here Q_{pulse} is the charge inside one pulse, t_{pulse} is the length of a pulse and f_{pulse} is the frequency at which pulses are extracted. Filling in the characteristics of the standard multi-bunch operation mode: $I_{\text{pulse}} = 2\,\text{A}$, $t_{\text{pulse}} = 1\,\mu\text{s}$, $f_{\text{pulse}} = 50\,\text{Hz}$ a averaged current of $I_{\text{avg}} = 0.1\,\text{mA}$ is reached.
Three cathodes were found to be usable since they share almost identical dimensions and fulfil the requirements. Their specifications are listed in Table 6.1.
Referring to the technical drawings (see Appendix A on pages 57-59), all specified dimensions vary from each other exclusively on a submillimeter scale. Therefore, it is unclear whether it is technically feasible to build a cathode holder that can accommodate all three cathodes without any modifications, or if it would be more appropriate to build a separate high-voltage cone for each cathode, or if there exists a better solution from a technical perspective. This matter cannot be conclusively evaluated at this point and should be left to

Name	Cathode Area	Emission-Current Density		Flange Size	Grid D_{GC}	Filament Current	Filament Voltage
Y845	0.5 cm^2	2.5 A cm^{-2}	1.25 A	CF2¾"	0.14 mm	1.4 A	6.0 V
NJK2221A	0.5 cm^2	10 A cm^{-2}	5 A	ICF70	?	1.6 A	6.7 V
HWEG 101244	1.0 cm^2	3 A cm^{-2}	3 A	CF2¾"	0.16 mm	2.2 A	6.3 V

Table 6.1: Specifications of the different dispenser cathodes identified to be suitable for the new gun assembly. The ICF70-flange is a Japanese norm, identical to the CF2¾" norm. Technical drawings of the different cathodes can be found in Appendix A on pages 57-59.

the judgment of the engineers in the working group. As already mentioned from their specifications all three cathodes are interesting for our applications. It is unknown how the different cathodes will perform in the TAPE operation mode and if there will be differences between them.

6.3 From Concept to 3D Model: Initial Design of the New Gun Assembly

As for the current electron gun CST [11] is used to create a three-dimensional model and simulate the electron beam inside the model. Based on the optimization ideas described in section 6.1 a model was set up. This model is suitable for the cathodes described in the previous section. It features a Pierce-type geometry as the current assembly does also. The modelled grid in front of the cathode corresponds to the one used in the current Y848-B cathode. Upon comparing Table 3.1 and Table 6.1, it is evident that the differences in grid dimensions, as far as indicated, are marginal. As the descriptions of the grids for the new cathodes are incomplete, the grid of the old cathode will continue to be modelled and simulated. The expected deviations are of negligible magnitude.
The geometry of the anode was initially derived from the existing design in the first iteration step. A CF150 vacuum flange was selected for the insulator to enable a larger high-voltage cone and provide sufficient space for the cathode, simplifying work within the high-voltage cone. The length of the insulator was modeled as 21.4 cm. This value was calculated as the mean of the sizes of various available insulators, which are roughly in the specification range. The insulator, which will finally be used, will be most likely specifically build for this application. Changes in its length will be compensated by the high-voltage cone to preserve the inner geometry. The distance between the anode and cathode (measured from the surface of the emitting material to the tip of the anode) was initially set to 15 mm, which was also adopted from the current design. A more precise constraint on this distance is calculated using the Child-Langmuir Law (see formula 2.8):

$$d = \sqrt{K \cdot U^{\frac{3}{2}} \cdot J^{-1}} \tag{6.2}$$

with the desired extraction current of $I = 2\,\mathrm{A}$ and the radius of the beam pipe being $r = 9\,\mathrm{mm}$. A lower limit for the current density can be determined, if one assumes, that the desired current is spread across the whole cross-section S of the aperture:

$$J = \frac{I}{S}\,; \qquad S \leq \pi r^2$$
$$\Rightarrow J \geq \frac{2\,\mathrm{A}}{\pi\,(9\,\mathrm{mm})^2} = 0.786\,\mathrm{A\,cm^{-2}}$$

Using this result in formula 6.2 yields an upper limit for the distance between the anode and cathode:

$$d \leq \sqrt{K \cdot (50\,\mathrm{kV})^{\frac{3}{2}} \cdot (0.786\,\mathrm{A\,cm^{-2}})^{-1}}$$
$$d \leq 5.762\,\mathrm{cm} \tag{6.3}$$

As can be deduced from the result, the space charge-limited emission mode is not a strong limitation in this gun. In chapter 4, it has already been described that high longitudinal field gradients have a positive effect on the beam properties, thus small distances between the cathode and anode are preferred. The breakdown voltage represents a lower limit for this distance, and it depends on the quality of the surfaces used and possibly the vacuum quality. In a vacuum of around 10^{-8} mbar, this limit typically lies in the range of $10\,\mathrm{kV\,mm^{-1}}$. Therefore the lower limit for the distance would be 5 mm. It is important to note in this context that the minimum distance between the anode (ground potential) and cathode (negative high potential) is meant here, and not the distance described when applying the Child-Langmuir law. In addition, this calculation does not include a safety margin to account for potential errors in the surfaces, inaccuracies in the positioning, or fluctuations in the voltage. Therefore, a larger distance between the anode and cathode should be chosen. The optimization of this parameter can be found in the following section. The following nomenclature will be used from now on:

$$d_{\mathrm{CA}} \leq 5.762\,\mathrm{cm}\,; \quad d_{\mathrm{min}} = 5\,\mathrm{mm} \tag{6.4}$$

where d_{CA} is the distance between the emitting surface of the cathode and the tip of the anode measured along the longitudinal axis and d_{min} is the minimal distance between anode and cathode.
In the technical drawing of the current electron gun (see Fig. **??**) one deviation from the Pierce geometry can be found: The opening of the cathode near the emitting surface corresponds to the Pierce geometry, but at a longitudinal distance of about 2mm, the slope angle of the surface changes from the Pierce angle $\Theta_{\mathrm{Pierce}} = 22.5°$ to $\Theta = 38°$. A constructive reason for these changes could not be found, which is why a physical reason is suspected. In the model of the new gun, it is provided that such an angle can be defined deviating from the Pierce angle, but it is not initially incorporated into the model. In the following section, this parameter will also be examined and optimized, even if this would lead to a deviation from the originally desired Pierce geometry. The basic design is shown in Figure 6.1. In the following section the performance of the electron gun will be optimized in an iterative process. To evaluate the performance the metrics defined in section 4.1.2 will be used, therefore the analysis will be similar to the one done for the existing gun setup in chapter 3. In addition to the physical point of view - defined in particular by the performance metrics - the operational point of view should also be taken into account in order to meet the elementary goal of a gun that is as reliable and durable as possible.

6.4 Optimization of Design Parameters

In the following sections, a number of simulations are described, aimed at optimizing the geometry of the new gun. All of these simulations will be able to describe the thermal operation of the cathodes, with the maximum extraction current being assumed in each case. A simulation of the TAPE operation mode was not possible within the scope of this thesis, since no simulation program could be found that covers the required physical areas and enables the required simulations and tracking of the electrons. For example, CST does not include the ability to describe the actual emission process and to simulate the behaviour of the thermal

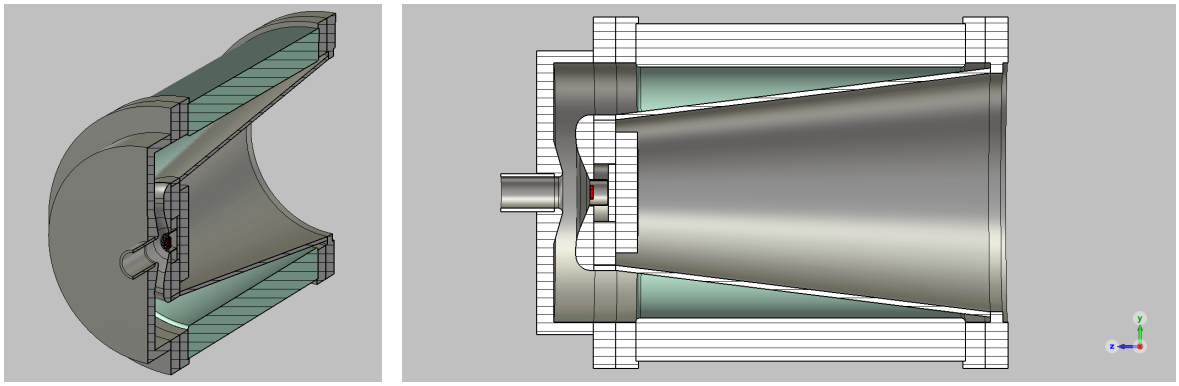

(a) Perspective view (b) Side view

Figure 6.1: The initial design of the new assembly, seen from a perspective and a side view. This model was designed as a first iteration step to implement the intended improvements. Some dimensions were taken from the old design after a review. The performance of the gun will be investigated in a similar way as in chapter 3. The depicted model will then be optimized in an iterative process, taking into account physical and operational aspects.

cathodes as photo-emitters. In the following, the optimization process that was carried out in the context of this work will be presented in more detail.
A highly simplified toy model was initially developed, to gain a better understanding for the possibilities of the optimisation of the gun performance. This model consisted solely of the two electrodes, which were designed according to the Pierce geometry. The dimensions of these electrodes already corresponded to those in the initial model presented above. This also applied to the geometry of the emitting surface of the cathode and the grid. The aim of this model was not to deliver scientifically reliable results, but, as already described, to understand the basic relationships between individual dimensions and their influence on the beam parameters and, based on this, to develop a plan for the iterative optimization of the actual model.

6.4.1 Toy model

Whilst the additional value of the toy model for the planning of the following analysis are apparent, its scientific validity is limited. Therefore an analysis of the simulations carried out with this model is neglected. The simplification of the model was intended to allow for a large number of simulations with small changes in geometry to be performed in a short amount of time. For this the distance between cathode and anode d_{CA}, the depth of the (Pierce-type) cone around the cathode d_{Pierce} and the deviation from the Pierce geometry by the introduction of a second angle Θ in the cathode cone - as described in the previous section - could be altered.
From the simulations with the toy model it was apparent, that there is no optimization possible for d_{CA} and d_{Pierce} separately, but that there is a link between the two parameters. Therefore suitable combinations of both parameters need to be identified first and then one of the parameters can be optimized. Based from this a plan for the optimization of the model for the new gun was derived:

i. **Identification of optimal combinations of d_{CA} and d_{Pierce}:** Several simulations should be carried out to evaluate different combinations of d_{CA} and d_{Pierce}. A investigation of possible values for d_{CA} was performed in section 6.3. The resulting boundary conditions are used: $10\,\mathrm{mm} \leq d_{\mathrm{CA}} \leq 20\,\mathrm{mm}$, $5\,\mathrm{mm} \leq d_{\mathrm{Pierce}} \leq 10\,\mathrm{mm}$. In the combination of both parameters it is important to remember the

requirement of $d_{\text{min}} = 5\,\text{mm}$. Only combinations of both parameters, which fulfil $d_{\text{CA}} - d_{\text{Pierce}} \geq 5\,\text{mm}$ are therefore used. It is sufficient to carry out this simulation only with one cathode.

ii. **Optimization of d_{CA}:** After optimal combinations are found the distance between anode and cathode can be optimized. This will be done in the same range of d_{CA} already used in the prior optimization step. For this analysis the combinations of the first step are used. This analysis will be done for all three cathodes.

iii. **Investigation of the influence of the second angle in the Pierce cone:** This was already mentioned in the previous section. Since the purpose of this deviation from the Pierce geometry is unclear it should be investigated. Investigation will occur in the range: $18° \leq \Theta \leq 42°$. Especially Θ_{Pierce} - the case, where the geometry is equivalent to the Pierce geometry - and $\Theta = 38°$ - the angle used in the current gun - are of particular interest.

The optimization process is explained in the following - ordered according to this plan - and the simulation results are described.

6.4.2 Identification of optimal combinations of d_{CA} and d_{Pierce}

As described above the first task is to identify combinations of the distance between anode and cathode and the depth of the cone around the cathode. The principle of finding combinations of this two dimensions to simulate those was also described previously. The evaluation of the performance will be based on the transverse emittances, the achieved extraction current and the beam divergence and envelope. The simulations were performed with the Eimac Y845 cathode, which is capable of delivering 1.25 A of electrons. This current is used in the simulations alongside the geometry of the cathode. In the following different values of d_{CA} will be evaluated separately.

$d_{\text{CA}} = 10\,\text{mm}$

The first simulation was done for $d_{\text{CA}} = 10\,\text{mm}$ and $d_{\text{Pierce}} = 5\,\text{mm}$. From the defined range for the depth of the cathode cone this is the only possible combination. However a small evaluation of this geometry was performed. The results of this evaluation are illustrated in Figure 6.2 and the values of the performance metrics at gun exit are also given in Table 6.2.

$d_{\text{Pierce}}/\text{mm}$	$\epsilon_x/\text{mm mrad}$	$\epsilon_z/\text{mm mrad}$	divergence/mrad	envelope/mm	I/A
5	10.1	10.1	61	8.57	0.96

Table 6.2: Values of the performance metrics at the gun exit. With the simulation parameters: $d_{\text{CA}} = 10\,\text{mm}$ and $d_{\text{Pierce}} = 5\,\text{mm}$. This simulation was performed with the Eimac Y845 cathode.

$d_{\text{CA}} = 12\,\text{mm}$

Also for this distance only one parameter combination is possible. Again the cathode cone will be simulated with a depth of $d_{\text{Pierce}} = 5\,\text{mm}$. The illustration of the performance metrics can be found in the appendix in Figure B.1. The values of the metrics at gun exit are summarized in Table B.1.

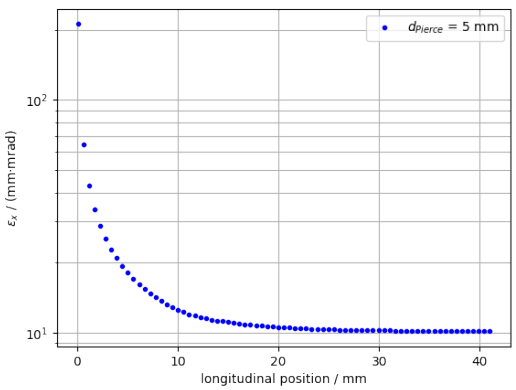

(a) Transverse Emittance in x-direction

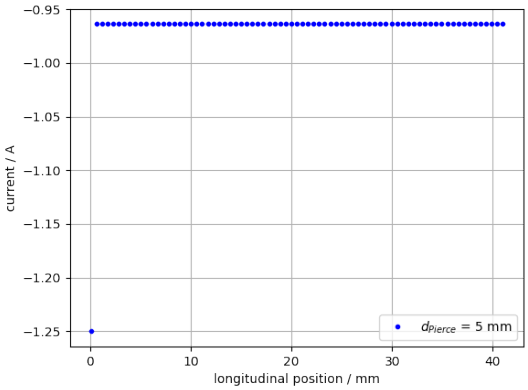

(b) Extraction Current

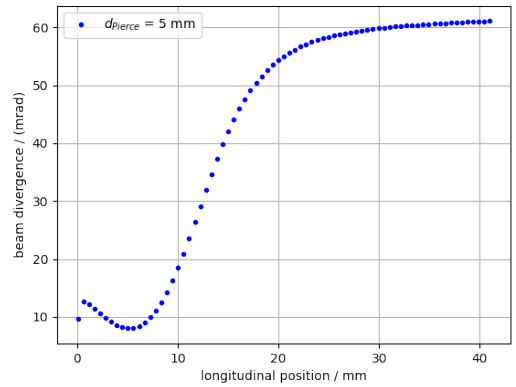

(c) Beam Divergence

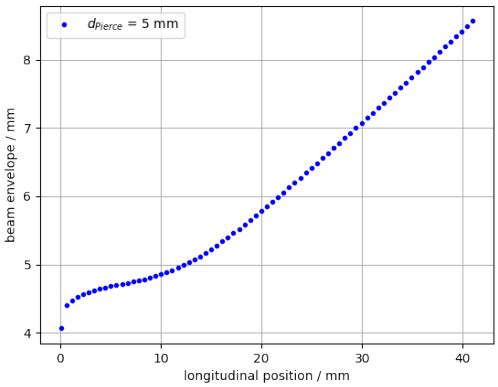

(d) Beam envelope

Figure 6.2: Evaluation of the simulations of the new assembly. The parameters of this simulations are those described for the initial gun design. In the scope of the evaluation $d_{\mathrm{CA}} = 10\,\mathrm{mm}$ and $d_{\mathrm{Pierce}} = 5\,\mathrm{mm}$ were used. The simulation was done using the Eimac Y845 cathode, which delivers an electron current of 1.25 A. One can see the evolution of the performance metrics, i.e. the transverse emittance (here in x-direction, since the problem is symmetric along the x- and y-axis, the emittances along both axes are equivalent), the extraction current, the beam divergence and the beam envelope, along the longitudinal axis. Here the emitting surface of the cathode is at $x = 0$. The term *plane position* refers to the position of the so-called monitors, which are used in CST[11] to determine beam parameters. This concept was already introduced in section 3.3. The values of the beam properties at gun exit are also given in Table 6.2.

d_{CA} = 14 mm

For this distance of anode and cathode two values for the depth of the cathode became possible, additional to the already used 5 mm of depth also a 8 mm deep cone was simulated. The evolution of the transverse emittance showed no significant difference between the two depths, which is also true for the extraction current. For the beam divergence and beam envelope small changes could be observed, these two quantities are depicted in Figure 6.3, a depiction of all four quantities can be found in Figure B.2. The values at gun-exit for the two simulations are again summarized in Table B.2. Referring to this values a small decrease in emittance, divergence and envelope is actually visible for a deeper cone. This is probably due to the fact, that there is a longer longitudinal region with a transverse electric field component due to the Pierce geometry, which leads to a more effective focussing. However these effects are very small. Remembering the distance between anode and cathode and that there could be problems if not enough security margin is taken into account, the combination of $d_{\mathrm{CA}} = 14\,\mathrm{mm}$ and $d_{\mathrm{Pierce}} = 5\,\mathrm{mm}$ is still favourable.

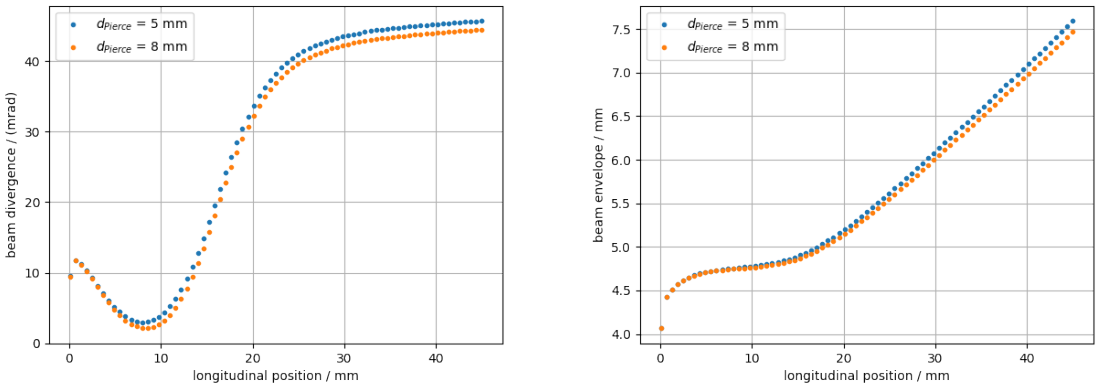

(a) Beam Divergence

(b) Beam envelope

Figure 6.3: Evaluation of the simulations of the new assembly. The parameters of this simulations are those described for the initial gun design. In the scope of the evaluation $d_{\mathrm{CA}} = 14\,\mathrm{mm}$ and two values for d_{Pierce} were used. The simulation was done using the Eimac Y845 cathode, which delivers an electron current of 1.25 A. Depicted is the longitudinal evolution of the beam divergence and beam envelope. All performance metrics are depicted in the appendix in Figure B.2. The values of the beam properties at gun exit are also given in Table B.2.

d_{CA} = 15 mm

This distance was initially chosen for the gun design. For this distance three different combinations are available. The simulation results are depicted in Figure B.3 and the performance metrics at gun exit are summarized in Table 6.3.
Again a small decrease of the transverse emittance is noticeable. The decrease of the beam divergence is smaller than in the evaluation before. Whilst the influence of the geometry change on the extraction current is again negligible, the beam envelope decreases for deeper cathode cones. When selecting a suitable combination of the two variables, it must be noted that changing the depth from 8 mm to 10 mm does not have a significant impact on the performance. Following the reasoning of the previous evaluation, the combination of $d_{\mathrm{CA}} = 15\,\mathrm{mm}$ and $d_{\mathrm{Pierce}} = 8\,\mathrm{mm}$ will be chosen for the further optimization process.

d_{Pierce}/mm	ϵ_x/mm mrad	ϵ_z/mm mrad	divergence/mrad	envelope/mm	I/A
5	7.1	7.1	43	7.44	0.94
8	6.9	6.9	42	7.29	0.94
10	6.9	6.9	42	7.28	0.94

Table 6.3: Values of the performance metrics at the gun exit. With the simulation parameters: $d_{\text{CA}} = 15\,\text{mm}$ and different values of d_{Pierce}. This simulation was performed with the Eimac Y845 cathode.

$d_{\text{CA}} = 17\,\text{mm}$

The observations made in this evaluations are well comparable with the ones for $d_{\text{CA}} = 15\,\text{mm}$. Therefore a more detailed description is omitted. The summary of the data is given in Table B.3 and the illustration can be found in the appendix (fig. B.4). For the further process the combination of $d_{\text{CA}} = 17\,\text{mm}$ and $d_{\text{Pierce}} = 8\,\text{mm}$ will be chosen.

$d_{\text{CA}} = 20\,\text{mm}$

Also, for an electrode spacing of 20 mm, no significant changes in the observations were made - as can be seen in Figure B.5. This is also reflected in the performance metrics at the gun exit (see Table B.4). For the simulations in the following section the combination of $d_{\text{CA}} = 20\,\text{mm}$ and $d_{\text{Pierce}} = 8\,\text{mm}$ will be used.
As the optimal combinations of the distance between anode and cathode and the depth of the cathode cone have been identified for all values of d_{CA}, which will be used in the upcoming section, it is now possible to investigate the influence of the cathode anode spacing for all three cathodes.

6.4.3 Optimization of d_{CA}

Based on the findings of the previous optimization, the influence of the distance between cathode and anode on the performance of the electron gun is examined. This investigation is conducted separately for all three cathodes. Subsequently, the findings are summarized and a distance that offers good performance for all three cathodes is determined.

Eimac Y845

For this simulations again the performance according to the simulation metrics was evaluated. The Y845 cathode, which has already been described before, can deliver at least an electron current of 1.25 A.
The simulation results for the Y845 cathode are shown in figure 6.4. The performance metrics at the gun exit for the different values of d_{CA} are given in table 6.4.
It can be seen that an increase in the distance of anode and cathode has a significant influence on the transverse emittance of the beam, reducing the value at gun exit from $\epsilon_x \approxeq \epsilon_z = 10.1\,\text{mm mrad}$ at $d_{\text{CA}} = 10\,\text{mm}$ to $\epsilon_x \approxeq \epsilon_z = 5.0\,\text{mm mrad}$ at $d_{\text{CA}} = 20\,\text{mm}$. Considered explicitly, the evolution of the beam divergence and beam envelope can be observed to contribute to and reflect the behaviour of emittance. Divergence is almost halved by doubling the distance between cathode and anode, while the beam envelope decreases from 8.57 mm at $d_{CA} = 10\,\text{mm}$ to 6.87 mm at $d_{CA} = 20\,\text{mm}$. This can be explained via the transversal fields in the gun. Inside and very near to the Pierce cone a focussing transverse field is present. There is also a transverse component of the electric field around the anode, but unlike that around the cathode, it is a defocussing component. Between these two areas the field lines are almost perfectly parallel and the transverse component

is negligible. By increasing the distance between cathode and anode, one increases the area with no transverse component. This region is also important for the focussing due to the Pierce geometry. The transverse electric field around the cathode changes the angular towards the longitudinal axis, for this to result in a focussing of the beam a drift section is needed, where this change of angular direction can be converted into a change of the transverse position. If the section between cathode and anode is too small, this cannot happen and the focussing will not be sufficient.
Regarding the extraction current it is apparent, that the influence of d_{CA} is not as significant as for the other performance metrics. An increase of the cathode anode spacing leads to a reduction of the achievable extraction current. This most probably a sign of space-charge effects. Therefore it should be observable even more distinct for the other cathodes with higher electron currents. In the simulations for the Y845 cathode we can only see an obvious difference between the current at $d_{CA} = 10\,\text{mm}$ and the other distances. Between those distances the differences are small.
Based on this evaluations, for the Y845 cathode higher distances between anode and cathode would even be preferable. Referring to the design goals summarized in Table 4.1 one can see that for values of $d_{CA} \geq 14\,\text{mm}$ the design goals for emittance and beam envelope can be met, the design goal regarding the beam divergence cannot be fulfilled independently on the value of D_{CA} in the simulated range.

d_{CA}/mm	ϵ_x/mm mrad	ϵ_z/mm mrad	divergence/mrad	envelope/mm	I/A
10	10.1	10.1	61	8.57	0.96
12	8.8	8.7	52	8.02	0.95
14	7.6	7.6	46	7.59	0.94
15	6.9	6.9	42	7.29	0.94
17	6.0	6.0	38	7.07	0.95
20	5.0	5.0	34	6.87	0.94

Table 6.4: Values of the performance metrics at the gun exit. With different values of d_{CA} and the corresponding values of d_{Pierce}. This simulation was performed with the Eimac Y845 cathode.

HWEG 101244

The HWEG101244 cathode has a extraction current rating of 3 A. It has also a larger emitting surface than the two other cathodes (comp. Table 6.1). This leads to a larger initial beam envelope, which necessitates a stronger focus. In Figure 6.5 the evolution of the performance metrics can again be observed along the longitudinal direction. We can observe a loss of electrons at the end of the assembly for the two smallest values of d_{CA}, this is expressed in a decrease of the extraction current. The reason behind this loss is an insufficiently strong focussing of the beam. The reason why this effect occurs for small distances between the cathode and the anode was described previously. A possible analogue, which should not remain unmentioned here, comes from the field of optics and is the observation of a beam at a small distance from the focusing lens, where the effect of the lens is still small. If a defocusing lens (in this case the anode) is placed too close to the focusing lens, a wide and still divergent beam is obtained. This can be observed by looking at the beam divergence and beam envelope in the evaluation of the simulation. The exact values of the performance metrics at the gun exit are given in Table B.5. They reflect the fact that a greater spacing can lead to better focus of the beam. However at values of d_{CA} of around 14 to 15 mm the limitation of the extraction current due to space-charge effects becomes stronger than the loss of electrons in the aperture. Therefore the distance between cathode and anode should be chosen in this range for this cathode.

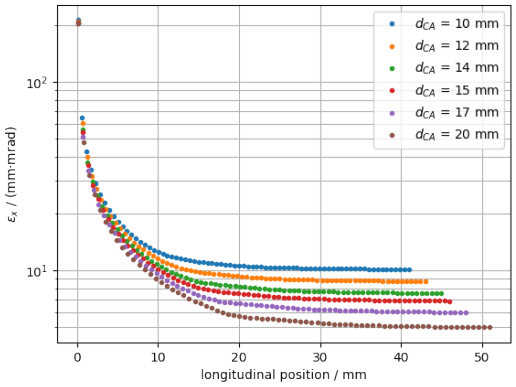

(a) Transverse Emittance in x-direction

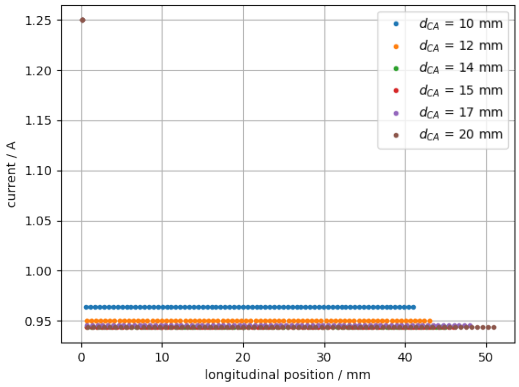

(b) Extraction Current

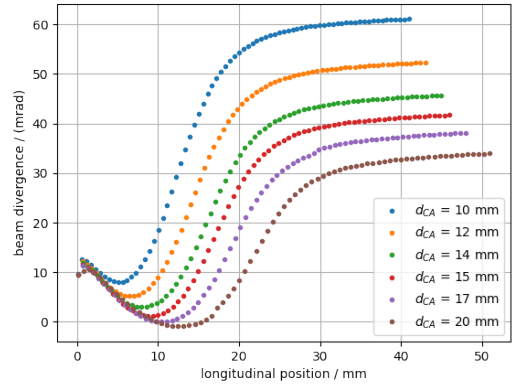

(c) Beam Divergence

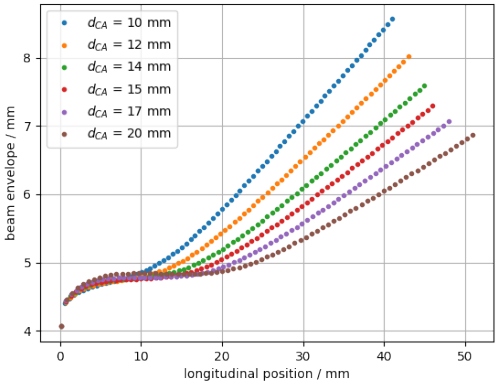

(d) Beam envelope

Figure 6.4: Evaluation of the simulations of the new assembly. For the simulation the identified pairs of the cathode anode spacing from the previous optimization step were used, all other dimensions correspond to those of the initial design. This simulation was done using the Eimac Y845 cathode, which delivers an electron current of 1.25 A. One can see the evolution of the performance metrics, i.e. the transverse emittance (here in x-direction, since the problem is symmetric along the x- and y-axis, the emittances along both axes are equivalent), the extraction current, the beam divergence and the beam envelope, along the longitudinal axis. Here the emitting surface of the cathode is at $x = 0$.

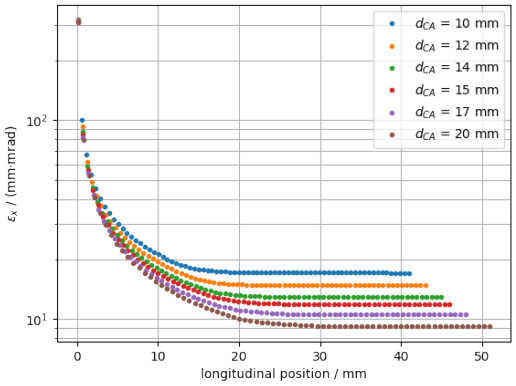

(a) Transverse Emittance in x-direction

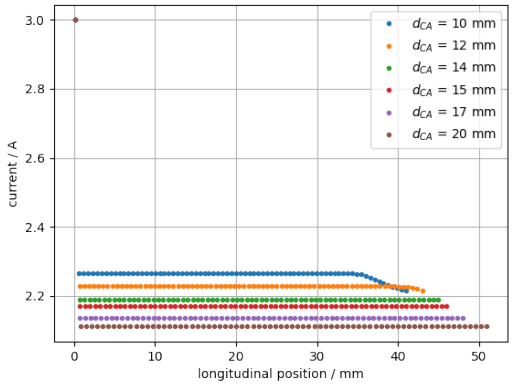

(b) Extraction Current

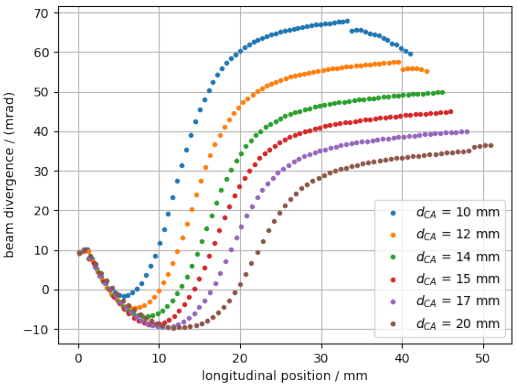

(c) Beam Divergence

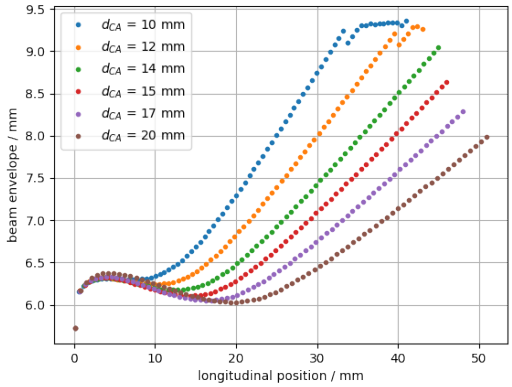

(d) Beam envelope

Figure 6.5: Evaluation of the simulations of the new assembly. For the simulation the identified pairs of the cathode anode spacing from the previous optimization step were used, all other dimensions correspond to those of the initial design. This simulation was done using the HWEG101244 cathode, which delivers an electron current of 3 A. One can see the evolution of the performance metrics, i.e. the transverse emittance, the extraction current, the beam divergence and the beam envelope, along the longitudinal axis. Here the emitting surface of the cathode is at $x = 0$. In the extraction current a small decrease towards the end of the assembly can be seen for the two smallest distances between cathode and anode. This means that electrons are lost within the anode aperture, because the beam is too broad at that position. This effect for small distances between the electrodes was already mentioned for the Eimac Y845 cathode. The small distance results in too less space for the focussing effect to decrease the transverse size of the beam.

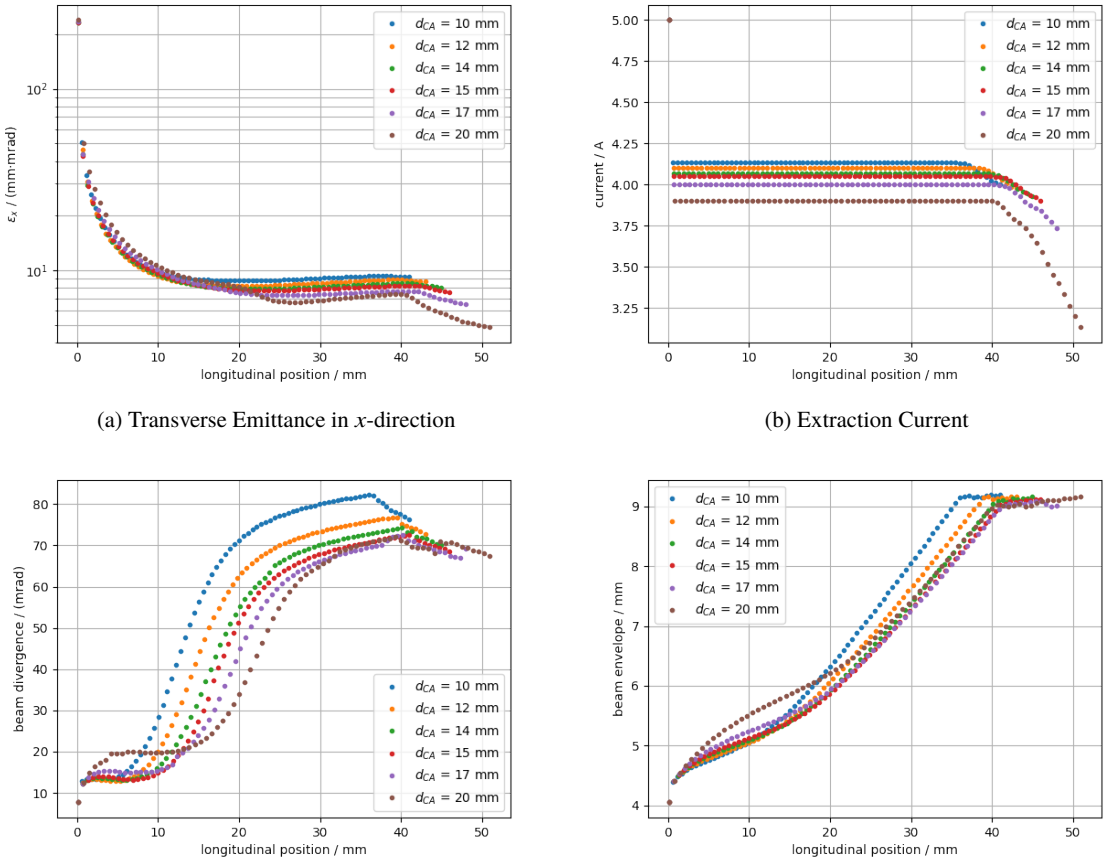

(a) Transverse Emittance in x-direction

(b) Extraction Current

(c) Beam Divergence

(d) Beam envelope

Figure 6.6: Evaluation of the simulations of the new assembly. For the simulation the identified pairs of the cathode anode spacing from the previous optimization step were used, all other dimensions correspond to those of the initial design. This simulation was done using the NJK2221A cathode, which delivers an electron current of 5 A. One can see the evolution of the performance metrics, i.e. the transverse emittance, the extraction current, the beam divergence and the beam envelope, along the longitudinal axis. Here the emitting surface of the cathode is at $x = 0$. One can observe a decrease in the extraction current towards the end of the assembly, this is a sign, that electrons are lost in the aperture of the anode. This is also visible in the other metrics, since electrons with a high transverse displacement are lost. This influences both the emittance as well as the divergence of the remaining electron beam. Furthermore the envelope is limited to the aperture of the anode.

NJK2221A

The NJK2221A cathode is capable of delivering up to 5 A of electron current. Therefore it is expected, that the space-charge effects have more impact in this simulation. The evolution of the performance metrics along the longitudinal direction is depicted in Figure 6.6, the values at gun exit can be found in Table B.6. In the longitudinal evolution of the performance metrics, there is one quite significant observation to mention: The extraction current decreases significantly towards the end of the assembly. This is a sign, that electrons are lost within the anode aperture, since the electron beam becomes too wide. This is a result of the repelling space-force. This effect is stronger if the distance between the anode and the cathode is increased. This

d_{CA}/mm	ϵ_x/mm mrad	ϵ_z/mm mrad	divergence/mrad	envelope/mm	I/A
10	9.3	8.91	82	9.15	4.13
12	8.9	8.4	76	8.95	4.10
14	8.5	7.9	74	8.84	4.07
15	8.2	7.7	72	8.92	4.05
17	7.7	7.1	72	8.85	4.00
20	7.4	6.8	71	8.97	3.90

Table 6.5: Values of the performance metrics at a position close to but before the loss of particles. This simulation was performed with the NJK2221A cathode.

difference can be explained by the strong space charge effects resulting from the high extraction current and the small emitting surface. In the area between the cathode and the anode, which has no transverse electric field, the space charge has an expanding effect and thus defocuses the beam. If this area is longer, the focusing effect of the Pierce geometry could be completely compensated, resulting again in a strongly divergent beam. This region can even aggravate the broadening of the beam, analogous to how it can assist focusing, depending on how much the angle towards the longitudinal direction of the individual particles changes due to the space-charge.
The loss of particles also means that the performance metrics at the gun exit are no longer as scientifically significant as before, this can also be seen in Figure 6.6: Beginning at the point in longitudinally direction, where electrons are lost first, an abrupt change in the evolution of the metrics can be observed. Therefore to compare the performance for different values of d_{CA} it is more sensible to compare the values taken at a position close to the point of first particle loss. This was done and the results are summarized in Table 6.5. Comparing the results of Table 6.5 one can see, that a increase of d_{CA} still results in a smaller emittance as well as a smaller beam divergence, but with a increased particle loss. With a cathode anode spacing of $d_{CA} = 15$ mm the design goal regarding the emittance of $\epsilon_x \leq 8.3$ mm mrad can be reached. A higher spacing would result in a higher particle loss and is therefore not desirable.
Summarising the results of the previous investigations, it can be stated that too small distances lead to a poorly focused beam and thus a greater emittance and are not suitable for achieving the design parameters. Especially for the cathode NJK2221A, however, a significant beam loss occurs also for high distances, which can be explained by space charge effects. A spacing of 14 mm appears to be a reasonable middle ground that delivers good performance for the three different cathodes. However, the simulations also show that the requirement for beam divergence cannot be met if a sufficient electron current is to be guaranteed or the two cathodes with particularly high extraction currents are used. It remains to be determined whether the pending optimization will be able to change this.

6.4.4 Investigation of the influence of the second angle in the Pierce cone

The last set of simulations, which is left to carry out, is the analysis of the influence of the second angle inside the cathode cone as described in section 6.3. The simulation of this second angle were carried out for five different values in the range of 18° to 42°, the geometry was taken from the previous optimisations and is thus: $d_{CA} = 15$ mm and $d_{Pierce} = 8$ mm. The results for the Eimac Y845 and the NJK2221A are given in the appendix in figures B.6 and B.7. The results for the HWEG101244 cathode are shown as an example in Figure 6.7. The simulation results of the different cathodes is summarized in Table 6.6. One can observe, that for bigger angles (which means a narrower cone) there are some improvements in the beam quality,

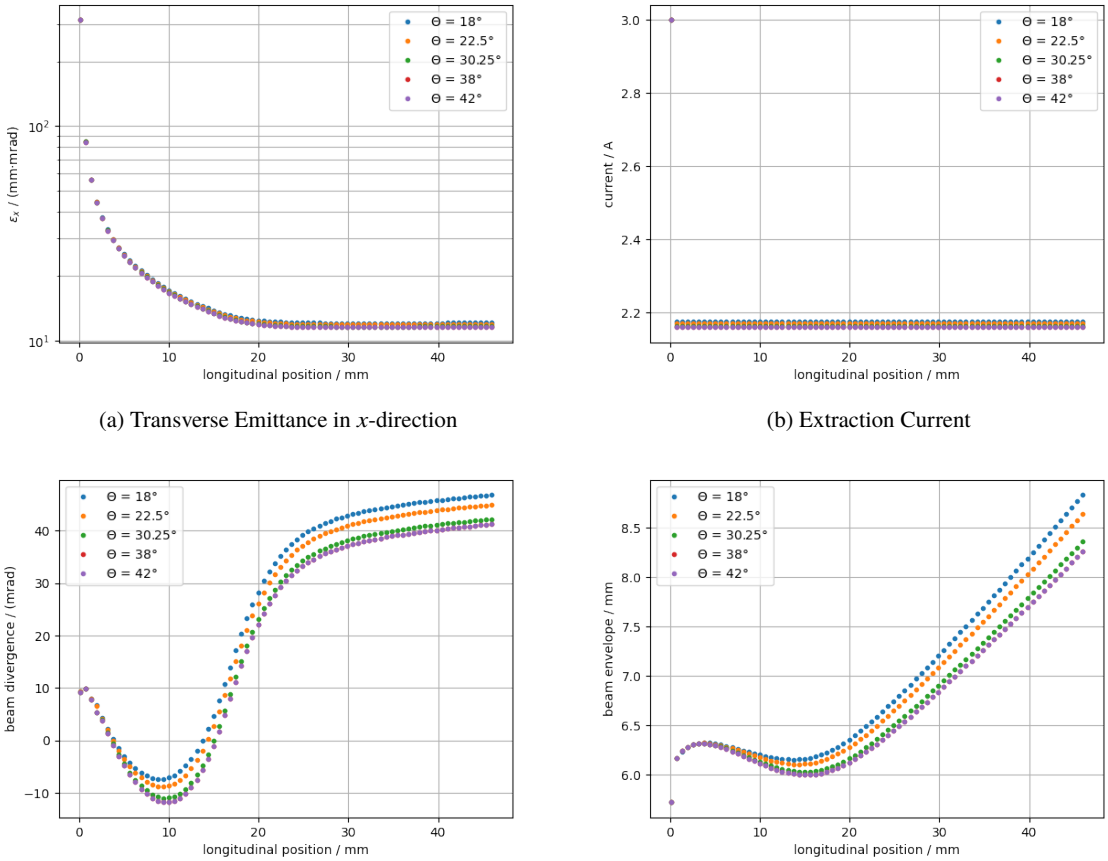

(a) Transverse Emittance in x-direction

(b) Extraction Current

(c) Beam Divergence

(d) Beam envelope

Figure 6.7: Evaluation of the simulations of the new assembly. For this simulation $d_{\mathrm{CA}} = 15\,\mathrm{mm}$ and $d_{\mathrm{Pierce}} = 8\,\mathrm{mm}$ was used. The value of the described second angle inside the cathode cone was changed. Where $\Theta = 22.5°$ corresponds to the normal Pierce geometry of the cone. This simulation was done using the HWEG101244 cathode, which delivers an electron current of 3 A. One can see the evolution of the performance metrics, i.e. the transverse emittance, the extraction current, the beam divergence and the beam envelope, along the longitudinal axis. Here the emitting surface of the cathode is at $x = 0$.

Cathode	Θ/°	ϵ_x/mm mrad	ϵ_z/mm mrad	divergence/mrad	envelope/mm	I/A
Y845	18.00	7.0	7.0	43	7.42	0.94
	22.50	6.9	6.9	42	7.29	0.94
	30.25	6.7	6.7	40	7.11	0.94
	38.00	6.6	6.6	40	7.04	0.95
	42.00	6.6	6.6	40	7.04	0.95
HWEG	18.00	12.1	12.1	47	8.83	2.18
101244	22.50	11.9	11.9	45	8.64	2.17
	30.25	11.6	11.7	42	8.36	2.16
	38.00	11.5	11.6	41	8.26	2.16
	42.00	11.5	11.6	41	8.26	2.16
NJK	18.00	7.7	7.1	68	9.13	3.89
2221A	22.50	7.7	7.1	68	9.12	3.89
	30.25	7.4	6.9	68	9.10	3.91
	38.00	7.4	6.9	68	9.10	3.91
	42.00	7.4	6.9	68	9.10	3.91

Table 6.6: Performance metrics for the different cathodes at gun exit in dependence of the second angle Θ in the cathode cone. For higher values of this angles - which means a narrower cone - slightly better focussing performance can be observed. However this effect is smaller for the cathodes with higher extraction current.

but especially for the cathodes with higher beam currents the effect becomes smaller. Therefore, it can be assumed that these changes are intended for the low extraction flows of the current gun. It is important to remember that the Pierce geometry is calculated for a gun in space charge limited mode, so it may not be optimal for small extraction currents. Since the influence of the change due to the second angle in the operating range of our cathodes is rather small, it was decided not to introduce a second angle, but to use a pure Pierce geometry in order not to unnecessarily increase the complexity of the setup.

6.4.5 Optimizing Beam Divergence and Transfer Efficiency with a Solenoid Magnet

In the previous sections it was mentioned that the design parameter defined in Table 4.1 regarding the beam divergence could not be matched for all cathodes, furthermore the problem of loosing electrons in the aperture of the anode when using the NJK2221A cathode was mentioned. Therefore it was necessary to conduct another optimization step. Including a solenoid magnet at the gun exit, as already mentioned in chapter 3. Detailed studies regarding the dimensions, position and strength of the magnet are out of scope of this work and should be repeated in combination with a full simulation of the new beamline connecting the gun to the Linac.

Simulations were performed analysing if the divergence and transfer efficiency can be optimized. As a solenoid an air coil with $N = 5\,000$ turns and a coil current of 5 A is used. Beam divergences between -10 mrad and 10 mrad were achieved for the different cathodes. It could be shown, that the loss of electrons in the aperture of the anode can successfully be prevented with the use of the solenoid. With the setting given, only emittances behind the solenoid in the order of 100 to 200 mm mrad are achievable. Preliminary investigations show that the magnetic field strength of the solenoid is overestimated as smaller strengths also feature smaller emittances. Although a significant increase in emittance can still be observed. Furthermore

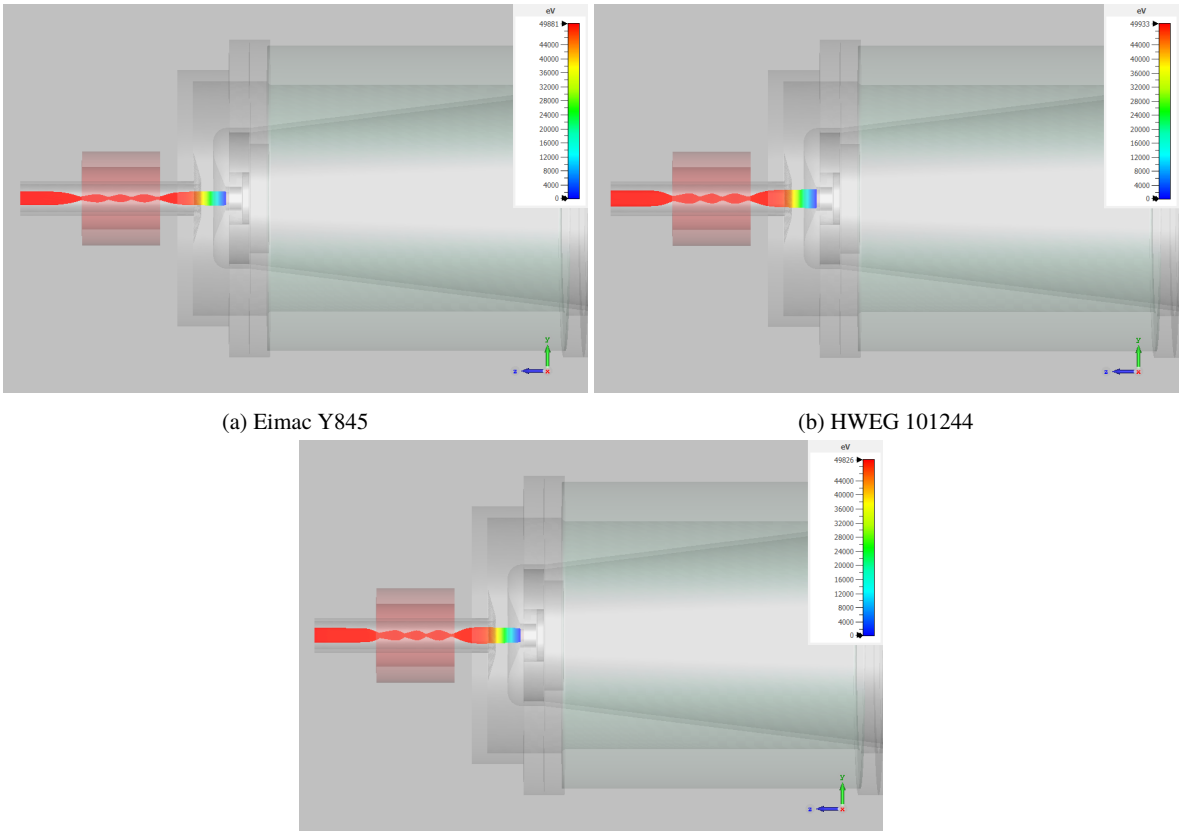

(a) Eimac Y845

(b) HWEG 101244

(c) NJK 2221A

Figure 6.8: Particle trajectories for the new electron gun design with a solenoid magnet (red structure) near gun exit. One can see, that the resulting electron beams are almost perfectly parallel. There are no longer electrons lost in the aperture of the anode.

collimation proves to be more difficult with smaller magnetic fields. Finding a suitable setting and solution to the problem should be pursued in combination with the precise design of the magnet optics of the subsequent beamline. In principle, however, the simulations show that the problems mentioned can be solved by installing a solenoid magnet when using cathodes with high extraction currents.

6.5 Performance Evaluation and Comparison with existing Electron Gun

Summarising the results of the previous investigations, it can be said that a geometry has been found that can be used well with all three cathodes. However, the increasing space charge effects with increasing current density of the cathodes pose a problem. Due to this effects, the requirements for beam envelope and beam divergence cannot be fulfilled for the cathodes HWEG 101244 and NJK 2221A. The larger diameter of the emitting surface of the HWEG 101244 cathode results in the emittance requirements not being met in this case. However, it can be assumed that the small deviation is tolerable. It could be shown that a solenoid magnet has a positive influence on the divergence and envelope of the beam. For the NJK 2221A cathode, the loss of electrons within the anode can also be prevented by a suitable magnet. The exact comparison of the design goals and the values achieved so far with the optimised design are shown in Table 6.7.

Parameter	Design Goal	Y845	HWEG 101244	NJK 2221A
ϵ_x / mm mrad	≤ 8.3	6.9	11.9	7.7
ϵ_z / mm mrad	≤ 8.3	6.9	11.9	7.1
beam divergence /mrad	≤ 22	42*	45*	68*
beam envelope /mm	≤ 8.00	7.29*	8.64*	9.12*
I/A	2.00	0.94	2.17	3.89*

Table 6.7: The achieved performance metrics for the different cathodes are compared to the original design goals. For the NJK2221A cathode it is important to remember, that these results include particles being lost at the anode aperture. The values marked by a star can be optimized by the use of a solenoid near to the gun exit.

6.6 Analysis of Mechanical Tolerances and Their Impact

Once the optimisation of the geometry is complete, the physical model was transferred into a preliminary mechanical model. The insulator showed up as been a design critical component, as it has to be manufactured by external companies. Due to the manufacturing process, deviations from the required geometry can hardly be corrected afterwards. It is imperative to examine the required tolerances closely so as not to degrade the performance of the gun. In the planning of the insulator, two variables turned out to be particularly important, as they strongly influence the transverse positioning of the cathode as well as the geometry of the electric field. These are the parallelism of the end plates (i.e. the outer surfaces of the vacuum flanges) and the coaxiality of the two flanges. The following section presents the investigations that were carried out to obtain suitable values for the tolerances on the two values.

6.6.1 Limited Parallelism of the Insulator End Plates

For the definition of the parallelism, one side of the structure (in this case one of the outer faces of the flanges) is defined as the reference plane. A second plane is then defined, perfectly parallel to the reference plane, and shifted by the length of the assembly so that it ends up at the design position of the plane whose parallelism is to be defined (the other flange). The tolerance is then given as $t_\parallel$ in mm. From the plane at the design position (now design plane), which is exactly parallel to the reference plane, two additional planes parallel to the design plane are defined, offset by $+t_\parallel/2$ and $-t_\parallel/2$ along the length of the part. To meet the tolerance, the surface must be located entirely within the volume spanned by these two planes. For a known tolerance and a known size of the surfaces underlying that tolerance, a maximum tilt of one surface relative to the other can be derived. This can then be used in the simulation to analyse the worst case for a given tolerance.
The investigations show a strong impact on the performance metrics depending on the tilt angle. With that, tolerances for the parallelism in the range between 0.1 mm and 0.4 mm are tolerable. As a representative, the detailed simulations here are shown for the Y845 cathide, but were performed for all cathodes and can be found in the appendix (see p. 70-71). The corresponding beam emittance, divergence, current and envelope are depicted in Figure 6.9. One can identify a difference for the non ideal cases, which is mostly due to additional particle loss. However the differences between the results in the simulated tolerance range are small considered the performance metrics. Further, the particle density distribution was examined in a plane

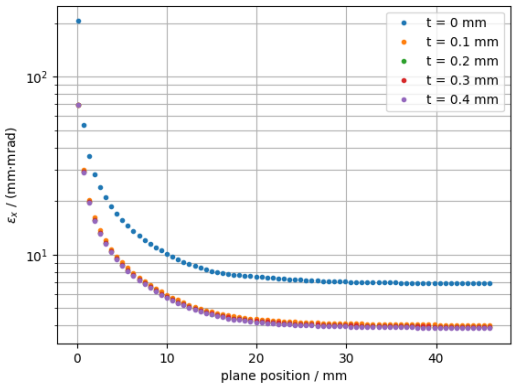

(a) Transverse Emittance in x-direction

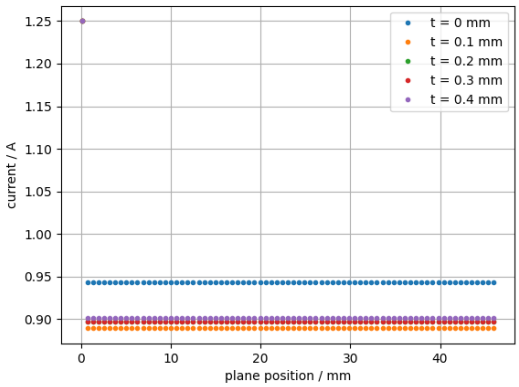

(b) Extraction Current

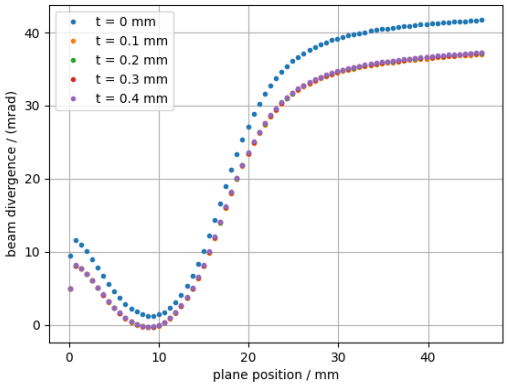

(c) Beam Divergence

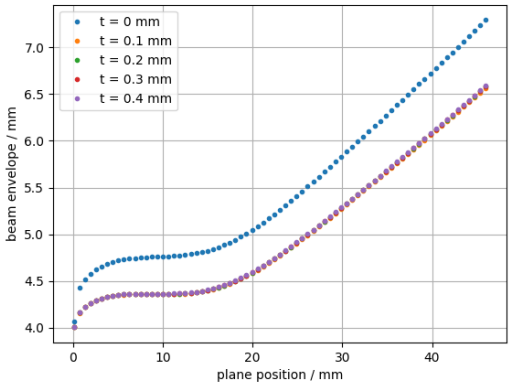

(d) Beam envelope

Figure 6.9: The performance metrics are evaluated for different values of the parallelism tolerance. A significant influence is visible for non ideal tolerance values. However the deviation between different values of the tolerance is small in the simulated range. The decrease in divergence, envelope and emittance is due to the additional particle loss.

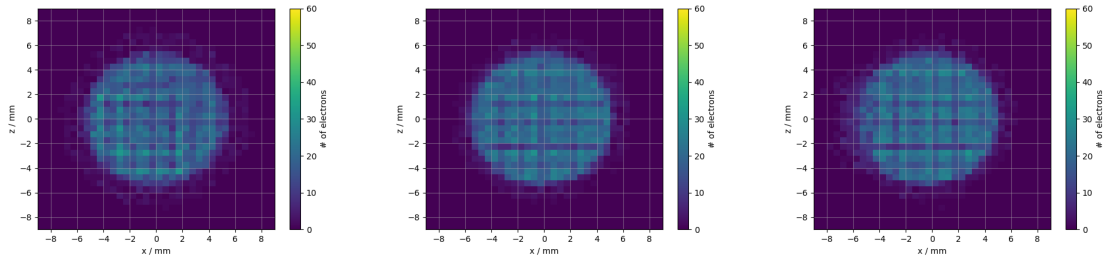

(a) $t_{\parallel} = 0.0\,\text{mm}$ (b) $t_{\parallel} = 0.1\,\text{mm}$ (c) $t_{\parallel} = 0.2\,\text{mm}$

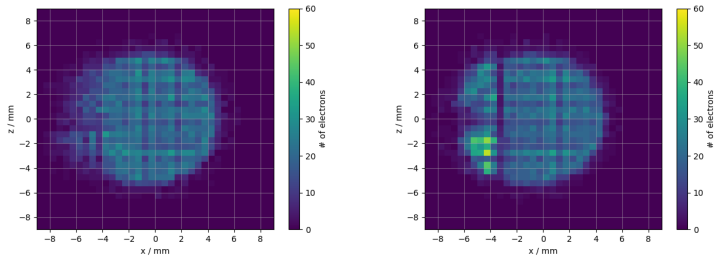

(d) $t_{\parallel} = 0.3\,\text{mm}$ (e) $t_{\parallel} = 0.4\,\text{mm}$

Figure 6.10: The distribution of electrons inside the beam was analysed for different values of the parallelism tolerance. Beginning from $t_{\parallel} = 0.2\,\text{mm}$ a small deviation in the distribution can be observed. With increasing values of the worst case tilt angle, which conforms to the given tolerance, increasing effects on the distribution are visible.

shortly after the gun exit. The results are depicted in Figure 6.10. It can be observed that there is a clear deviation from the ideal case for higher tolerances. Which result in a very non-uniform electron distribution. This is highly undesirable and could result in additional particle loss further down the beam line. Since the results are comparable for the other cathodes it was decided to request a tolerance of $t_{\parallel} = 0.2\,\text{mm}$.

6.6.2 Limited Coaxiality of the Insulator Flanges

Coaxiality is defined in a similar way as parallelism. Here the centre of one flange is defined as the reference, the centre of the second flange must lie within a circle of diameter $t_{\circledcirc}$ around the reference. Since this tolerance directly influences the transverse position of the cathode it is expected to have an influence on the performance of the gun.
The first analysis step was again to evaluate the performance metrics, these can be found on pages 72-74. Based on this observation a tolerance of $t_{\circledcirc} = 1\,\text{mm}$ is desirable, but at this stage it has not been definitively established whether this tolerance is achievable or economically viable. Therefore, a final decision on the exact value of this tolerance is still pending.

CHAPTER 7

Outlook and Conclusion

Final Design and Concept

Due to the condition of the injector described above, the investigation of the current cathode could only be carried out on the basis of simulations within the scope of this thesis. Design objectives for the new electron gun were derived from these investigations. A review of known electron gun types was carried out and presented, based on publications on the completion or planning of guns of these types or further experimental validations. The new gun is designed as a hybrid gun. Thermionic dispenser cathodes are used both as thermal and as photocathodes to suit the different operating modes. The advantages of this concept are reliability, multi-functionality and space efficiency, allowing two modes of operation to be provided in almost the same space as before. The new electron gun uses a static electric field to accelerate the particles, while the Pierce geometry is used to obtain a more focused electron beam. The acceleration distance between the anode and cathode has been optimised to 15 mm. Several optimisation steps have been carried out to achieve the desired beam characteristics. The possibility of further optimisation by using a solenoid close to the gun exit was demonstrated.
Regarding the feasibility of the TAPE operation preliminary laser properties were derived and the requirements were judged to be rather easy to fulfil. Further possible conflicts in the hybrid combination of both operation modes were analysed and largely excluded.

Comparison with Original Design Goals

The objectives for the design of the electron gun were introduced in chapter 4. After the optimisation steps, the beam characteristics obtained with the different cathodes were analysed. Compared with the design targets, it was found that the emittances for two of the three cathodes could be met. The other cathode has a larger emitting surface, which has the disadvantage of a higher emittance, but the differences are rather small and negotiable. At the moment, beam divergence and envelope are a persistent problem in the preliminary design, but it has been shown that well aligned magnet optics of the transfer beamline to the Linac are able to resolve these (comp. Section 6.4.5). With the cathodes identified as suitable, the targeted current upgrade can be achieved. A comparison of the achieved and desired performance metrics was summarized in Table 6.7.

Future Research and Development

It has been shown that the concept described is suitable for replacing the current electron gun. However, it was pointed out in the introduction that the replacement of the electron gun is only one step in solving the problems at the injector. Further steps introduce the replacement of the transfer beam line to the Linac, planning for the magnet optics, diagnostics and the vacuum system.
The aim is not only to increase the research possibilities at the injector itself, but also to plan a test stand where all kinds of beam parameters can be measured. On such a test stand it would be possible to measure beam profiles, charges, emittances, energy distributions within the beam and the dependence on various adjustable parameters such as heating power or grid volatage. In particular, the TAPE mode of operation can be analysed there, as there are currently no simulations and very limited experience from other groups. The framework BDSIM [51] was discovered, which is a combination of a simulation of individual particles and their interaction (here: Geant4 [52]) and a particle tracking code (like elegant [53]). This tool could potentially be used in the future to simulate the TAPE mode of operation.
It would be of great benefit to study the different cathodes and their applicability in TAPE mode. As a second step the laser parameters can be optimized for the particular cathode. With the test stand, these measurements could be carried out without interfering with the normal operation of the accelerator, increasing the research possibilities on the field of TAPE operation mode. In addition, recurring tasks, as the preparation and activation of a new cathode can be achieved at the test stand, improving the reliability.

Detailed Design Drawings and Schematics

NJK2221A

■ GENERAL DESCRIPTION

NJK2221A is an electron gun includes the Ir coated dispenser cathode and indirect type heater for getting electron emission. This electron gun is also preparing a grid electrode.

■ CATHODE SPECIFICATIONS

Cathode type: Ir coated dispenser cathode
Cathode diameter: 8 mm / Area: 0.5 cm^2
Current density: 10 A/cm^2
Heater voltage: 6.7 V
Heater current: 1.6 A
Flange type: ICF-70

■ OUTLINE

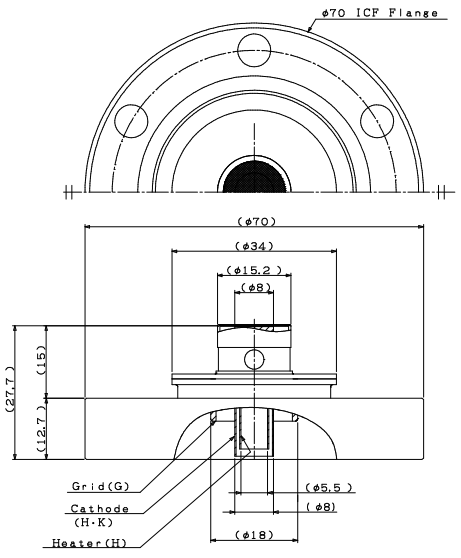

(Dimensions are expressed in “mm”.)

＊Above Specifications are subject to change without notice.

Nisshinbo Micro Devices Inc.

Reference No.:	Rev.:	Sheet:
DS-K2221A	07E	2

Data-sheet of the Nisshinbo Micro Devices NJK2221A cathode

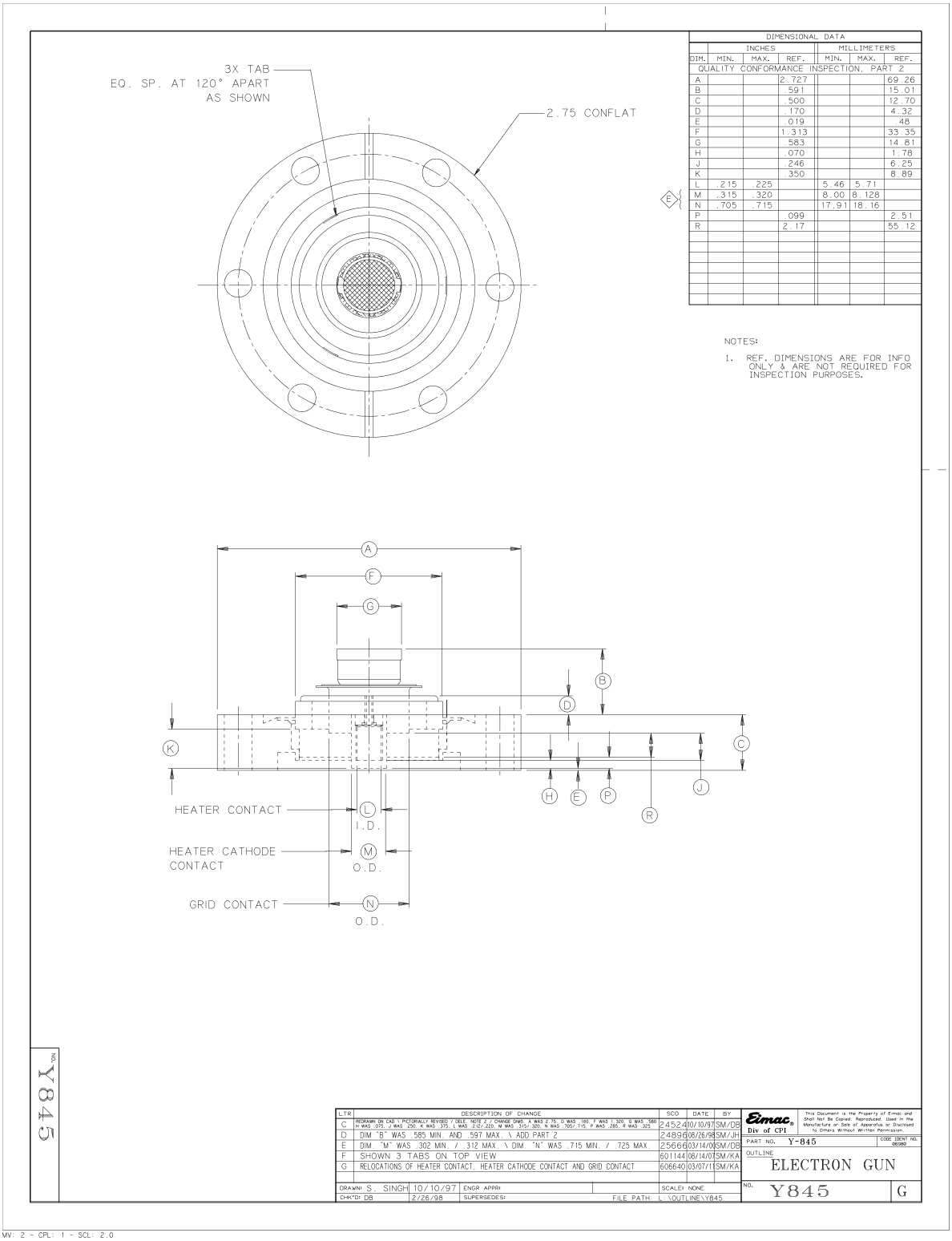

DIM.	INCHES MIN.	INCHES MAX.	INCHES REF.	MILLIMETERS MIN.	MILLIMETERS MAX.	MILLIMETERS REF.
QUALITY CONFORMANCE INSPECTION, PART 2						
A			2.727			69.26
B			.591			15.01
C			.500			12.70
D			.170			4.32
E			.019			.48
F			1.313			33.35
G			.583			14.81
H			.070			1.78
J			.246			6.25
K			.350			8.89
L	.215	.225		5.46	5.71	
M	.315	.320		8.00	8.128	
N	.705	.715		17.91	18.16	
P			.099			2.51
R			2.17			55.12

LTR	DESCRIPTION OF CHANGE	SCO	DATE	BY
C	REDRAWN ON CAD \ PICTORIALLY REVISED / DELE. NOTE 2 / CHANGE DIMS. K WAS 2.75, D WAS .180, F WAS 1.320, G WAS .580, H WAS .075, J WAS .250, K WAS .375, L WAS .212/.220, M WAS .315/.320, N WAS .705/.715, P WAS .285, R WAS .325	24524	10/10/97	SM/DB
D	DIM "B" WAS .585 MIN. AND .597 MAX. \ ADD PART 2	24896	08/26/98	SM/JH
E	DIM. "M" WAS .302 MIN. / .312 MAX. \ DIM. "N" WAS .715 MIN. / .725 MAX.	25666	03/14/00	SM/DB
F	SHOWN 3 TABS ON TOP VIEW	601144	08/14/07	SM/KA
G	RELOCATIONS OF HEATER CONTACT, HEATER CATHODE CONTACT AND GRID CONTACT	606640	03/07/11	SM/KA

DRAWN: S. SINGH 10/10/97 | ENGR APPR: | SCALE: NONE
CHK'D: DB 2/26/98 | SUPERSEDES: | FILE PATH: L:\OUTLINE\Y845

MV: 2 - CPL: 1 - SCL: 2.0

Technical drawing of the CPI Eimac Y845 cathode

HeatWave Labs, Inc.

TB-193

Model HWEG-101244 Electron Gun

Conflat Size	2 3/4”
Grid-Cathode Spacing (DGK)	160 microns (cold)
Emission, Typical*	3A @ E_C=100V
Cathode Area	1.0cm^2
Cathode Diameter	Ø0.44”
Cathode Heater Voltage*	6.3V
Cathode Heater Current, Typ.*	2.2A
Cathode Type	Dispenser
Cathode Lifetime**	>>10,000 Hours

*Actual values are subject to anode and system configurations.
**Cathode lifetimes are theoretical and under ideal conditions.

101244 Gun shown is sealed
in its shipping/storage container.

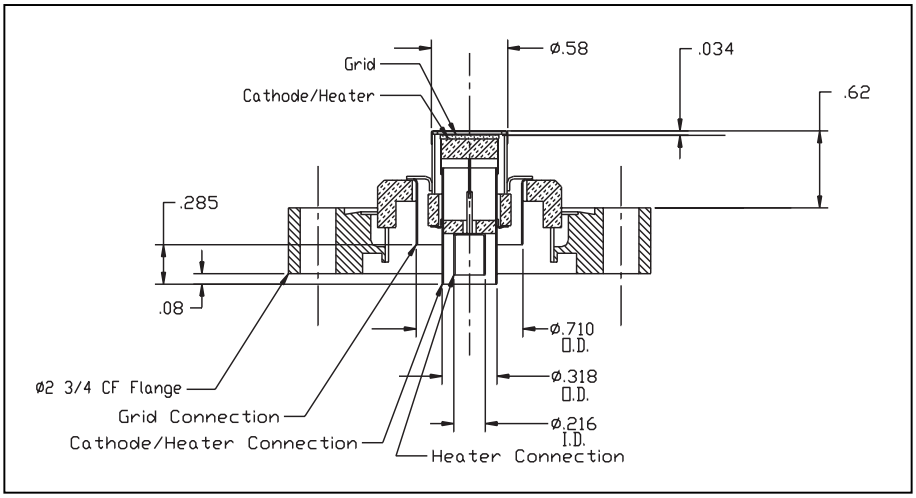

Rev. Date 9/9/02

Phone: (831) 722-9081 Fax: (831) 722-5491 Website: www.cathode.com E-mail: techsales@cathode.com

Data-sheet of the HeatWaveLabs HWEG101244 cathode

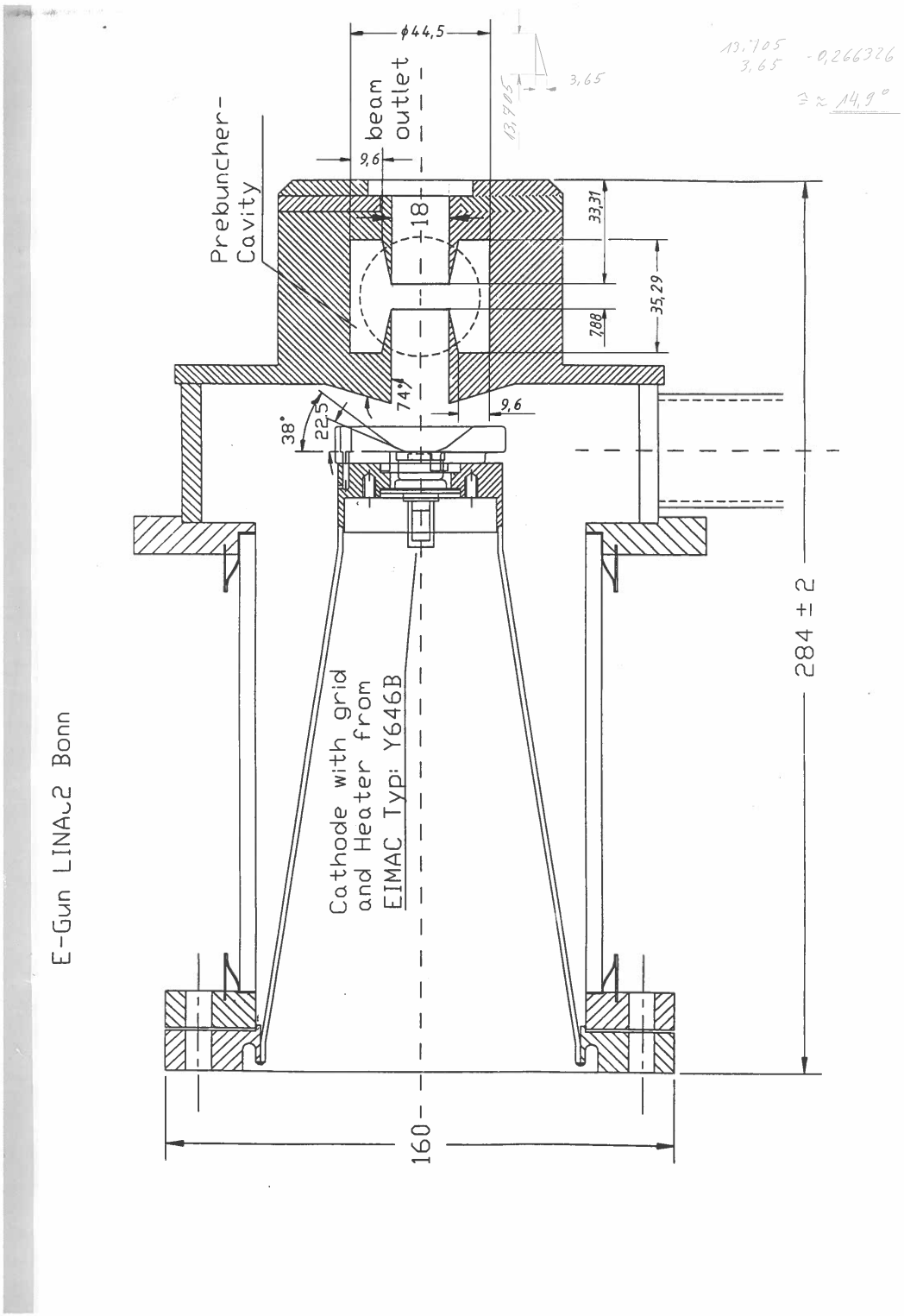

Figure A.1: Technical drawing of the current electron gun at LINAC2

APPENDIX **B**

Simulation Results and Data Analysis

B.1 Tables

d_{Pierce}/mm	ϵ_x/mm mrad	ϵ_z/mm mrad	divergence/mrad	envelope/mm	I/A
5	8.7	8.7	52	8.02	0.95

Table B.1: Values of the performance metrics at the gun exit. With the simulation parameters: $d_{\text{CA}} = 12\,\text{mm}$ and $d_{\text{Pierce}} = 5\,\text{mm}$. This simulation was performed with the Eimac Y845 cathode.

d_{Pierce}/mm	ϵ_x/mm mrad	ϵ_z/mm mrad	divergence/mrad	envelope/mm	I/A
5	7.6	7.6	46	7.59	0.94
8	7.4	7.4	44	7.47	0.94

Table B.2: Values of the performance metrics at the gun exit. With the simulation parameters: $d_{\text{CA}} = 14\,\text{mm}$ and different values of d_{Pierce}. This simulation was performed with the Eimac Y845 cathode.

d_{Pierce}/mm	ϵ_x/mm mrad	ϵ_z/mm mrad	divergence/mrad	envelope/mm	I/A
5	6.2	6.2	40	7.24	0.94
8	6.0	6.0	38	7.07	0.94
10	6.0	5.9	38	7.02	0.94

Table B.3: Values of the performance metrics at the gun exit. With the simulation parameters: $d_{\text{CA}} = 17\,\text{mm}$ and different values of d_{Pierce}. This simulation was performed with the Eimac Y845 cathode.

d_{Pierce}/mm	ϵ_x/mm mrad	ϵ_z/mm mrad	divergence/mrad	envelope/mm	I/A
5	5.2	5.2	36	7.08	0.94
8	5.0	5.0	34	6.87	0.94
10	5.0	5.0	34	6.85	0.94

Table B.4: Values of the performance metrics at the gun exit. With the simulation parameters: $d_{\text{CA}} = 20\,\text{mm}$ and different values of d_{Pierce}. This simulation was performed with the Eimac Y845 cathode.

d_{CA}/mm	ϵ_x/mm mrad	ϵ_z/mm mrad	divergence/mrad	envelope/mm	I/A
10	17.0	17.0	60	9.36	2.21
12	14.8	14.8	55	9.27	2.22
14	12.9	12.9	50	9.05	2.19
15	11.9	11.9	45	8.64	2.17
17	10.5	10.6	40	8.29	2.14
20	9.2	9.2	37	7.99	2.11

Table B.5: Values of the performance metrics at the gun exit. With different values of d_{CA} and the corresponding values of d_{Pierce}. This simulation was performed with the HWEG101244 cathode.

d_{CA}/mm	ϵ_x/mm mrad	ϵ_z/mm mrad	divergence/mrad	envelope/mm	I/A
10	9.2	8.8	76	9.19	4.00
12	8.7	8.2	73	9.16	3.98
14	8.1	7.5	70	9.16	3.93
15	7.6	7.0	69	9.11	3.90
17	6.5	5.9	69	9.01	3.73
20	4.9	4.2	68	9.16	3.13

Table B.6: Values of the performance metrics at the gun exit. With different values of d_{CA} and the corresponding values of d_{Pierce}. This simulation was performed with the NJK2221A cathode. The values at gun exit have to be considered very carefully in this simulation since a loss of particles in the anode aperture can be observed, which means that particles with high transverse displacement - and therefore probably also a big angle with regard to the longitudinal axis - are lost. This leads to a reduction of emittance, divergence and envelope of the remaining particle ensemble. Therefore these metrics should be reevaluated at a position close to but before the loss of particles. This can be seen in table 6.5.

B.2 Figures

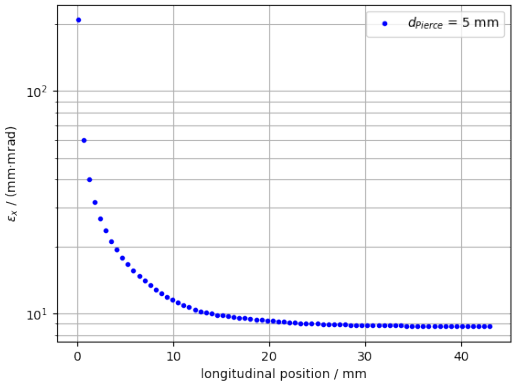

(a) Transverse Emittance in x-direction

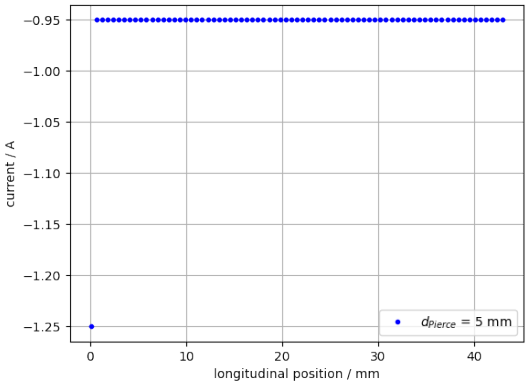

(b) Extraction Current

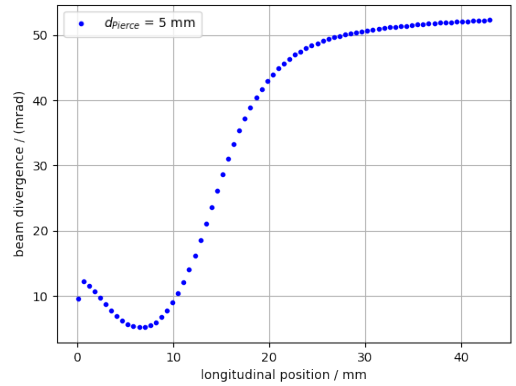

(c) Beam Divergence

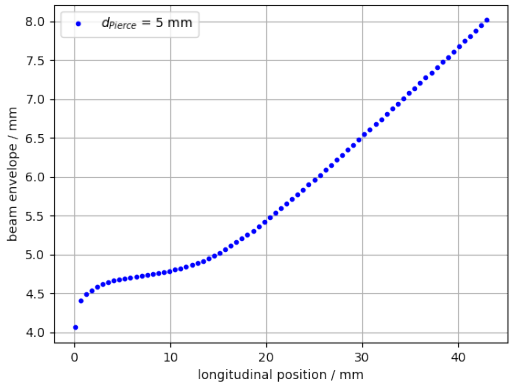

(d) Beam envelope

Figure B.1: Evaluation of the simulations of the new assembly. The parameters of this simulations are those described for the initial gun design. In the scope of the evaluation $d_{\mathrm{CA}} = 12\,\mathrm{mm}$ and $d_{\mathrm{Pierce}} = 5\,\mathrm{mm}$ were used. The simulation was done using the Eimac Y845 cathode, which delivers an electron current of 1.25 A. One can see the evolution of the performance metrics.

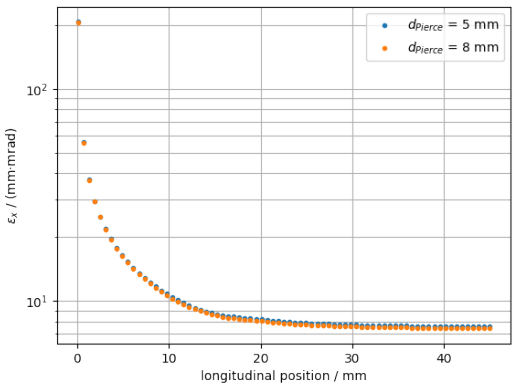

(a) Transverse Emittance in x-direction

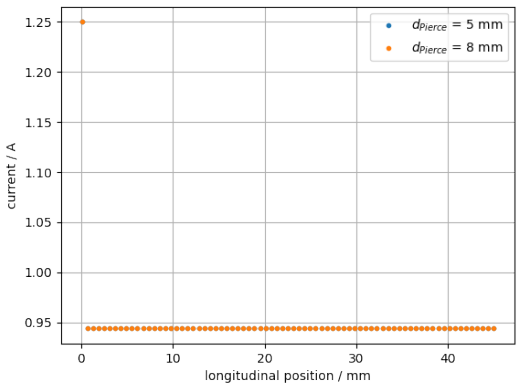

(b) Extraction Current

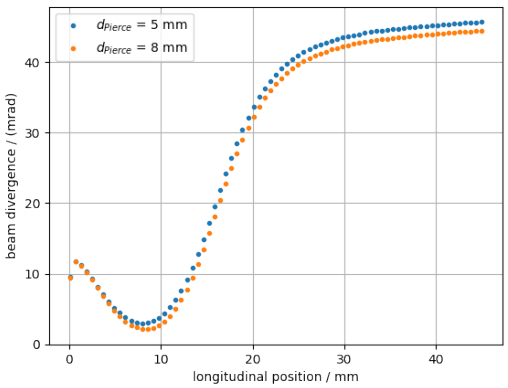

(c) Beam Divergence

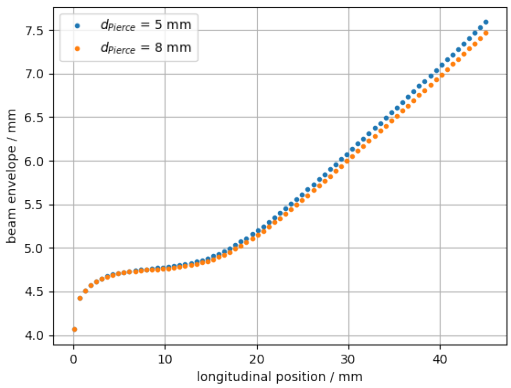

(d) Beam envelope

Figure B.2: Evaluation of the simulations of the new assembly. The parameters of this simulations are those described for the initial gun design. In the scope of the evaluation $d_{\mathrm{CA}} = 14\,\mathrm{mm}$ and different values of d_{Pierce} were used. The simulation was done using the Eimac Y845 cathode, which delivers an electron current of 1.25 A. One can see the evolution of the performance metrics.

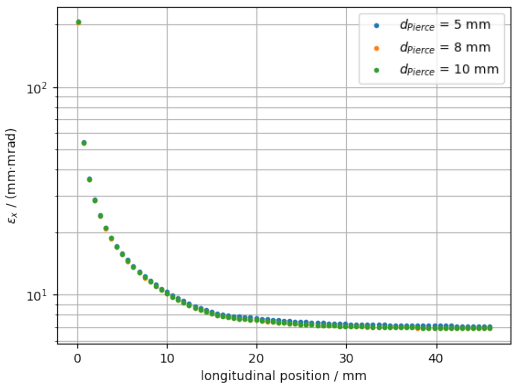

(a) Transverse Emittance in x-direction

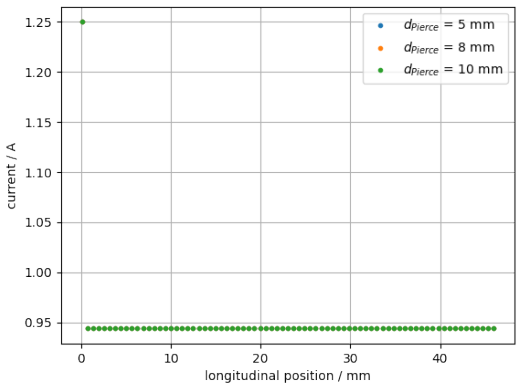

(b) Extraction Current

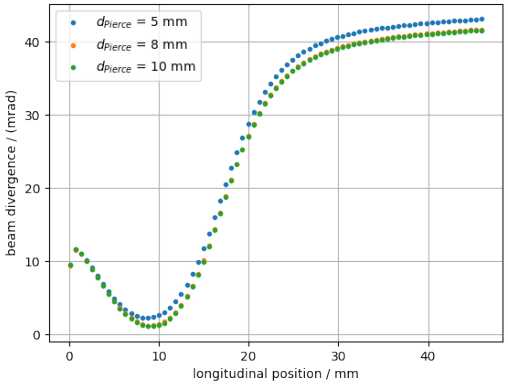

(c) Beam Divergence

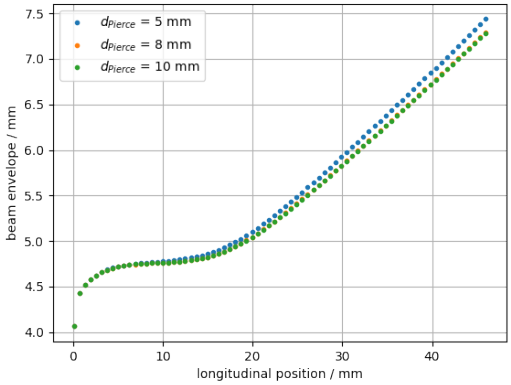

(d) Beam envelope

Figure B.3: Evaluation of the simulations of the new assembly. The parameters of this simulations are those described for the initial gun design. In the scope of the evaluation $d_{\mathrm{CA}} = 15\,\mathrm{mm}$ and different values of d_{Pierce} were used. The simulation was done using the Eimac Y845 cathode, which delivers an electron current of 1.25 A. One can see the evolution of the performance metrics.

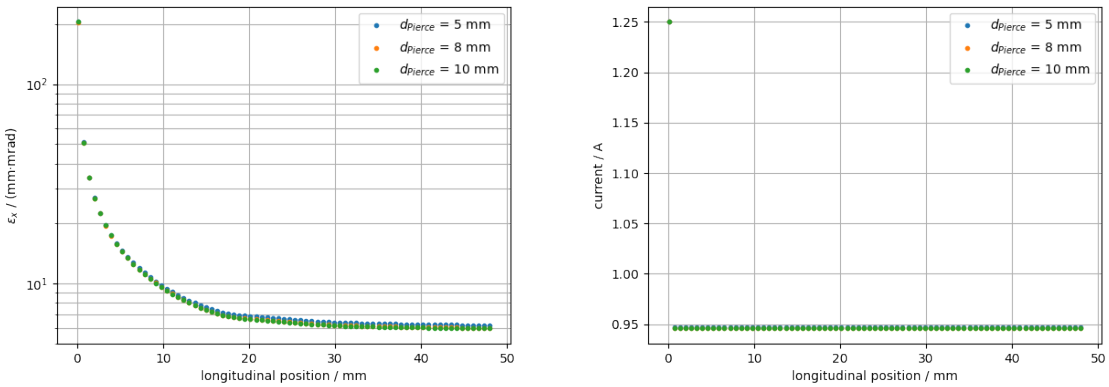

(a) Transverse Emittance in x-direction

(b) Extraction Current

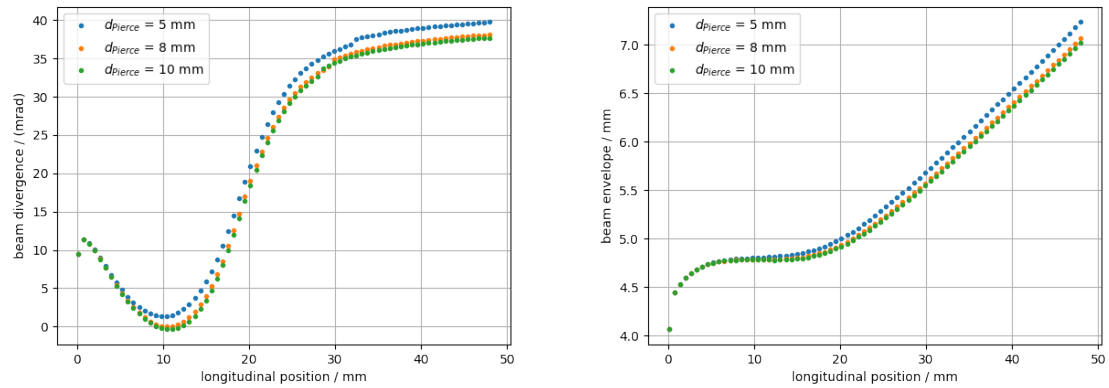

(c) Beam Divergence

(d) Beam envelope

Figure B.4: Evaluation of the simulations of the new assembly. The parameters of this simulations are those described for the initial gun design. In the scope of the evaluation $d_{\mathrm{CA}} = 17\,\mathrm{mm}$ and different values of d_{Pierce} were used. The simulation was done using the Eimac Y845 cathode, which delivers an electron current of 1.25 A. One can see the evolution of the performance metrics.

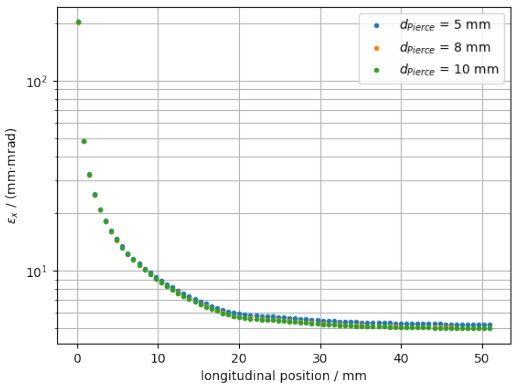

(a) Transverse Emittance in x-direction

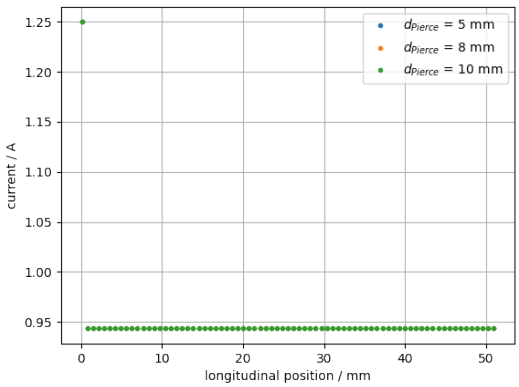

(b) Extraction Current

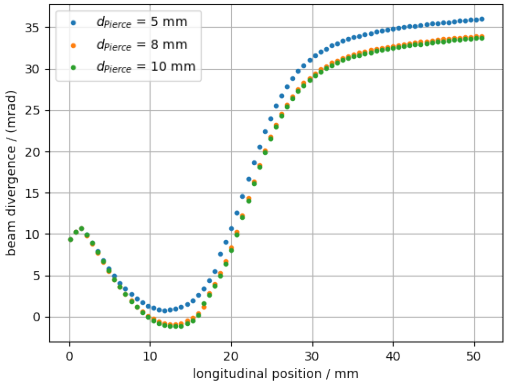

(c) Beam Divergence

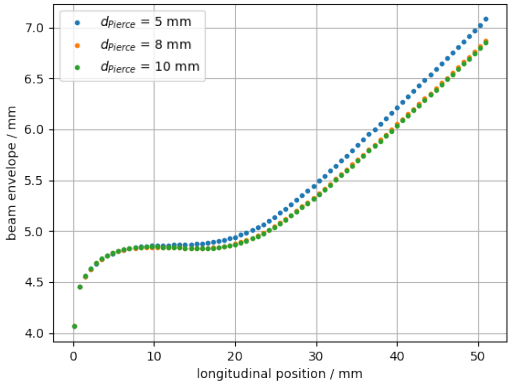

(d) Beam envelope

Figure B.5: Evaluation of the simulations of the new assembly. The parameters of this simulations are those described for the initial gun design. In the scope of the evaluation $d_{\mathrm{CA}} = 20\,\mathrm{mm}$ and different values of d_{Pierce} were used. The simulation was done using the Eimac Y845 cathode, which delivers an electron current of 1.25 A. One can see the evolution of the performance metrics.

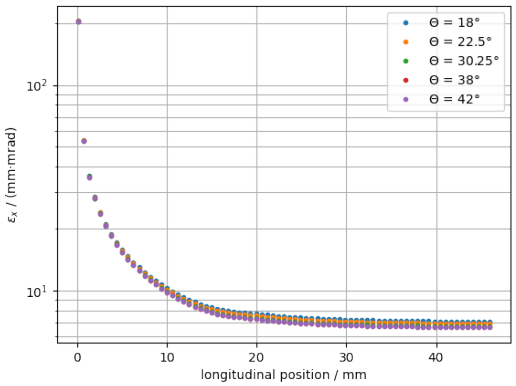

(a) Transverse Emittance in x-direction

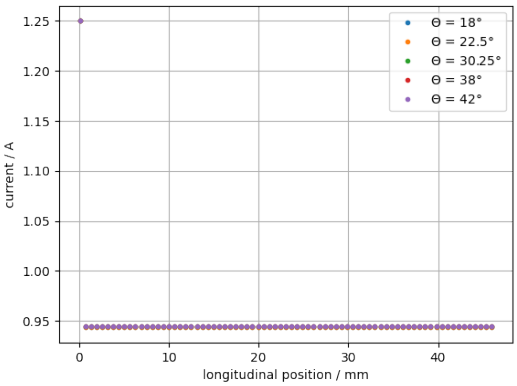

(b) Extraction Current

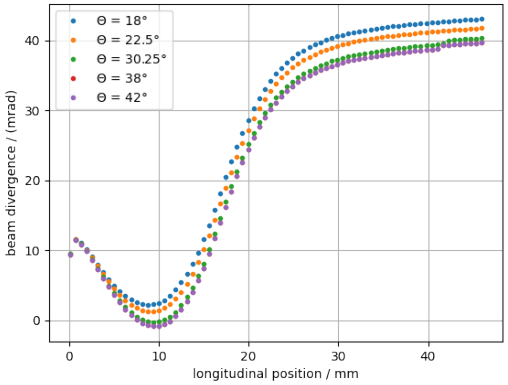

(c) Beam Divergence

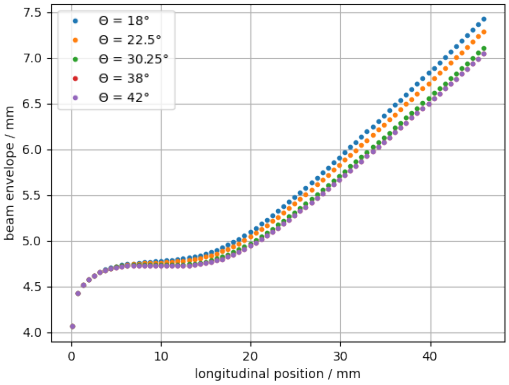

(d) Beam envelope

Figure B.6: Evaluation of the simulations of the new assembly. For this simulation $d_{\mathrm{CA}} = 15\,\mathrm{mm}$ and $d_{\mathrm{Pierce}} = 8\,\mathrm{mm}$ was used. The value of the described second angle inside the cathode cone was changed. Where $\Theta = 22.5°$ corresponds to the normal Pierce geometry of the cone. This simulation was done using the Eimac Y845 cathode, which delivers an electron current of 1.25 A. One can see the evolution of the performance metrics, i.e. the transverse emittance, the extraction current, the beam divergence and the beam envelope, along the longitudinal axis. Here the emitting surface of the cathode is at $x = 0$.

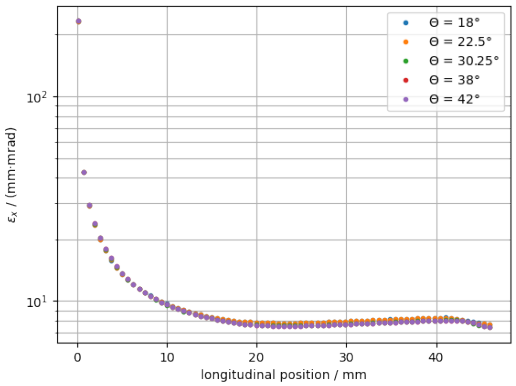

(a) Transverse Emittance in x-direction

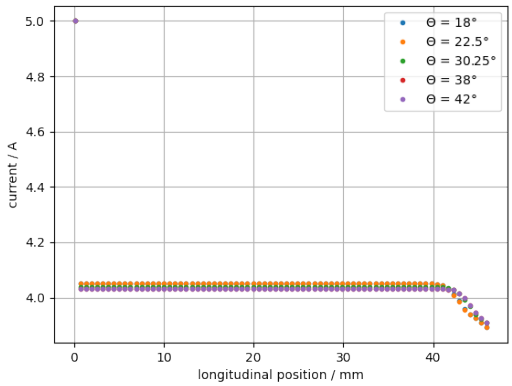

(b) Extraction Current

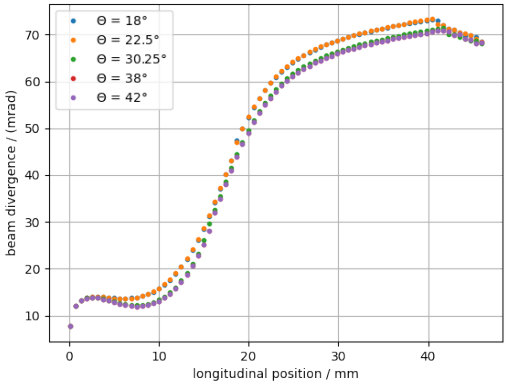

(c) Beam Divergence

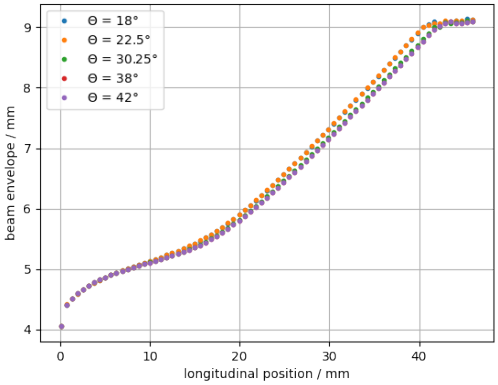

(d) Beam envelope

Figure B.7: Evaluation of the simulations of the new assembly. For this simulation $d_{\mathrm{CA}} = 15\,\mathrm{mm}$ and $d_{\mathrm{Pierce}} = 8\,\mathrm{mm}$ was used. The value of the described second angle inside the cathode cone was changed. Where $\Theta = 22.5°$ corresponds to the normal Pierce geometry of the cone. This simulation was done using the NJK2221A cathode, which delivers an electron current of 5 A. One can see the evolution of the performance metrics, i.e. the transverse emittance, the extraction current, the beam divergence and the beam envelope, along the longitudinal axis. Here the emitting surface of the cathode is at $x = 0$.

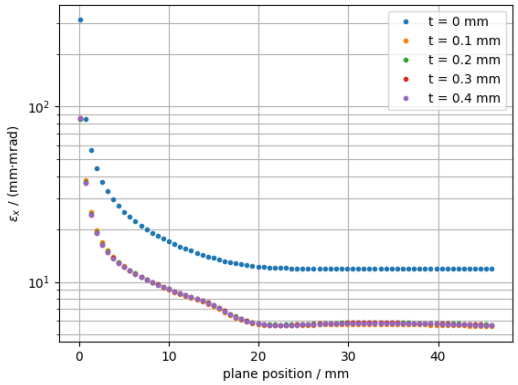

(a) Transverse Emittance in x-direction

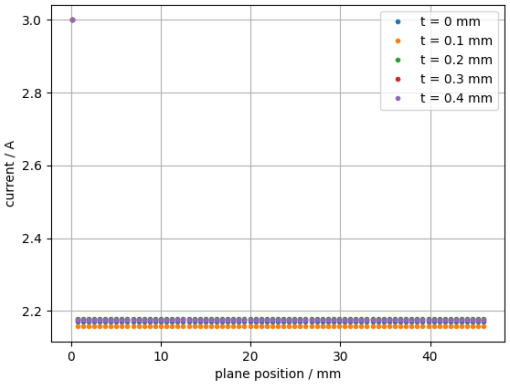

(b) Extraction Current

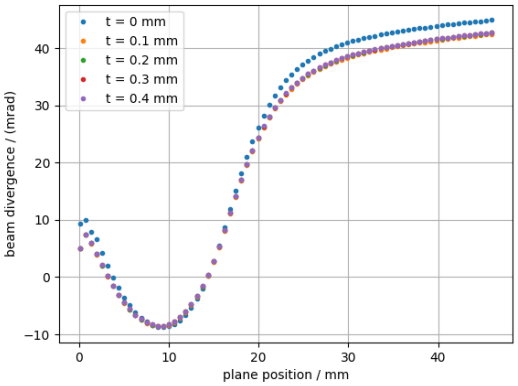

(c) Beam Divergence

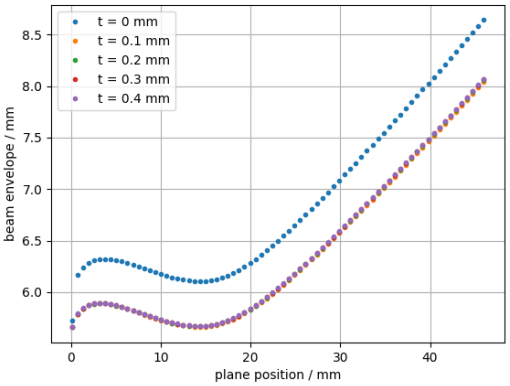

(d) Beam envelope

Figure B.8: The performance metrics are evaluated for different values of the parallelism tolerance. A significant influence is visible for non ideal tolerance values. However the deviation between different values of the tolerance is small in the simulated range. The decrease in divergence, envelope and emittance is due to the additional particle loss.

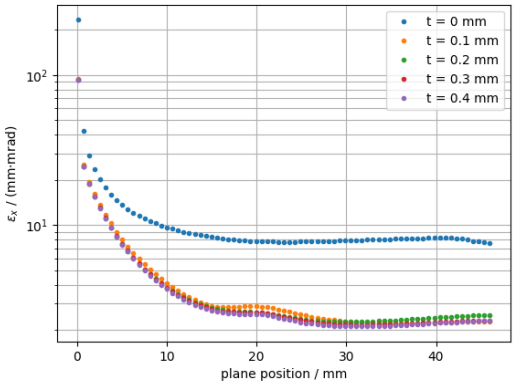

(a) Transverse Emittance in x-direction

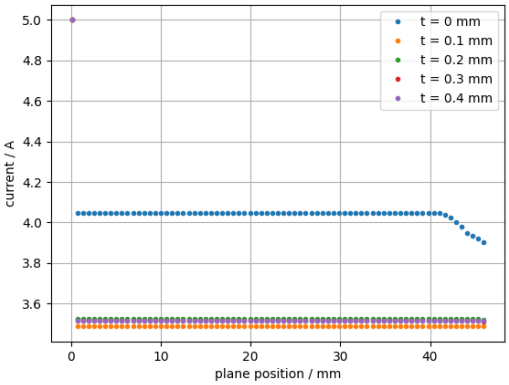

(b) Extraction Current

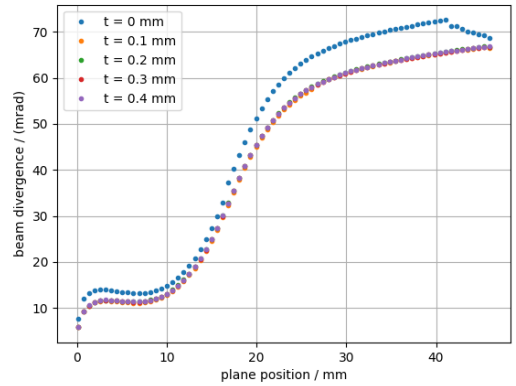

(c) Beam Divergence

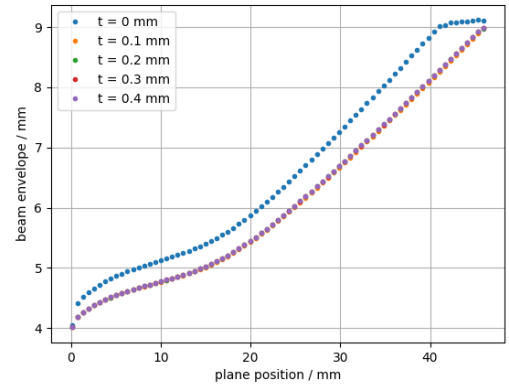

(d) Beam envelope

Figure B.9: The performance metrics are evaluated for different values of the parallelism tolerance. A significant influence is visible for non ideal tolerance values. However the deviation between different values of the tolerance is small in the simulated range. The decrease in divergence, envelope and emittance is due to the additional particle loss.

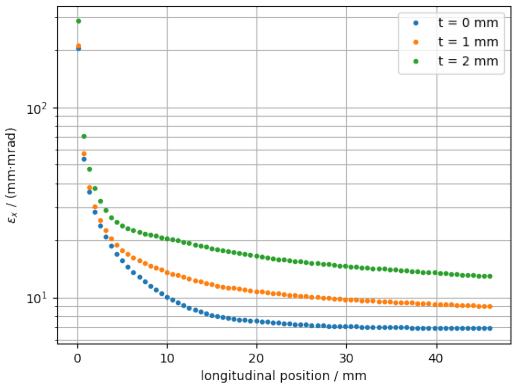

(a) Transverse Emittance in x-direction

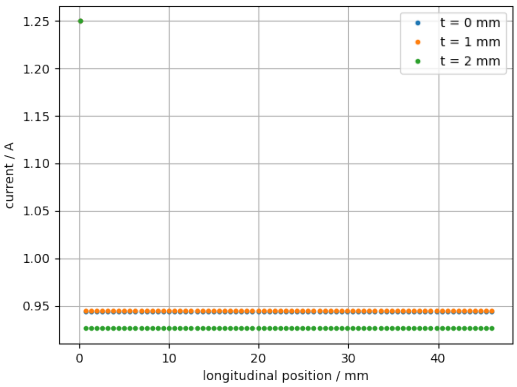

(b) Extraction Current

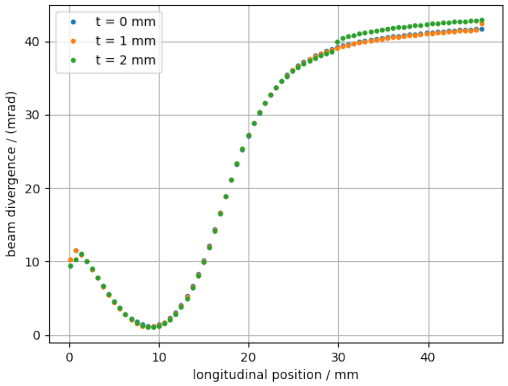

(c) Beam Divergence

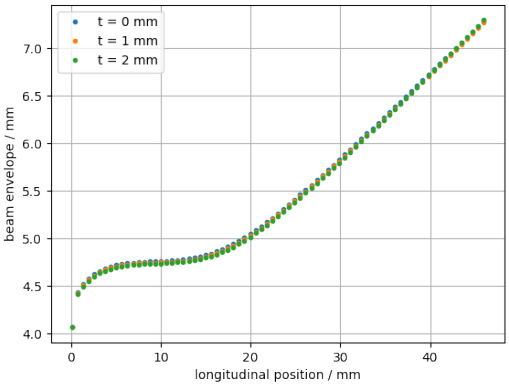

(d) Beam envelope

Figure B.10: The performance metrics are evaluated for different values of the coaxiality tolerance. A significant influence is visible for non ideal tolerance values. However the deviation between different values of the tolerance is small in the simulated range. The decrease in divergence, envelope and emittance is due to the additional particle loss.

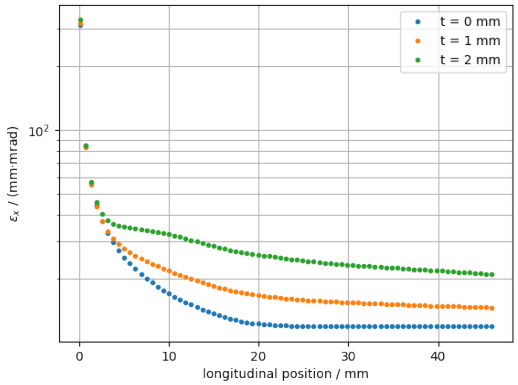

(a) Transverse Emittance in x-direction

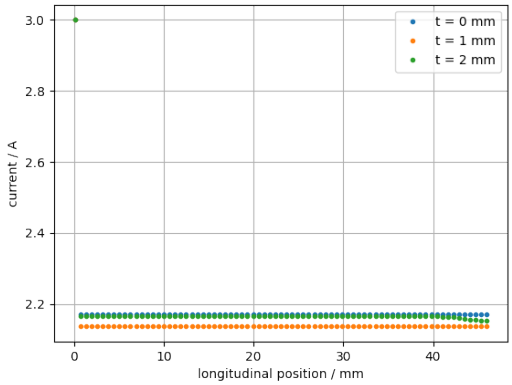

(b) Extraction Current

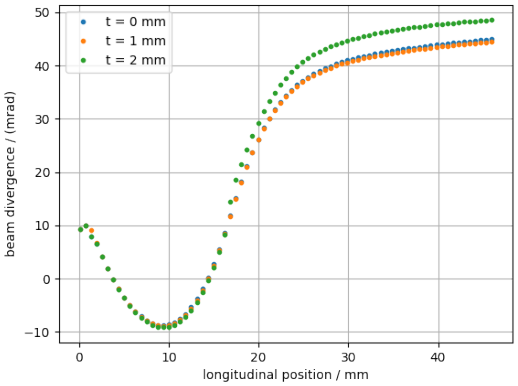

(c) Beam Divergence

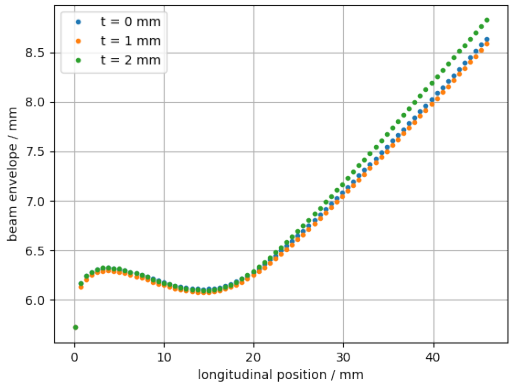

(d) Beam envelope

Figure B.11: The performance metrics are evaluated for different values of the coaxiality tolerance for the HWEG 101244 cathode. A significant influence is visible for different tolerance values. For a tolerance of $t_{\circledcirc} = 1\,\text{mm}$ the effects are predominantly small, only in the case of emittance is a clear effect discernible.

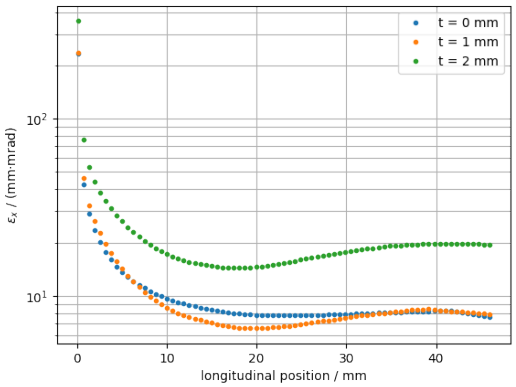

(a) Transverse Emittance in x-direction

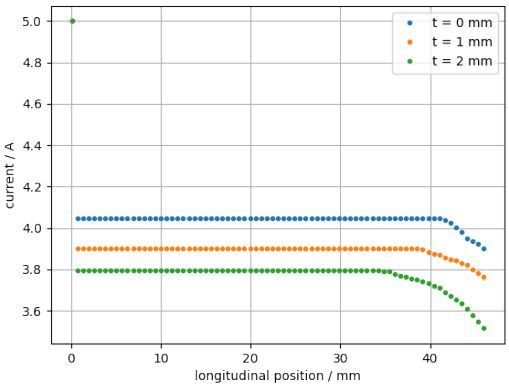

(b) Extraction Current

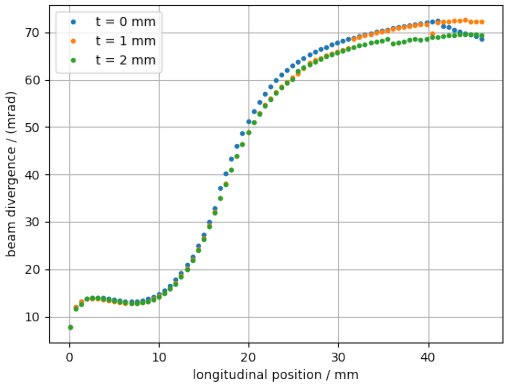

(c) Beam Divergence

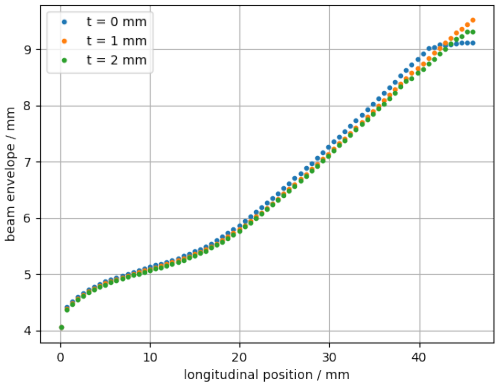

(d) Beam envelope

Figure B.12: The performance metrics are evaluated for different values of the coaxiality tolerance for the NJK 2221A cathode. The effects are mainly visible for the current and the emittance.

Bibliography

[1] Beck, Reinhard and Thoma, Ulrike, *Spectroscopy of baryon resonances*, EPJ Web Conf. **134** (2017) 02001 (cit. on p. 1).

[2] Schmieden, Hartmut and Klein, Friedrich, *Photoproduction of Mesons*, EPJ Web Conf. **134** (2017) 03001 (cit. on p. 1).

[3] M. Schedler, *Intensitäts- und Energieerhöhung an ELSA*, PhD thesis: Rheinische Friedrich-Wilhelms-Universität Bonn, 2015 (cit. on p. 3).

[4] Fabian Klarner, *Konzeption, Aufbau und Inbetriebnahme eines neuen Vorbeschleunigersystems an ELSA*, PhD thesis: Rheinische Friedrich-Wilhelms-Universität Bonn, 2011 (cit. on pp. 3, 8, 21, 22).

[5] F. Hinterberger, *Physics of particle accelerators and ion optics. With 149 illustrations, calculated examples, and 99 exercise problems with complete solutions*, Springer, 1997 (cit. on pp. 4, 7, 10, 12).

[6] H. Wiedemann, *Particle accelerator physics*, Springer Nature, 2015 (cit. on p. 4).

[7] J. R. Pierce, *Theory and Design of Electron Beams*, 2nd ed., D. van Nostrand Company, Inc.´, 1954 (cit. on p. 9).

[8] D. C. Faircloth, *Particle Sources*, 2021, arXiv: 2103.13231 [physics.acc-ph] (cit. on p. 10).

[9] S. V. Kutsaev, *Electron bunchers for industrial RF linear accelerators: theory and design guide*, The European Physical Journal Plus **136** (2021) 446 (cit. on pp. 12, 13).

[10] *ELECTRON SOURCES, Communications and Power Industries Electron Guns*, CPI - Communications and Power Industries, (visited on 08/02/2023) (cit. on p. 15).

[11] *CST Studio Suite, Electromagnetic field simulation software*, Dassault Systèmes, 2023, (visited on 08/02/2023) (cit. on pp. 15, 16, 37, 41).

[12] F. Klarner, *Ein neues Injektorsystem zur Erzeugung von Einzelpulsen für den Elektronenbeschleuniger ELSA*, Diplom: Physikalisches Institut der Universität Bonn, 2006, chap. Der Linearbeschleuniger Linac 1 und sein Injektor, (visited on 27/06/2022) (cit. on pp. 21, 24, 26).

[13] D. Proft, personal communication, 2022 (cit. on p. 22).

[14] K. Baptiste et al.,
A CW normal-conductive RF gun for free electron laser and energy recovery linac applications,
Nuclear Instruments and Methods in Physics Research Section A: Accelerators, Spectrometers, Detectors and Associated Equipment **599** (2009) 9, ISSN: 0168-9002 (cit. on p. 23).

[15] F. Löhl et al., "High current and high brightness electron sources",
IPAC 2010 - 1st International Particle Accelerator Conference, 2010 (cit. on p. 23).

[16] D. H. Dowell, J. W. Lewellen, D. Nguyen and R. Rimmer,
The status of normal conducting RF (NCRF) guns, a summary of the ERL2005 workshop,
Nuclear Instruments and Methods in Physics Research Section A: Accelerators, Spectrometers, Detectors and Associated Equipment **557** (2006) 61, Energy Recovering Linacs 2005,
ISSN: 0168-9002 (cit. on p. 23).

[17] A. Matveev et al.,
Simulation and experimental study of beam dynamics in NovoFEL RF gun and its beamline,
AIP Conference Proceedings **2299** (2020) 020006,
eprint: https://aip.scitation.org/doi/pdf/10.1063/5.0030844
(cit. on p. 23).

[18] E. d. Prepared by the staff of CPI, ed., *Care and feeding of power grid tubes*, 5th ed.,
CPI, EIMAC Division, San Carlos, CA 94070, USA, 2003, chap. 2 39, (visited on 27/06/2022)
(cit. on p. 24).

[19] J.-Y. Gao et al., *A review on recent progress of thermionic cathode*, Tungsten **2** (2020) 289
(cit. on p. 24).

[20] R. Thomas, J. Gibson, G. Haas and R. Abrams,
Thermionic sources for high-brightness electron beams,
IEEE Transactions on Electron Devices **37** (1990) 850 (cit. on p. 24).

[21] P. K. Roy et al., *Study of a laser-heated electron gun*,
Review of Scientific Instruments **67** (1996) 4098,
eprint: https://doi.org/10.1063/1.1147577 (cit. on p. 24).

[22] F. Giori, L. A. MacKenzie and E. J. McKinney, *Laser-induced thermionic emission*,
Applied Physics Letters **3** (1963) 25, eprint: https://doi.org/10.1063/1.1753860
(cit. on p. 24).

[23] I. Munawar, I. Ghalib Ul, F. Muhammad Ayub and Z. Zusheng,
Electron Beam Guns for High Energy Electron Accelerators: An Overview,
Journal of Modern Physics **2013** (2013) (cit. on p. 24).

[24] B. Dunham, *Introduction to Electron Guns for Accelerators*, Talk,
Cornell Laboratory for accelerator-based sciences and education, 2008, (visited on 27/06/2022)
(cit. on p. 24).

[25] W. Hillert, M. Gowin and B. Neff, eds., *The 50 kV inverted source of polarized electrons at ELSA*,
14th International Spin Physics Symposium SPIN2000 (2000), Osaka, 2000, (visited on 27/06/2022)
(cit. on p. 24).

[26] M. Hoffmann and other, eds., *The polarized electron beam at ELSA*, 14th International Spin Physics Symposium SPIN2000 (2000), Osaka, 2000, (visited on 27/06/2022) (cit. on p. 24).

[27] W. Hillert, M. Gowin and B. Neff, "A new injector for polarized electrons at ELSA", *GDH 2000*, World Scientific, 2001 283 (cit. on p. 24).

[28] W. Hillert, M. Gowin and B. Neff, "A 50 kV inverted polarized gun", *Proc. Low Energy Polarized Electron Workshop, St. Petersburg*, 1998 (cit. on p. 24).

[29] W. Hillert, *Erzeugung eines Nutzstrahls spinpolarisierter Elektronen an der Beschleunigeranlage ELSA*, 2000 (cit. on p. 24).

[30] D. Mihalcea, P. Piot et al., *Simulation of Field-Emission Cathodes for High Current Electron Injectors*, Proceedings of LINAC08, Victoria, Canada (2008) (cit. on p. 25).

[31] D. Pigache and G. Fournier, *Secondary-emission electron gun for high pressure molecular lasers*, Journal of Vacuum Science and Technology **12** (1975) 1197 (cit. on p. 25).

[32] K. L. Jensen, D. W. Feldman, N. A. Moody and P. G. O'Shea, *A photoemission model for low work function coated metal surfaces and its experimental validation*, Journal of Applied Physics **99** (2006) 124905, eprint: https://doi.org/10.1063/1.2203720 (cit. on p. 25).

[33] B. Leblond, *Short pulse photoemission from a dispenser cathode under the 2nd, 3rd and 4th harmonics of a picosecond Nd: YAG laser*, Nuclear Instruments and Methods in Physics Research Section A: Accelerators, Spectrometers, Detectors and Associated Equipment **317** (1992) 365, ISSN: 0168-9002 (cit. on p. 25).

[34] H. Bergeret, M. Boussoukaya, R. Chehab, B. Leblond and J. Le Duff, *Short pulse photoemission from a dispenser cathode*, Nuclear Instruments and Methods in Physics Research Section A: Accelerators, Spectrometers, Detectors and Associated Equipment **301** (1991) 389, ISSN: 0168-9002 (cit. on p. 25).

[35] K. Torgasin et al., *Thermally assisted photoemission effect on CeB 6 and LaB 6 for application as photocathodes*, Physical Review Accelerators and Beams **20** (2017) 073401 (cit. on p. 25).

[36] R. Yen, J. Liu and N. Bloembergen, *Thermally assisted multiphoton photoelectric emission from tungsten*, Optics Communications **35** (1980) 277, ISSN: 0030-4018 (cit. on p. 25).

[37] J. Schmerge et al., "SSRL performance enhancements", *Journal of Physics: Conference Series*, vol. 425, 4, IOP Publishing, 2013 042011 (cit. on p. 26).

[38] S. Gierman et al., "Operating a Tungsten Dispenser Cathode in Photo-Emission Mode", *Particle Accelerator Conference (PAC 09)*, 2010 MO6RFP088 (cit. on pp. 26, 28–30).

[39] S. Thorin, N. Čutić, F. Lindau, S. Werin and F. Curbis, *Photocathode operation of a thermionic RF gun*, Nuclear Instruments and Methods in Physics Research Section A: Accelerators, Spectrometers, Detectors and Associated Equipment **606** (2009) 291, ISSN: 0168-9002 (cit. on pp. 26, 28, 30, 31).

[40] S. Thorin, N. Čutić, F. Lindau, S. Werin and F. Curbis,
"Characterisation of the BEAM from thermionic RF-gun adapted for photo cathode operation", 2009 310 (cit. on pp. 26, 28).

[41] S. Guharay, L. Len and F. Mako,
"High-current micro-pulse electron guns and accelerator applications",
PACS2001. Proceedings of the 2001 Particle Accelerator Conference (Cat. No. 01CH37268), vol. 3, IEEE, 2001 2084 (cit. on p. 26).

[42] L. Liao, M. Zhang, Q. Gu, W.-C. Fang and M.-H. Zhao,
Multipacting analysis in micro-pulse electron gun, Chinese Physics C **37** (2013) 117004 (cit. on p. 26).

[43] L. Liao, M. Zhang, M. Zhao and Q. Gu, *Novel design of a micro-pulse electron gun*,
Nuclear Instruments and Methods in Physics Research Section A: Accelerators, Spectrometers, Detectors and Associated Equipment **729** (2013) 381, ISSN: 0168-9002 (cit. on p. 26).

[44] F. M. Mako and W. Peter, "A high-current micro-pulse electron gun",
Proceedings of International Conference on Particle Accelerators, IEEE, 1993 2702 (cit. on p. 26).

[45] D. Yang et al., *Study on the maximum stable output of a novel s-band micro-pulse electron gun*, AIP Advances **8** (2018) 075313 (cit. on p. 26).

[46] D. Yang et al., "Design and Research of a Micro-Pulse Electron Gun",
38th Int. Free Electron Laser Conf.(FEL'17), Santa Fe, NM, USA, August 20-25, 2017, JACOW, Geneva, Switzerland, 2018 466 (cit. on p. 26).

[47] L. Liao, M. Zhang, Q. Gu, W. Fang and M. Zhao,
"Studying of multipacting in micro-pulse electron gun", *Proceedings of IPAC2013, Shanghai, China* 383 (cit. on p. 26).

[48] K. L. Jensen, D. W. Feldman, N. A. Moody and P. G. O'Shea, *A photoemission model for low work function coated metal surfaces and its experimental validation*,
Journal of Applied Physics **99** (2006) 124905 (cit. on p. 30).

[49] W. Demtröder, "Laser", *Experimentalphysik 3: Atome, Moleküle und Festkörper*,
Berlin, Heidelberg: Springer Berlin Heidelberg, 2016 251, ISBN: 978-3-662-49094-5 (cit. on p. 31).

[50] *LightPipes for Python*, version 2.1.3, 2019 (cit. on pp. 31, 32).

[51] L. N. et al., *BDSIM: An Accelerator Tracking Code with Particle-Matter Interactions*, 2020 (cit. on p. 56).

[52] S. Agostinelli et al., *GEANT4–a simulation toolkit*, Nucl. Instrum. Meth. A **506** (2003) 250 (cit. on p. 56).

[53] M. Borland, *elegant: A Flexible SDDS-Compliant Code for Accelerator Simulation*,
Advanced Photon Source LS-287, 2000 (cit. on p. 56).

List of Figures

List of Tables

Acknowledgements

I would like to thank Prof. Dr. Desch for supervising my Master's thesis and for providing me with this topic. I was very grateful to be able to work in the ELSA group again after my bachelor thesis and to be able to personally contribute to the accelerator.

I would like to thank Prof. Dr. Schmieden for agreeing to act as coreferee.

I would especially like to thank Dennis Proft for his extensive supervision of my thesis and for always having his door open. I would like to thank him and the group for their trust, allowing me to contribute my ideas to a significant extent. It was much appreciated.

At this point I would also like to thank Philipp Hänisch, who supported the project from the technical side and triggered some of my analyses, always keeping feasibility in mind. He was also always available to discuss changing plans or answer technical questions.

I would also like to thank Michael Switka for his support with all sorts of questions, especially but not exclusively about all sort of optics related ones.

I would like to thank Dr. Frank Vewinger for his help in evaluating the laser properties and for his continued support of the project and future tests and the search for a temporary laser system for them.

Special thanks to both Dr. Sara Thorin of MAX-lab and Dr. William Jeff Corbett of SSRL for their contributions and for sharing their experience with TAPE-type guns.

I would like to thank Dennis Proft, Dennis Sauerland and Michael Switka for proofreading the thesis.

Last but not least, I would like to thank the whole ELSA team - especially the "Jungvolk" - for their support, comments and ideas during this thesis, which helped me a lot.

I would also like to thank my family and friends who have supported me throughout my entire studies, especially during stressful times. Without them I would not be where I am today.

Thank you all!